Field-scale quantification of methane and nitrous oxide agricultural emissions using micrometeorological approaches

by

Chinthaka Weerasekara

B.S., University of Peradeniya, 2010
M.S., Kansas State University, 2019

AN ABSTRACT OF A DISSERTATION

submitted in partial fulfillment of the requirements for the degree

DOCTOR OF PHILOSOPHY

Department of Agronomy
College of Agriculture

KANSAS STATE UNIVERSITY
Manhattan, Kansas

2025

Abstract

Methane (CH_4) and nitrous oxide (N_2O) emissions from agricultural systems are significant contributors to global greenhouse gas (GHG) emissions, and accurate quantification of these emissions is essential for improving GHG inventories and evaluating mitigation strategies. This research employs the eddy covariance (EC) technique, artificial neural networks (ANN), and footprint analysis to address key challenges, such as spatial variability, data gaps, and footprint limitations, in measuring GHG emissions in dynamic agricultural environments. The objectives of this study were to: 1) assess the performance of the EC technique for measuring N_2O and CH_4 fluxes in agricultural systems; 2) develop ANN models to fill gaps in N_2O flux data; and 3) evaluate CH_4 emission rates from grazing systems using EC and footprint models.

The first study focused on N_2O emissions measured using the EC technique in two contrasting agricultural environments: a cattle feedlot and a winter wheat field. In the cattle feedlot, average N_2O fluxes were low (0.0062 μ mol m^{-2} s^{-1}) during winter, with emission spikes that were not consistently linked to precipitation or temperature changes due to frozen soil conditions. In contrast, the winter wheat field exhibited higher variability, with emission rates peaking at 0.03 μ mol m^{-2} s^{-1} during warm, moist periods following nitrogen fertilization and rainfall. Footprint analysis in the cattle feedlot revealed that up to 70% of the measured flux contributions came from outside the feedlot boundary, driven by manure runoff and off-site sources. In the winter wheat field, N_2O fluxes were more evenly distributed within the footprint and closely associated with fertilizer applications and subsequent precipitation events. These findings demonstrate the necessity of continuous high-frequency measurements to capture the full temporal and spatial variability of N_2O fluxes in agricultural systems.

The second study applied artificial neural networks (ANN) to fill data gaps in N_2O flux measurements at winter wheat fields. Data gaps, caused by equipment malfunctions, low-turbulence conditions, and extreme weather events, can significantly affect the accuracy of long-term flux data. The ANN models were trained using environmental variables, such as soil moisture, temperature, and wind speed, and demonstrated strong performance, achieving a coefficient of determination ($R^2 > 0.85$) between predicted and observed fluxes. At the winter wheat field, the ANN model successfully reconstructed missing flux data due to cold weather and sensor failures and filled gaps during elevated N_2O emissions following fertilization. These results highlight the importance of using advanced gap-filling techniques, such as ANN, to maintain the integrity of long-term GHG datasets, particularly in complex agricultural systems.

The third study focused on quantifying CH_4 emissions from grazing systems using the eddy covariance (EC) technique in combination with flux scaling based on footprint analysis. Controlled CH_4 release experiments were conducted to simulate emissions from a small herd of cattle, allowing for the assessment of the EC system's accuracy in estimating CH_4 fluxes. The results revealed that CH_4 fluxes were consistently underestimated, with the calculated emission rates clustering around 30% of the actual release rate. This underestimation was linked to the footprint model’s difficulty in fully capturing contributions from the source area, especially at lower fetch percentages. Increasing the fetch to 90% improved source coverage but introduced instability and errors. These findings emphasize the need for more accurate footprint models to account for varying wind conditions and terrain complexities in grazing environments.

The integration of these studies underscores the importance of continuous high-frequency measurements in capturing the variability of N_2O and CH_4 emissions in agricultural systems. Due to uncontrollable factors such as equipment failures and adverse weather conditions, data gaps are

inevitable, making gap-filling techniques like ANN crucial for ensuring data continuity. Footprint analysis further improves the accuracy of emission estimates by addressing spatial variability in emission sources, particularly in grazing systems. This research advances the understanding of GHG emissions from livestock and crop production systems, contributing to more accurate emission inventories and the development of effective mitigation strategies in agriculture.

Field-scale quantification of methane and nitrous oxide agricultural emissions using micrometeorological approaches

by

Chinthaka Weerasekara

B.S., University of Peradeniya, 2010
M.S., Kansas State University, 2019

A DISSERTATION

submitted in partial fulfillment of the requirements for the degree

DOCTOR OF PHILOSOPHY

Department of Agronomy
College of Agriculture

KANSAS STATE UNIVERSITY
Manhattan, Kansas

2025

Approved by:

Major Professor
Eduardo Alvarez Santos

Copyright

© Chinthaka Weerasekara 2025.

Abstract

Methane (CH_4) and nitrous oxide (N_2O) emissions from agricultural systems are significant contributors to global greenhouse gas (GHG) emissions, and accurate quantification of these emissions is essential for improving GHG inventories and evaluating mitigation strategies. This research employs the eddy covariance (EC) technique, artificial neural networks (ANN), and footprint analysis to address key challenges, such as spatial variability, data gaps, and footprint limitations, in measuring GHG emissions in dynamic agricultural environments. The objectives of this study were to: 1) assess the performance of the EC technique for measuring N_2O and CH_4 fluxes in agricultural systems; 2) develop ANN models to fill gaps in N_2O flux data; and 3) evaluate CH_4 emission rates from grazing systems using EC and footprint models.

The first study focused on N_2O emissions measured using the EC technique in two contrasting agricultural environments: a cattle feedlot and a winter wheat field. In the cattle feedlot, average N_2O fluxes were low (0.0062 μ mol m^{-2} s^{-1}) during winter, with emission spikes that were not consistently linked to precipitation or temperature changes due to frozen soil conditions. In contrast, the winter wheat field exhibited higher variability, with emission rates peaking at 0.03 μ mol m^{-2} s^{-1} during warm, moist periods following nitrogen fertilization and rainfall. Footprint analysis in the cattle feedlot revealed that up to 70% of the measured flux contributions came from outside the feedlot boundary, driven by manure runoff and off-site sources. In the winter wheat field, N_2O fluxes were more evenly distributed within the footprint and closely associated with fertilizer applications and subsequent precipitation events. These findings demonstrate the necessity of continuous high-frequency measurements to capture the full temporal and spatial variability of N_2O fluxes in agricultural systems.

The second study applied artificial neural networks (ANN) to fill data gaps in N_2O flux measurements at winter wheat fields. Data gaps, caused by equipment malfunctions, low-turbulence conditions, and extreme weather events, can significantly affect the accuracy of long-term flux data. The ANN models were trained using environmental variables, such as soil moisture, temperature, and wind speed, and demonstrated strong performance, achieving a coefficient of determination ($R^2 > 0.85$) between predicted and observed fluxes. At the winter wheat field, the ANN model successfully reconstructed missing flux data due to cold weather and sensor failures and filled gaps during elevated N_2O emissions following fertilization. These results highlight the importance of using advanced gap-filling techniques, such as ANN, to maintain the integrity of long-term GHG datasets, particularly in complex agricultural systems.

The third study focused on quantifying CH_4 emissions from grazing systems using the eddy covariance (EC) technique in combination with flux scaling based on footprint analysis. Controlled CH_4 release experiments were conducted to simulate emissions from a small herd of cattle, allowing for the assessment of the EC system's accuracy in estimating CH_4 fluxes. The results revealed that CH_4 fluxes were consistently underestimated, with the calculated emission rates clustering around 30% of the actual release rate. This underestimation was linked to the footprint model’s difficulty in fully capturing contributions from the source area, especially at lower fetch percentages. Increasing the fetch to 90% improved source coverage but introduced instability and errors. These findings emphasize the need for more accurate footprint models to account for varying wind conditions and terrain complexities in grazing environments.

The integration of these studies underscores the importance of continuous high-frequency measurements in capturing the variability of N_2O and CH_4 emissions in agricultural systems. Due to uncontrollable factors such as equipment failures and adverse weather conditions, data gaps are

inevitable, making gap-filling techniques like ANN crucial for ensuring data continuity. Footprint analysis further improves the accuracy of emission estimates by addressing spatial variability in emission sources, particularly in grazing systems. This research advances the understanding of GHG emissions from livestock and crop production systems, contributing to more accurate emission inventories and the development of effective mitigation strategies in agriculture.

Table of Contents

List of Figures xiv
List of Tables xvii
Acknowledgments xviii
Chapter 1 - General introduction 1
1.1 The eddy covariance technique 2
1.1.1 Advantages of eddy covariance 6
1.1.2 Challenges and data processing 6
1.1.3 Applications in agricultural systems 7
1.2 Outline and objectives 8
Chapter 2 - Measurements of nitrous oxide from agriculture systems using the eddy covariance technique 10
2.1 Abstract 10
2.2 Introduction 11
2.3 Material and methods 17
2.3.1 Site description and instrument setup 17
Site 01 17
Site 02 18
2.3.2 Flux measurements 19
2.3.3 Time lag compensation 20
2.3.4 Air density corrections 20
2.3.5 Spectral corrections 21
2.3.6 Statistical analysis: 23
Normality testing 23
Homogeneity of variance testing 24
One-Way ANOVA 25
Kruskal-Wallis test 25
Fisher's exact test 26
2.4 Results 28
2.4.1 N_2O emission from beef cattle 28

Environmental factors 28
Spatial variability of N_2O flux 30
Temporal variability of N_2O flux 31
2.4.2 N_2O emission from cropland 32
Environmental factors 32
Spatial variability of N_2O flux 34
2.5 Discussion 39
2.5.1 Temporal and spatial variability 39
2.5.2 Impact of missing data 40
Chapter 3 - Evaluating the applicability of neural networks for gap filling N_2O flux data 42
3.1 Abstract 42
3.2 Introduction 43
3.3 Material and methods 46
3.3.1 Site description 46
3.3.2 Flux measurements 47
3.3.3 Using cross-correlation to identify the lags between N_2O flux, soil temperature, and soil moisture content. 48
3.3.4 Gap filling approaches. 49
Linear interpolation 49
Artificial neural network 49
Development and optimization of an artificial neural network 52
3.3.5 The relative importance of driving variables for the ANN model 54
3.3.6 Evaluation of gap filling methods 55
3.3.7 Total flux uncertainty 55
3.3.8 Data selection for training the ANN and the evaluation performance of the gap filling methods. 56
3.4 Results 57
3.4.1 Environmental conditions 57
3.4.2 Data screening 58
3.4.3 Neural network training 60
3.4.4 Performance of gap filling methods 62

3.5 Discussion 67
3.5.1 Challenges of data gaps in N_2O emission studies 67
3.5.2 Evaluation of gap-filling methods 67
3.5.3 Study limitations and future directions 69
Chapter 4 - Assessing the use of eddy covariance and flux scaling to estimate methane emissions from a simulated herd of cattle in a grazing system. 70
4.1 Abstract 70
4.2 Introduction 71
4.3 Material and methods 78
4.3.1 Site description and instrument setup 78
4.3.2 Flux calculation 80
4.3.3 Flux footprint calculation 81
4.3.4 Flux scaling 83
4.4 Results 85
4.4.1 Eddy covariance fluxes 85
4.4.2 Footprint analysis 85
4.4.3 Fluxes from the surrounding area 87
4.4.4 Emissions from the artificial source 87
4.5 Discussion 91
4.5.1 Impact of temporal resolution on flux estimates 91
4.5.2 Footprint analysis and source area coverage 91
4.5.3 Challenges in scaling methodologies 92
4.5.4 Future directions and methodological advancements 93
Chapter 5 - Overall discussion and conclusion 95
5.1 Summary and conclusions 95
Study 1: N_2O emissions from agricultural fields using the eddy covariance technique 95
Study 2: Gap-filling of N_2O flux data using artificial neural networks 96
Study 3: CH_4 emissions from grazing systems using eddy covariance and footprint analysis 97
5.2 Implications for agriculture in the United States 99
5.2.1 Advancing sustainable practices in U.S. agriculture 99

5.2.2 Enhancing national GHG inventories 100
5.2.3 Supporting policy and incentive programs 100
5.3 Positioning U.S. agriculture as a global leader 101
References 102

List of Figures

Figure 1-1: Main component and their placement of an eddy covariance system..... 5
Figure 2-1: Layout of the experimental site the beef cattle stocker unit in Manhattan, KS. Insets: (a) flux tower..... 17
Figure 2-2: Layout of the experimental site, NEON Kona experimental field. Blue circles show the location of the soil moisture and soil temperature sensors. Insets: (a) instrument setup, (b) Flux tower. 18
Figure 2-3: 30-min values of intervals (a) N_2O fluxes, and (b) air temperature and precipitation. 28
Figure 2-4: Distance from the flux tower to the 'x' mark representing the upwind distance from the tower contributing to 70% of the total flux for 30-minute intervals. Color of the 'x' represents the flux value. 30
Figure 2-5: Hourly average of N_2O fluxes in Beef stocker unit. The central blue line in each box indicates the median, central diamond indicates the mean, and the bottom and top edges of the box indicate the 25th and 75th percentiles, respectively. The whiskers are extended to the most extreme data point that is no more than 1.5 times the interquartile range (IQR) from the edge of the box. The black circle sign represents outliers that lie beyond the whiskers. 32
Figure 2-6: 30-min values of (a) N_2O fluxes with red vertical line indicating the fertilization event 07 March 2021 (47 kg N ha−1), (b) soil temperature and water content at 5cm depth. 33
Figure 2-7:Wind rose and N_2O flux magnitudes during the experimental period. The N_2O flux was grouped based on the flux magnitude bins represented by the different colors in the graph. 36
Figure 2-8: Hourly average of N_2O flux in winter wheat field. The central blue line in each box indicates the median, central diamond indicates the mean, and the bottom and top edges of the box indicate the 25th and 75th percentiles, respectively. The whiskers are extended to the most extreme data point that is no more than 1.5 times the interquartile range (IQR) from the edge of the box. The black circle sign represents outliers that lie beyond the whiskers. 38

Figure 3-1: Layout of the NEON Kona experimental field. Blue circles show the location of the soil moisture and soil temperature sensors. Insets: (a) instrument setup, (b) Flux tower. 46
Figure 3-2: Workflow for developing and optimizing an artificial neural network (ANN) for filling gaps in N_2O flux data 52
Figure 3-3: Daily values of air temperature and precipitation. 57
Figure 3-4: Comparisons between fluxes obtained using two different EC systems: closed-path and open-path systems. Data on the graphs are half-hourly fluxes. Redline is the 1:1 line. 59
Figure 3-5: Frequency distribution of the consecutive missing data points. 60
Figure 3-6: Architecture of the Artificial Neural Network (ANN) for N_2O Flux Prediction. 60
Figure 3-7: Training status of the artificial neural network (ANN) model using the MSE. MSE for the training data set shows in the blue line, green lines show the MSE for the validation data set and the red shows the MSE for the test data set. The MSE for the validation data decreases from beginning up to 32nd epoch and minimum MSE achieved at the 32nd epoch. 61
Figure 3-8: Correlation between the actual values and the ANN predicted values, orange line shows the hypothetical prefect correlation, and the green line shows the best fitted line to show the relationship between the actual values and the predicted values..... 62
Figure 3-9: Relationship between missing data points and coefficient of determination (R^2), biased error (BE) and root mean square error (RMSE) for the relationship between measured N_2O fluxes and estimated fluxes using linear interpolation and artificial neural networks. 64
Figure 3-10: Segment of the gap filled N_2O time series that include original data and different data gap sizes. The error bar shows the standard error. 65
Figure 4-1: Layout of the experimental site the Rannells' Flint Hills Prairie Preserve. Insets: (a) flux tower, (b) gas manifold enclosure and point sources used to release CH_4 at a known rate, and (c) gas manifold and manifold control system. 80
Figure 4-2: Coverage of the source area by (a) 80% footprint fetch and (b) 90% footprint fetch at 9.00 p.m. December 01st 2022. Red point represents the position of the flux tower and green box represents the artificial source area. 86

Figure 4-3: Time series of 30-min values of (a) wind speed and direction, (b) relative contribution of the source area provided by the footprint model, and (c) estimated CH_4 flux during controlled CH_4 release event on December 01 2022. 88
Figure 4-4:Time series of 30 min of (a) wind speed and direction, (b) relative contribution of the source area, and (c) estimated CH_4 flux during controlled CH_4 release event on February 03, 2023..... 89

List of Tables

Table 2-1: Contingency table 34

Acknowledgments

I extend my deepest gratitude to my advisor, Dr. Eduardo Alvarez Santos, for his unwavering support, invaluable guidance, and mentorship throughout my Ph.D. journey. His expertise and insights have been crucial in shaping both my research and professional growth.

I am also immensely thankful to my Ph.D. committee members for their invaluable contributions to my research. Dr. Brian Washburn, Dr. Jean Stiner, and Dr. Stephen Welch provided rigorous feedback and essential advice that greatly enhanced the quality of my work.

I am deeply grateful to the National Science Foundation for their financial support, which was vital to the completion of my research. This funding not only facilitated my work but also enriched my development as a scientist.

A special thank you goes to my family, whose endless love and encouragement kept me motivated and grounded. Their belief in my abilities has been a constant source of strength.

Finally, I wish to acknowledge my friends and colleagues, whose companionship and support have brought solace and joy throughout this challenging and rewarding journey.

Chapter 1 - General introduction

Agriculture plays a pivotal role in the global greenhouse gas (GHG) budget, accounting for a substantial portion of anthropogenic methane (CH_4) and nitrous oxide (N_2O) emissions. In the United States, methane is largely produced through enteric fermentation in ruminants and manure management, while nitrous oxide is predominantly emitted from agricultural soils as a byproduct of microbial processes such as nitrification and denitrification. These processes are often driven by nitrogen inputs from synthetic fertilizers and organic waste such as livestock excreta. Both gases have much higher global warming potentials (GWPs) than carbon dioxide (CO_2), with CH_4 being approximately 28 times and N_2O about 300 times more potent over a 100-year period (IPCC 2014). Due to their high potency and long atmospheric lifetimes, CH_4 and N_2O are key drivers of climate change. Accurate measurement and effective mitigation of these emissions are therefore essential, especially in regions like Kansas, where agriculture plays a dominant role in the economy and landscape.

The contribution of agriculture to GHG emissions is multifaceted. In livestock systems, ruminant digestion processes produce CH_4 as a natural byproduct of microbial activity in the animal's stomach (enteric fermentation), which is then exhaled or eructed. In addition, livestock manure stored in anaerobic conditions (e.g., lagoons, pits) generates methane through the breakdown of organic material. Similarly, in crop production systems, nitrogen fertilization significantly enhances soil microbial activity, leading to increased emissions of N_2O through nitrification and denitrification (Smith et al. 2014, De Klein and Harvey 2012). The intensification of agricultural practices in recent decades such as increased nitrogen fertilizer use and the expansion of large-scale livestock operations has amplified these emissions globally (Davidson 2009).

Accurately measuring agricultural emissions is challenging due to the inherent spatial and temporal variability of these sources. Emissions of N_2O are highly episodic, with fluxes spiking after rainfall or fertilizer application and varying significantly with seasonal dynamics and temperature fluctuations. (Butterbach-Bahl et al. 2013). Static chamber techniques, one of the most commonly used methods for measuring trace gas emissions from soils, have provided valuable insights into the biogeochemical processes driving N_2O and CH_4 emissions (Davidson et al. 2000).

Chambers offer precision and are relatively simple to use, allowing for direct measurements of gas fluxes over small areas. However, this method is constrained by its limited spatial and temporal resolution. Chambers capture emissions over small, localized areas and can only measure fluxes at discrete points in time, often missing key emission "events" that occur outside of measurement intervals (Rochette and Eriksen-Hamel 2008). As a result, they often underestimate total fluxes, especially in systems where emissions are highly variable or episodic.

To overcome the limitations of static chambers, micrometeorological techniques such as the eddy covariance (EC) method have become more widely adopted. The EC technique is a high-frequency method that measures gas exchange between the land surface and atmosphere, capturing fluxes over larger areas and across varied landscapes in real-time. This method calculates fluxes based on the covariance between fluctuations in vertical wind speed and gas concentrations, making it ideal for studying GHG emissions in complex agricultural environments (Baldocchi 2003). One of the main strengths of the EC technique is its ability to continuously monitor gas fluxes, allowing researchers to capture "hot spots" (areas with significantly higher fluxes than surrounding areas) and "hot moments" (periods of intense flux activity) (Groffman et al. 2009).

1.1 The eddy covariance technique

The eddy covariance (EC) technique is a sophisticated and widely used micrometeorological method for directly measuring turbulent fluxes of gases, energy, and momentum between the earth's surface and the atmosphere. It provides critical insights into ecosystem-atmosphere exchanges, especially for greenhouse gases (GHGs) such as carbon dioxide (CO_2), methane (CH_4), and nitrous oxide (N_2O). The technique operates on the principle of atmospheric turbulence, which refers to the chaotic and irregular motions of air that dominate the transport of heat, moisture, and gases in the lower atmosphere (Stull 1988). These turbulent motions, or "eddies," transport gases vertically, making them the primary drivers of gas exchange.

At the core of the EC technique is Reynolds decomposition, a mathematical framework that separates instantaneous measurements into their mean and fluctuating components. This allows the calculation of fluxes based on the covariance between fluctuations in vertical wind speed.

$$w' = w - \overline{w} \quad (1)$$

$$c' = c - \overline{c} \quad (2)$$

Where:

w is the vertical wind speed, c the gas concentration (e.g., CH_4, N_2O, CO_2), $\overline{w}$ and $\overline{c}$ are the time-averaged vertical wind speed and gas concentration, w' and c' are the fluctuations in vertical wind speed and gas concentration, respectively.

The eddy covariance flux (F) is then calculated as the mean covariance between the fluctuations in vertical wind speed w' and the fluctuations in gas concentration c' over a specified time period (typically 30 minutes). This is represented as:

$$F = \overline{w'c'} \quad (3)$$

This equation essentially describes how much of the gas (e.g., CH_4 or N_2O) is being transported vertically by turbulent eddies. Positive flux values indicate upward transport from the surface to the atmosphere, while negative values indicate downward transport or deposition from the atmosphere to the surface (Aubinet et al. 2012). This method is powerful because it directly measures the turbulent fluxes responsible for gas exchange, without the need for models or assumptions about diffusion rates, making it one of the most direct and reliable methods for measuring ecosystem-atmosphere gas exchanges (Baldocchi 2003).

An EC system typically consists of:

1. **Sonic Anemometer**: Measures the three-dimensional components of wind speed (*u, v, w*) at high frequencies (10–20 Hz) using ultrasonic pulses.
2. **Gas Analyzer**: Detects real-time concentrations of target gases (e.g., CH_4, N_2O, CO_2, H_2O). Depending on the target gases, the analyzer might employ techniques such as infrared absorption or laser spectroscopy.
3. **Data Acquisition System**: Records high-frequency data from the instruments for subsequent processing.

These instruments are mounted on towers or masts at a height sufficient to represent the area under study, referred to as the **flux footprint**. This footprint encompasses the spatial area contributing to the flux measurements, which varies based on factors such as wind speed, surface roughness, and measurement height. Proper placement and calibration of the system are critical for obtaining representative data. Figure 1-1 illustrates a typical EC setup, showing the placement of the sonic anemometer, gas analyzer, and data acquisition systems.

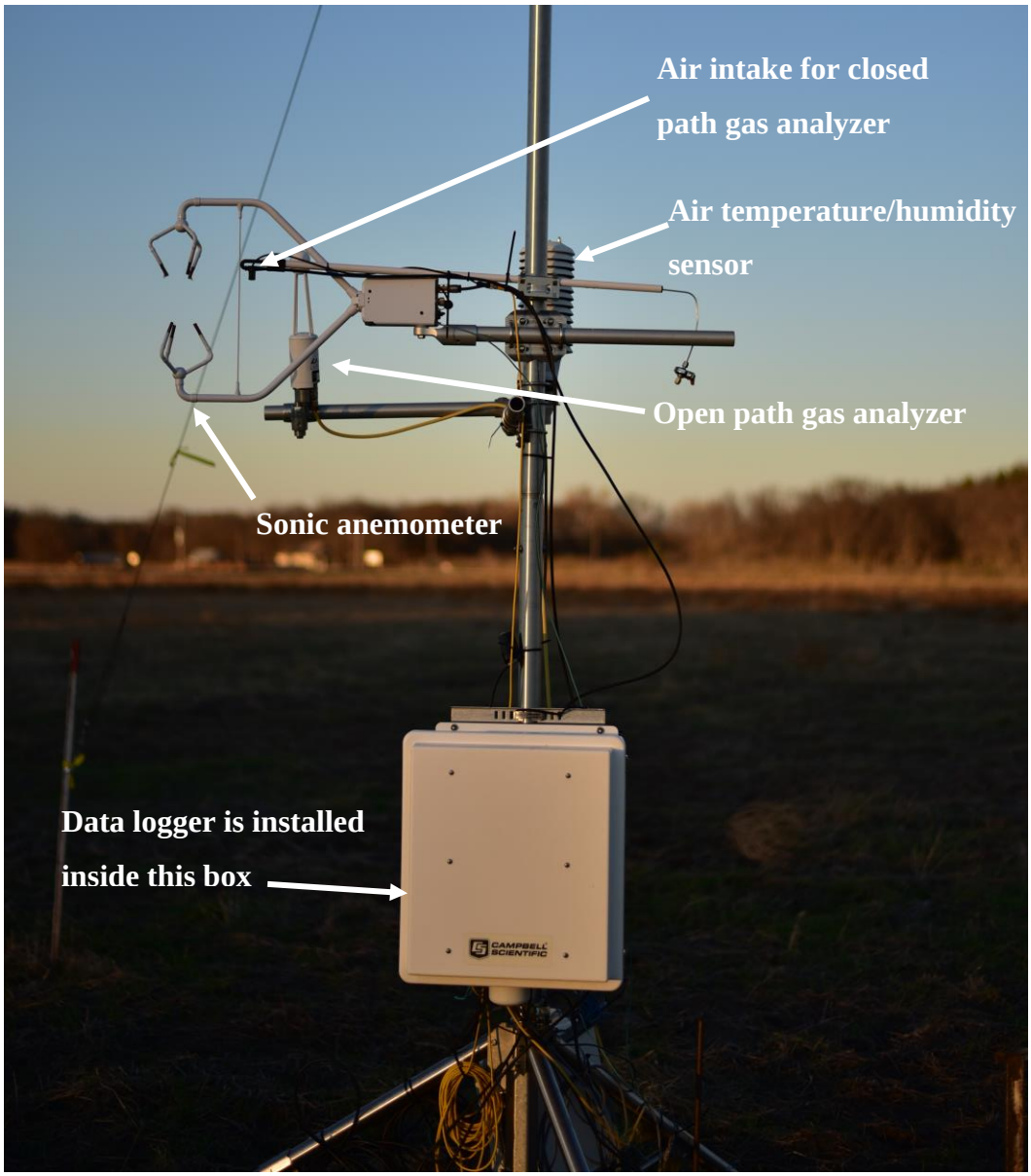

Figure 1-1: Main component and their placement of an eddy covariance system.

1.1.1 Advantages of eddy covariance

One of the greatest strengths of the EC technique is its ability to provide **continuous, high-frequency measurements** of gas fluxes in real time. Unlike static chambers, which only capture localized emissions at discrete time points, the EC method measures fluxes over larger spatial areas and extended periods. This capability makes it particularly effective for identifying "hot spots" (areas with disproportionately high emissions) and "hot moments" (times of intense flux activity).

The method is especially valuable for studying the temporal dynamics of GHG emissions, capturing variability on daily, seasonal, and interannual scales. For instance, it can reveal how emissions respond to environmental drivers like temperature, precipitation, and management practices. Additionally, it avoids reliance on assumptions about diffusion rates, making it one of the most direct and reliable methods for measuring ecosystem-atmosphere gas exchanges (Baldocchi 2003).

1.1.2 Challenges and data processing

Despite its strengths, the EC technique is not without challenges. It requires careful handling of **high-frequency data**, which must undergo extensive processing to ensure accuracy. Corrections are applied for:

- **Air Density Fluctuations**: The Webb-Pearman-Leuning (WPL) correction adjusts for the effects of air density changes on gas concentrations (Webb et al. 1980).
- **Spectral Attenuation**: Corrects for the loss of high-frequency signals due to sensor limitations (Moncrieff et al. 1997).
- **Time Lag Adjustments**: Accounts for the delay between measurements by the anemometer and gas analyzer (Aubinet et al. 2012).

Additionally, the EC method can struggle under low-turbulence conditions, leading to data gaps. These gaps, often caused by equipment malfunctions or extreme weather, can undermine the accuracy of long-term flux estimates. Advanced gap-filling techniques, such as artificial neural networks (ANNs), are increasingly employed to address this limitation.

1.1.3 Applications in agricultural systems

The eddy covariance method has revolutionized our understanding of GHG fluxes in agricultural systems, particularly in terms of capturing the temporal dynamics of emissions and their response to environmental and management variables. By providing continuous measurements, the EC method offers insights into the daily, seasonal, and interannual variability of emissions, which is crucial for creating accurate GHG budgets (Baldocchi, Dennis and Falge, Eva and Gu, Lianhong and Olson, Richard and Hollinger, David and Running, Steve and Anthoni, Peter and Bernhofer, Ch and Davis, Kenneth and Evans 2001). Additionally, the method covers a much larger spatial footprint than static chambers, making it possible to account for variability across landscapes, including areas with diverse management practices or varying environmental conditions.

However, the eddy covariance technique is not without its challenges. One of the key limitations of the EC technique is the difficulty in applying it to heterogeneous environments, such as grazing systems. In these systems, emissions are influenced by animal movement, terrain complexity, and changing wind direction, which can complicate the calculation of accurate fluxes (Laubach et al. 2013). Another significant issue is the occurrence of data gaps in EC measurements. These gaps are often caused by equipment malfunctions, extreme weather conditions, or low-turbulence periods when the EC method struggles to capture meaningful flux data (Papale et al. 2006). Unaddressed, such gaps can undermine the accuracy of long-term flux estimates and create uncertainties in emission inventories.

To mitigate the impact of data gaps, advanced data modeling techniques such as artificial neural networks (ANNs) have been increasingly employed. ANNs are computational models inspired by the neural networks of the human brain and are capable of recognizing complex, non-linear relationships in data (Taki et al. 2019). In the context of GHG flux measurements, ANNs have shown promise in accurately predicting missing flux data by learning from existing environmental data (Bigaignon et al. 2020). This approach allows for more complete datasets and reduces the uncertainty associated with data gaps, improving the robustness of GHG flux estimates over time.

This research is divided into three interconnected studies, each addressing key challenges in the measurement and modeling of GHG emissions from livestock and crop production systems.

1.2 Outline and objectives

This thesis addresses the challenges associated with measuring and modeling greenhouse gas (GHG) emissions in agricultural systems through three interconnected studies, each targeting key methodological and analytical gaps. Together, these studies aim to improve the accuracy of GHG inventories and provide actionable insights for sustainable agricultural management.

Study 1: Investigating N_2O Emissions in Diverse Agricultural Systems

This study examines nitrous oxide (N_2O) emissions in two contrasting environments: a cattle feedlot and a winter wheat field. The eddy covariance (EC) technique is employed to capture temporal and spatial variability in emissions, with footprint analysis used to identify dominant contributing areas.

Outcome:

This research highlights the spatial and temporal variability of N_2O emissions, uncovering key emission drivers under different environmental conditions and management practices. These findings provide a detailed understanding of how N_2O fluxes vary across agricultural systems, helping to refine emission reduction strategies.

Study 2: Gap-Filling Techniques for N_2O Flux Data

This study compares the effectiveness of artificial neural networks (ANNs) and linear interpolation methods in filling gaps in 30-minute N_2O flux data. These gaps arise from equipment downtime, low turbulence, or other technical issues that hinder continuous data collection. The study evaluates the suitability and reliability of these methods for long-term datasets.

Outcome:

This work identifies the most effective gap-filling approach, enhancing data continuity and robustness. By providing a systematic comparison, the study ensures a more reliable method for completing datasets, which is critical for accurately estimating long-term emissions.

Study 3: Measuring CH_4 Emissions in Grazing Systems

This study focuses on methane (CH_4) emissions from grazing systems, employing EC measurements and footprint modeling to address the challenges of dynamic environments. Controlled CH_4 release experiments are conducted to validate methods for estimating emissions from individual animals.

Outcome:

The study underscores the complexity of measuring CH_4 emissions in grazing systems and highlights the need for improved footprint models to capture the spatial and temporal variability unique to these systems. The findings advocate for model enhancements to better reflect the dynamic nature of grazing environments.

Collective Contributions

Together, these studies advance the methodologies for measuring and modeling GHG emissions in agriculture, offering critical improvements in the accuracy and reliability of emission estimates. For Kansas, these findings align agricultural productivity with climate change mitigation efforts by informing sustainable management practices and improving GHG inventories. This work bridges the gap between research and practical applications, supporting both local and global initiatives to reduce agricultural emissions.

Chapter 2 - Measurements of nitrous oxide from agriculture systems using the eddy covariance technique

2.1 Abstract

Nitrous oxide (N_2O) is a potent greenhouse gas and a major contributor to both climate change and stratospheric ozone depletion. Emissions from agriculture, particularly from manure management and nitrogen fertilization, represent a significant portion of global N_2O emissions. This study investigates N_2O emissions from two distinct agricultural systems a beef cattle feedlot and a winter wheat field using the eddy covariance (EC) technique.

N_2O emissions were monitored from November 2019 to January 2020 in a small beef cattle feedlot and from November 2020 to May 2021 in a winter wheat field. The feedlot study demonstrated that average N_2O fluxes were low (0.0062 μ mol m^{-2} s^{-1}), with occasional spikes in emissions, likely driven by sporadic thawing events and manure decomposition. The footprint analysis revealed that a substantial portion of emissions originated from areas outside the cattle feedlot, suggesting that indirect emissions from manure runoff contributed significantly to the overall N_2O budget. In the winter wheat field, average N_2O flux was 0.01 μ mol m^{-2} s^{-1}, with emission spikes closely tied to fertilization and rainfall events. These spikes were attributed to increased microbial activity triggered by warm, moist soil conditions that enhanced nitrification and denitrification processes. Both sites exhibited significant temporal and spatial variability in N_2O emissions, underscoring the importance of continuous high-frequency measurements for accurate GHG inventory reporting. The results demonstrate that environmental factors such as soil temperature, moisture, and management practices play critical roles in driving N_2O emissions. The study also highlights the challenges of missing data due to equipment malfunctions and adverse weather conditions, emphasizing the need for reliable gap-filling techniques to accurately quantify cumulative N_2O emissions.

2.2 Introduction

N_2O is a powerful greenhouse gas (GHG) and an important contributor to climate change. It has a global warming potential approximately 300 times greater than carbon dioxide (CO_2) over a 100-year time frame (IPCC 2014). Although N_2O constitutes only a small fraction of the total atmospheric GHG concentration, its potent warming effect and long atmospheric lifetime up to 114 years results in a larger radiative forcing/concentration than carbon dioxide and methane. Moreover, N_2O is the single most significant ozone-depleting substance emitted today, highlighting its dual threat to both climate and stratospheric ozone (Ravishankara et al. 2009).
The increase of N_2O concentration in the atmosphere is largely driven by human activities, particularly agricultural practices. Since the pre-industrial era, atmospheric concentrations of N_2O have risen by approximately 20%, largely due to increased nitrogen fertilizer use, livestock production, and other agricultural intensification processes (Davidson 2009). Agriculture accounts for more than 50% of total anthropogenic N_2O emissions, with estimates ranging from 1.7 to 4.8 Tg N_2O-N annually, out of a global total range of 2.8 to 8.9 Tg N_2O-N per year (Ciais et al. 2013). This contribution underscores the central role of agriculture in the global nitrogen cycle and the importance of understanding N_2O dynamics for climate change mitigation efforts.

Nitrous oxide is produced naturally as part of the nitrogen cycle, primarily through microbial processes in soils and water bodies. These processes include nitrification, the aerobic oxidation of ammonium (NH_4^+) to nitrate (NO_3^-), and denitrification, the anaerobic reduction of NO_3^- to gaseous nitrogen (N_2) (Firestone and Davidson 1989). In both processes, N_2O is an intermediate product. While N_2O is produced naturally in terrestrial and aquatic ecosystems, human activities especially those related to agriculture have greatly accelerated its release into the atmosphere (Vitousek et al. 1997). The introduction of synthetic nitrogen fertilizers, expansion of legume cultivation, and intensified livestock production have fundamentally altered the global nitrogen cycle, leading to increased N_2O emissions (Galloway et al. 2008).

The application of synthetic and organic nitrogen fertilizers is one of the largest sources of N_2O emissions from agricultural soils. Nitrogen fertilizer provides the substrate for nitrification and denitrification, the key microbial processes responsible for N_2O production (Davidson, Eric A. Verchot 2000). The application of nitrogen fertilizers, especially in excess of plant needs, can lead

to substantial losses of nitrogen to the atmosphere in the form of N_2O. In addition, fertilization can stimulate soil microbial activity, leading to the rapid conversion of nitrogen into gaseous forms. The type, timing, and rate of fertilizer application, as well as soil conditions, can significantly affect the magnitude of N_2O emissions (Thomson et al. 2012).

Livestock production is another major source of N_2O emissions, primarily through the deposition of animal excreta on pastures. Urine and dung from grazing animals create localized areas of high nitrogen concentration, resulting in "hot spots" of N_2O emissions (De Klein and Harvey 2013). These emissions can be particularly high when grazing occurs on nitrogen-rich pastures or during periods of high soil moisture, which promote denitrification. Additionally, intensive livestock systems, such as confined animal feeding operations (CAFOs), contribute to N_2O emissions through the storage and management of manure. The anaerobic decomposition of organic matter in manure piles or lagoons can result in substantial N_2O production, especially if manure is not properly managed (Chadwick et al. 2011).

Since the advent of the Green Revolution in the mid-20^{th} century, the global use of synthetic nitrogen fertilizers has increased dramatically. This surge in nitrogen inputs, along with the intensification of livestock production, has led to a corresponding rise in N_2O emissions (Galloway et al. 2008). The global agricultural system has become the dominant source of reactive nitrogen in the environment, surpassing natural biological nitrogen fixation (Fowler et al. 2013). This has far-reaching consequences, not only for global climate change but also for ecosystems and human health.

In addition to its role as a potent GHG, N_2O emissions contribute to the depletion of stratospheric ozone, a protective layer that shields the Earth from harmful ultraviolet radiation (Ravishankara et al. 2009). The impact of N_2O on the ozone layer has become more pronounced in recent decades, as other ozone-depleting substances, such as chlorofluorocarbons (CFCs), have been phased out under international agreements like the Montreal Protocol. As a result, reducing N_2O emissions has become a key objective for both climate change mitigation and ozone layer protection.

Accurately measuring N_2O emissions is crucial for improving national greenhouse gas inventories, developing mitigation strategies, and advancing our understanding of the biogeochemical processes that drive these emissions. However, the spatial and temporal variability of N_2O fluxes poses significant challenges for measurement (Flechard et al. 2007). Emissions can vary greatly depending on soil type, climate, management practices, and the timing of nitrogen inputs, making it difficult to obtain representative measurements.

The static chamber method is the most widely used technique for measuring N_2O fluxes from agricultural soils. Chambers are placed over a small area of soil, and gas samples are collected periodically to determine the concentration of N_2O. This method is relatively simple and cost-effective, making it ideal for small-scale experiments and comparative studies of different treatments (Davidson et al. 2000). Chambers can also be used to measure fluxes under controlled conditions, such as after fertilizer application or irrigation.

Despite its widespread use, the static chamber method has several limitations. One of the main challenges is the difficulty of capturing the temporal variability of N_2O emissions, which are often episodic and influenced by specific events like rainfall or fertilizer application (Groffman et al. 2009). Chambers provide only a snapshot of emissions at a given moment, and their small surface area (typically less than 1 m^2) makes it difficult to capture spatial variability (Rochette and Eriksen-Hamel 2008). Moreover, the enclosed environment within the chamber can alter soil conditions, such as temperature and gas exchange, potentially leading to biased estimates of N_2O fluxes (De Klein and Harvey 2012).

To overcome the limitations of chamber methods, micrometeorological techniques have been developed to measure N_2O emissions continuously and over larger areas. These methods rely on measuring gas concentration gradients and wind velocity data to estimate fluxes between land surface and atmosphere. The most commonly used micrometeorological methods for N_2O measurement include the flux gradient method, relaxed eddy accumulation, and eddy covariance (Baldocchi 2003).

The flux gradient method, based on Fick's law of diffusion, measures the vertical gradient of gas concentrations and assumes that the flux is proportional to this gradient (Rochette and Eriksen-Hamel 2008). While the flux gradient method provides continuous measurements, it requires accurate estimates of atmospheric stability and turbulence, which can be difficult to obtain in highly variable agricultural environments (Jayasundara et al. 2007). Relaxed eddy accumulation, on the other hand, is a direct micrometeorological method that measures trace gases in updrafts and downdrafts of air (Desjardins et al. 2010). Although it can be used for a wide range of gases, including N_2O, its application is limited by the need for specialized equipment and complex data processing.

The eddy covariance (EC) technique has emerged as a robust and efficient method for measuring GHG fluxes, including N_2O, CO_2, CH_4, and water vapor (H_2O), from agricultural ecosystems. EC measures the covariance between vertical wind speed and gas concentration fluctuations to calculate the net flux of gases between the land surface and the atmosphere. This technique has several advantages over other methods, as it provides continuous, high-frequency data over extended periods and covers a larger spatial area (Baldocchi 2003).

Until recently, the use of the EC technique for measuring N_2O was limited by the challenges of detecting N_2O concentrations at the high temporal resolution required for accurate flux calculations (Cowan et al. 2014a). Early EC systems for N_2O required frequent calibration, pre-drying of air samples, and complex cryogenic systems for cooling the laser spectrometers, making them difficult to deploy in the field (Kroon et al. 2007). However, advancements in laser spectroscopy, particularly the development of tunable diode lasers (TDLAS) and quantum cascade lasers (QCL), have made it possible to measure N_2O fluxes more accurately and with lower maintenance requirements (Cowan et al. 2014b, Cowan et al. 2015).

These new technologies, such as the continuous-wave quantum cascade laser (CW-QCL) and mid-infrared (mid-IR) lasers, have significantly advanced the capabilities of eddy covariance (EC) systems. CW-QCLs, known for their high sensitivity and selectivity, have reduced power consumption and operational complexity, enabling longer-term field deployments and greater spatial coverage (Huang et al. 2014). Mid-IR lasers further enhance EC systems by leveraging

their ability to detect trace gases like methane (CH_4), nitrous oxide (N_2O), and ammonia (NH_3) with high precision due to strong absorption features in the mid-infrared region. These innovations have expanded the applicability of EC systems in studying GHG fluxes across diverse environments, offering more reliable and accurate measurements critical for advancing our understanding of ecosystem-atmosphere gas exchanges (Shen et al. 2024).

The EC technique has been applied successfully in various agricultural environments to measure GHG fluxes. In croplands, for example, Merbold et al. (2014) used EC to measure N_2O emissions in a commercial cornfield, capturing the dynamic response of N_2O fluxes to fertilization and precipitation events. Similarly, Huang et al. (2014) demonstrated the utility of EC for measuring N_2O emissions from managed grasslands, showing the technique's ability to capture both spatial and temporal variability in N_2O fluxes. These studies have highlighted the potential of EC to provide continuous, integrated measurements of N_2O emissions over large areas, improving our understanding of the factors driving N_2O fluxes in agricultural systems.

In livestock systems, the EC technique has been used to measure GHG fluxes in beef cattle feedlots, providing valuable data on the contributions of different surfaces, such as pens, alleys, and manure storage areas (Baum et al. 2008). Footprint analysis is often used in these systems to determine the area of influence for EC measurements, ensuring that the fluxes measured by the EC system represent the entire source area (Sun et al. 2015).

While the EC technique offers significant advantages for measuring N_2O emissions, several challenges remain. One of the key challenges is the requirement for a homogeneous source area, as the technique assumes that the fluxes measured at a single point are representative of the entire landscape (Baldocchi 2003). In heterogeneous agricultural systems, such as grazed pastures or fields with varying soil properties, this assumption may not hold, leading to potential errors in flux estimates.

Another challenge is the high cost of EC equipment and the need for specialized expertise to set up and maintain the system. EC systems require precise calibration, data processing, and corrections for various factors, such as air density and spectral losses, to ensure accurate flux

measurements (Aubinet et al. 2000). Additionally, the power requirements for running EC systems, especially in remote or off-grid locations, can be prohibitive, though recent advancements in low-power analyzers have begun to address this issue (Cowan, N. J. and Norman, P. and Famulari, D. and Levy, P. E. and Reay, D. S. and Skiba 2015).

Despite these challenges, the EC technique remains a valuable tool for measuring N_2O emissions, particularly in agricultural systems where spatial and temporal variability is high. By providing continuous, high-frequency data, EC can capture the "hot moments" and "hot spots" of N_2O emissions, offering a more complete picture of the processes driving GHG fluxes in agricultural ecosystems.

This study aims to address the limitations of traditional measurement techniques by utilizing the eddy covariance technique to measure N_2O emissions in two contrasting agricultural environments: a beef cattle feedlot and a winter wheat field. The primary objectives of this research are to:

1. Evaluate the performance of a closed-path eddy covariance system for quantifying N_2O emissions in both a livestock-based system and a crop-based system.
2. Assess the temporal variability of N_2O fluxes in response to environmental conditions such as soil moisture, temperature, and nitrogen inputs.
3. Investigate the spatial variability of N_2O emissions within each system and determine the extent to which the EC system can capture emission "hot spots" and "hot moments."

By providing continuous, high-frequency measurements of N_2O emissions, this research will contribute to a better understanding of the drivers of N_2O fluxes in agricultural systems and improve the accuracy of GHG inventories. Additionally, the insights gained from this study will inform the development of more effective mitigation strategies for reducing N_2O emissions from both livestock operations and crop production systems.

2.3 Material and methods

2.3.1 Site description and instrument setup

Site 01

The feedlot study was carried out at the Kansas State University Beef Stocker Research Unit located near Manhattan, Kansas. The study site was characterized by a nearly flat topography, and the feedlot housed 288 cows in pens measuring 70 meters in length (north to south) and 60 meters in width (east to west). The measurement period spanned from late November 2019 to early January 2020, capturing gaseous emissions both from enteric fermentation of the cattle and from manure management. A flux tower was situated at the northeast corner of the study area. During the fall to winter months, the prevailing winds in the Manhattan area are typically from the north and south. The site is bordered by open, ungrazed pasture on all sides, ensuring stable background concentrations that are close to typical atmospheric levels.

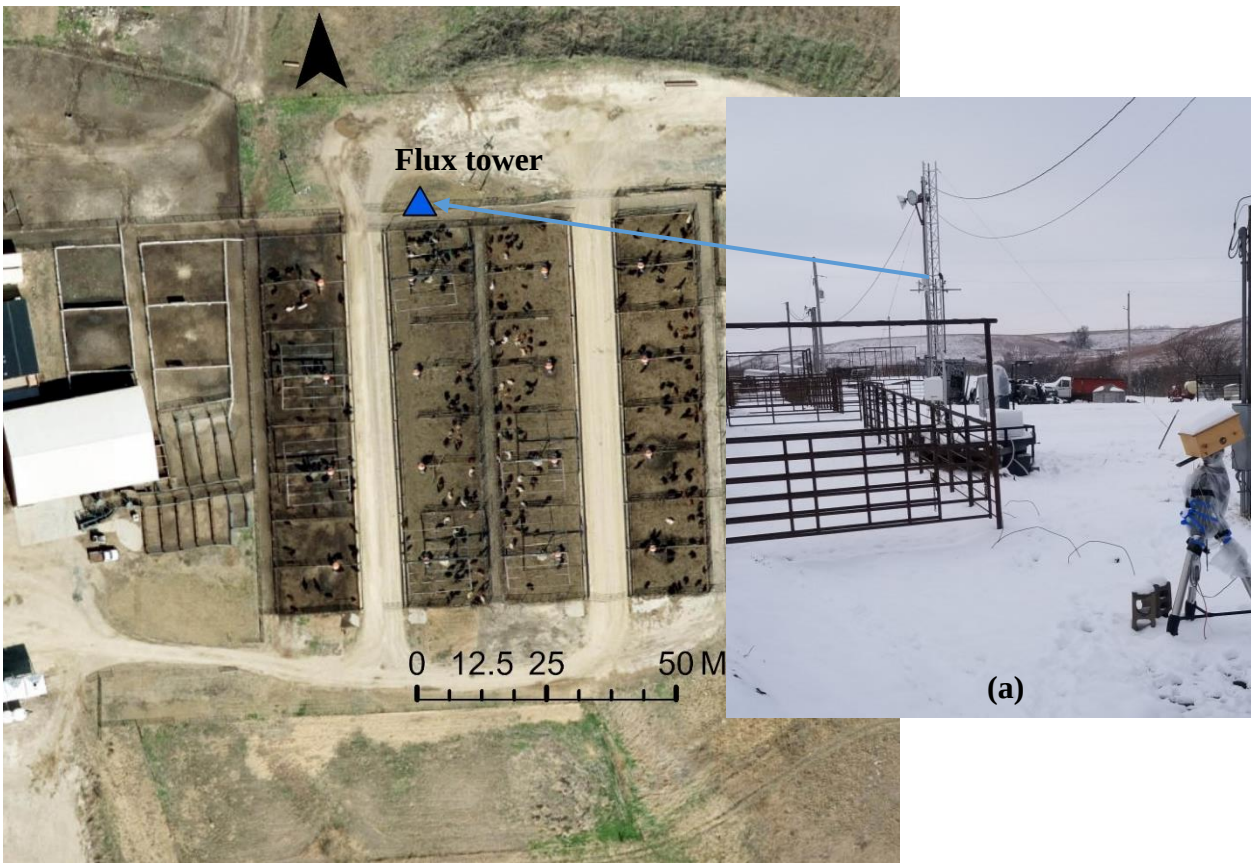

Figure 2-1: Layout of the experimental site the beef cattle stocker unit in Manhattan, KS. Insets: (a) flux tower.

Site 02

The winter wheat study was carried out at the NEON Kona experimental field (N 39.110, W 96.612) in Manhattan, Kansas, from November 2020 to May 2021. The field covers a total area of 16.1 hectares and has a nearly flat topography with a slope of less than 5%. Winter wheat was planted on October 8th, 2020, at a seeding rate of 166.6 kg seeds/ha. The first nitrogen fertilizer application was on September 16th, 2020, at a rate of 44.8 kg of nitrogen per hectare, using a mix of UAN (28-0-0) and ATS (12-0-0-26) sprayed onto the soil surface. The second application took place on March 7th, 2021, with 47 kg of nitrogen per hectare as UAN (28-0-0) sprayed onto both the soil and plant surfaces.

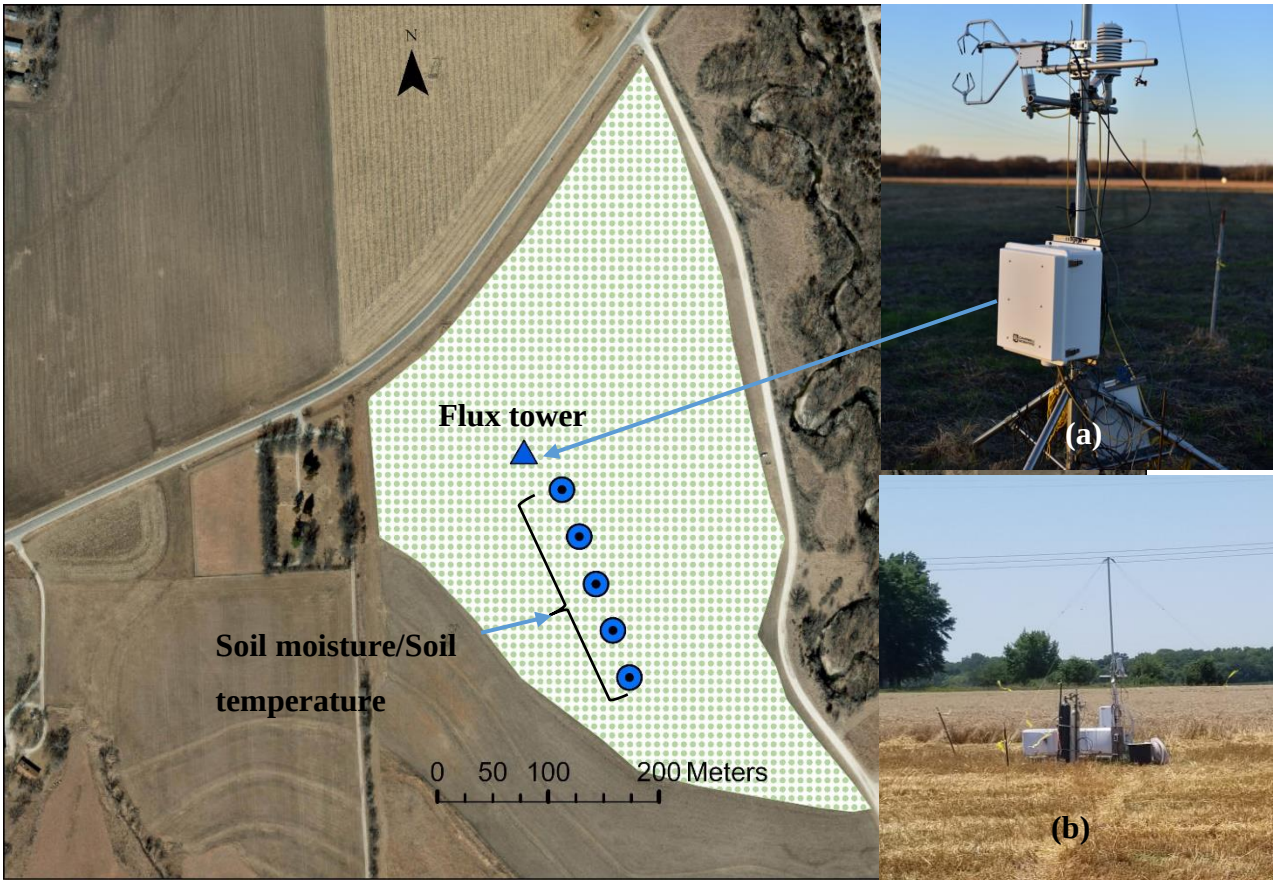

Figure 2-2: Layout of the experimental site, NEON Kona experimental field. Blue circles show the location of the soil moisture and soil temperature sensors. Insets: (a) instrument setup, (b) Flux tower.

2.3.2 Flux measurements

Fluxes of N_2O, CO_2, and latent heat were measured using the eddy covariance (EC) technique. The three orthogonal components of wind velocity and temperature were recorded with a sonic anemometer (CSAT3B, Campbell Sci., Logan, UT). Mixing ratios of CO_2 and N_2O were determined using a closed-path tunable-diode laser absorption spectroscopy (TDLAS) gas analyzer (TGA 200A, Campbell Sci., Logan, UT). At Site 02 only, an open-path gas analyzer (LI-7500, LI-COR, Lincoln, NE) was additionally deployed to measure CO_2 and water vapor (H_2O) concentrations. This allowed for direct comparison of CO_2 fluxes and enhanced data screening at site 02. The closed-path analyzer's air intake, the open-path gas analyzer (at Site 02), and the sonic anemometer were mounted on a tower (site 01: 3.5 m, site 02: 2.25 m) above the ground. Air temperature and relative humidity were measured using a standard air temperature and moisture probe (HMP 50, Campbell Sci.). Air samples were drawn to the gas analyzer through a 7.6-meter high-density polyurethane tube connected to the air intake, which included a vortex flow mechanism, an insect screen, and a high-flow filter equipped with a 10 μm filter membrane to ensure particulate removal. Air was drawn through the sampling tube by a vacuum pump (Edwards nXDS15i, Edwards Ltd, UK) at a rate of 5 liters per minute. The signals from the sonic anemometer, the closed-path gas analyzer, and the open-path gas analyzer were recorded at 10 Hz using a data logger (CR3000, Campbell Sci.).

The 30-minute average gas fluxes were calculated by analyzing the raw data using the eddy covariance software package EddyPro (v. 7.6, Licor). The data processing steps adhered to the standard protocol described by Nemitz et al. (2018), including spike removal (Vickers and Mahrt 1997), double coordinate rotation, time lag compensation (Fan et al. 1990), and spectral corrections (Horst 1997). Flux quality was controlled using flag values as suggested by (Foken et al. 2004). Additionally, CO_2 flux values calculated using the open-path gas analyzer data were used to filter out the closed-path data, only N_2O fluxes corresponding to congruent CO_2 fluxes from both analyzers were accepted. A similar approach was used by Prajapati and Santos (2017), to filter out the methane fluxes in their study. A detailed comparison of open-path and closed-path flux measurements is presented in the results section of Chapter 3

2.3.3 Time lag compensation

Time lags between the sonic anemometer and gas analyzer signals arise from several factors, such as the physical separation between wind and gas measurement devices, and differences in the processing and digitization of electronic signals (Aubinet et al. 2012). In closed-path systems, additional delays occur due to the travel time of air parcels through the sampling tube and interactions between gases and the tube walls. These delays cause gas concentrations to be measured later than wind velocity, making accurate time lag determination essential to avoid underestimating fluxes (Moravek et al. 2013).

In these studies, covariance maximization method was used to identify the time lags (Fan et al. 1990). For the closed-path EC system, time lags were identified within a reasonable search window. This step is particularly crucial under low flux conditions, where the measured signals can be noisy, potentially resulting in unrealistic time lag values (Detto et al. 2011). The EddyPro software established a plausibility window during preprocessing, statistically determining the time lags for the closed-path system and their range of variation. Considering the relationship between water vapor time lags and relative humidity, nominal time lags and plausibility windows were determined for different classes of relative humidity.

2.3.4 Air density corrections

Fluctuations in temperature and water vapor in the air can lead to variations in trace gas concentrations that are unrelated to the turbulent transport of the trace gas of interest, necessitating appropriate density corrections for accurate flux computations. For open-path analyzers, fluxes of CO_2 (*Fc*) and H_2O (*Fv*) are corrected using the method proposed by Webb et al. (1980), expressed as:

$$\overline{Fc} = \overline{w'\rho_c'} + \mu_m \left(\frac{\overline{\rho_c}}{\overline{\rho_d}}\right) \overline{w'\rho_v'} + (1 + \mu_m \sigma) \left(\frac{\overline{\rho_c}}{\overline{\theta}}\right) \overline{w'\theta'} \quad \textbf{4}$$

$$F_v = (1 + \mu_m \sigma) \left[\overline{w'\rho_v'} + \left(\frac{\overline{\rho_v}}{\overline{\theta}}\right) \overline{w'\theta'}\right] \quad \textbf{5}$$

where w represents the vertical wind velocity, ρ denotes molar density, and the subscripts $\boldsymbol{c}$, d, and v refer to CO_2, dry air, and water vapor, respectively. Here, $\mu_m = \left(\frac{m_d}{m_v}\right)$ is the molar mass ratio of dry air to water vapor, $\sigma = \frac{\overline{\rho_c}}{\overline{\rho_d}}$ and θ is the potential temperature. Overbars indicate mean values, and prime symbols denote deviations from the mean.

In contrast, TGA 200A closed-path gas analyzer, which dries the sample air via an air dryer, can directly measure the mixing ratios, thereby eliminating the need for density corrections. The air dryers' function by directing humidity in the sample air through the walls of Nafion tubing, where it is carried away by a purge flow. As the sample air travels through the inside of the tubing, the purge air flows in the opposite direction outside the tubing, removing water vapor due to the vapor pressure difference. This process requires a very dry purge flow (−40 °C dew point) with a flow rate at least twice that of the sample flow (Campbellsci). The purge flow is typically provided by a portion of the sample flow split off at the dryer outlet, with pressure reduced to meet the purge requirements efficiently.

One of the significant advantages of closed-path instruments is their ability to minimize the need for density corrections by measuring the number density of the target species at a stable temperature and pressure within the optical cavity. By applying the ideal gas law to derive the total number density in the cavity from P and T, these instruments can report the mole fraction of the target species. This is achieved by dividing its spectroscopically measured number density by the total number density, allowing for direct measurement of the dry air mole fraction without density corrections during post-processing in the absence of H_2O.

2.3.5 Spectral corrections

Spectral corrections are essential in eddy covariance (EC) systems to account for frequency losses that can lead to the underestimation of fluxes. These losses stem from various factors including inadequate sampling frequency, sensor separation, finite sampling duration, and, in closed-path systems, the presence of sampling tubes and filters as well as the residence time in the sampling

cell (Aubinet et al., 2012). This study applied several established methods to address these spectral losses.

Low-frequency losses, which can arise from factors such as inadequate sampling frequency and finite sampling duration, were corrected using the method proposed by Moncrieff et al. (2005). This method involves adjusting the measured flux to account for the attenuation of low-frequency fluctuations by applying the following equation:

$$F_t = \frac{F_m}{1 + \left(\frac{\omega_n}{\omega_c}\right)^2} \quad \textbf{6}$$

where F_t is the corrected flux, F_m is the measured flux, ω_n is the natural frequency, which represents the characteristic frequency of the flux signal, and ω_c is the cut-off frequency of the system, determined by its sampling and averaging characteristics.

High-frequency losses for the open-path analyzer were addressed using the analytical method proposed by Moncrieff et al. (1997). This method compensates for the damping of high-frequency signals, which can occur due to the response time of the sensors and the spatial separation between the sensors and the analyzers. The correction is implemented through a transfer function that adjusts the measured flux to approximate the true flux.

For the closed-path system, the spectral correction procedure proposed by Horst (1997) was applied, which relies on the Kansas co-spectra (Kaimal et al., 1972). This method accounts for spectral attenuation caused by sampling tubes, filters, and the residence time of the air sample within the system. The correction is expressed as:

$$\frac{(w's')_m}{(w's')_t} = \frac{1}{1 + \left(\frac{2\pi n_m \tau_c \bar{u}}{z}\right)^{\alpha}} \quad \textbf{7}$$

where $(w's')_m$ is the measured scalar flux (covariance between vertical wind speed w and scalar concentration s), $(w's')_t$ is the true scalar flux, $\bar{u}$ is the mean horizontal wind speed at

measurement height h, τ_c is the characteristic time constant of the EC system, α is a stability dependent constant (α =7/8 for neutral and unstable stratification, $z/L \leq 0$ and α =1 for stable stratification, $z/L > 0$, and $\boldsymbol{n_m}$ is the dimensionless frequency at which the logarithmic cospectrum peaks. This method ensures that the corrected flux values accurately reflect the true fluxes by compensating for high-frequency losses inherent in the closed-path system.

2.3.6 Statistical analysis:

To evaluate whether there is diurnal variability in N_2O fluxes and spatial variability across measurement locations, a combination of statistical methods was employed. Normality testing and homogeneity of variance assessments were conducted to ensure the data met the assumptions for parametric analyses. For diurnal variability, one-way ANOVA was used to compare mean fluxes across different time intervals, typically grouped into hourly or categorical time blocks. When the data did not satisfy parametric assumptions, the non-parametric Kruskal-Wallis test was applied to examine differences in median flux values among these time intervals. To analyze spatial variability, flux measurements from different wind directions were compared using similar methods, depending on the normality and variance properties of the data. By employing these statistical approaches, the analysis provided insights into temporal patterns of N_2O emissions throughout the day and identified potential spatial heterogeneity in fluxes across sampling locations.

Normality testing

To assess whether the data met the assumption of normality required for parametric analyses, the **Shapiro-Wilk Test** was used in conjunction with **quantile-quantile (Q-Q) plots**. The Shapiro-Wilk Test is particularly effective for small to medium-sized datasets and calculates a test statistic that tests the null hypothesis that the data are normally distributed (Shapiro and Wilk 1965). This test provides a rigorous statistical basis for determining deviations from normality. Additionally, Q-Q plots offered a visual inspection by plotting the quantiles of the data against the theoretical quantiles of a normal distribution. Deviations from the diagonal line in these plots indicate

potential departures from normality (Wilk and Gnanadesikan, 1968). Both methods were used to evaluate whether the residuals of the dataset conformed to the assumption of normality.

The hypotheses tested were as follows:

- **Null Hypothesis (H_0):** The data follow a normal distribution.
- **Alternative Hypothesis (H_1):** The data do not follow a normal distribution.

The interpretation was based on the p-values obtained:

- **$p \leq 0.05$:** Reject the null hypothesis, indicating that the data are not normally distributed.
- **$p > 0.05$:** Fail to reject the null hypothesis, suggesting that the data are consistent with normality.

This combined approach of statistical testing and visualization ensured that any deviations from normality were detected, providing a foundation for subsequent analyses.

Homogeneity of variance testing

Homogeneity of variance, a critical assumption for parametric tests such as ANOVA, was assessed using **Levene's Test** and, where appropriate, **Bartlett's Test**. Levene's Test evaluates the equality of variances by analyzing the absolute deviations of each observation from its group mean, making it robust to non-normal data distributions (Brown and Forsythe, 1974). Bartlett's Test, on the other hand, is sensitive to deviations from normality and was applied when data transformations achieved approximate normality (Bartlett, 1937). These tests were used to construct a comprehensive evaluation of variance homogeneity.

The hypotheses tested were:

- **Null Hypothesis (H_0):** Variances are equal across groups.
- **Alternative Hypothesis (H_1):** Variances are not equal across groups.

The results were interpreted as follows:

- **$p \leq 0.05$:** Reject the null hypothesis, indicating heterogeneity of variances.
- **$p > 0.05$:** Fail to reject the null hypothesis, suggesting homogeneity of variances.

This rigorous evaluation ensured that assumptions underlying subsequent parametric tests were met, enhancing the reliability of the results.

One-Way ANOVA

To analyze differences in group means, **One-Way Analysis of Variance (ANOVA)** was employed. This test partitions the total variance into components attributable to within-group and between-group variability, producing an FFF-statistic to determine whether observed differences are statistically significant (Edwards 2005). One-Way ANOVA was selected for its robustness and suitability for comparing three or more independent groups.

The hypotheses tested were:

- **Null Hypothesis (H_0):** All group means are equal.
- **Alternative Hypothesis (H_1):** At least one group mean is significantly different.

Post hoc pairwise comparisons were conducted using the Tukey-Kramer method, which adjusts for multiple comparisons to control the family-wise error rate (Tukey, 1949). Results were interpreted based on the FFF-statistic and p-values:

- **$p \leq 0.05$:** Reject the null hypothesis, indicating significant differences among group means.
- **$p > 0.05$:** Fail to reject the null hypothesis, suggesting no significant differences among group means.

ANOVA provided a robust framework for identifying significant differences, and the Tukey-Kramer method allowed for precise identification of group-wise disparities.

Kruskal-Wallis test

When data violated the assumptions of normality or homogeneity of variance, the **Kruskal-Wallis Test**, a non-parametric alternative to ANOVA, was used. This test compares the ranks of data across groups to evaluate differences in their central tendencies (Kruskal and Wallis 1952). It is particularly useful for analyzing skewed or heteroscedastic datasets.

The hypotheses tested were:

- **Null Hypothesis (H_0):** All group medians are equal.
- **Alternative Hypothesis (H_1):** At least one group median is significantly different.

Post hoc comparisons were conducted using Dunn's Test, with a Bonferroni correction applied to adjust for multiple comparisons and maintain statistical rigor (Dunn 1964). The tests were performed using [statistical software], The interpretation was based on p-values:

- **$p \leq 0.05$:** Reject the null hypothesis, indicating significant differences among group medians.
- **$p > 0.05$:** Fail to reject the null hypothesis, suggesting no significant differences among group medians.

This test was chosen for its flexibility in handling non-normal data, ensuring reliable and interpretable results even under conditions of assumption violations.

Fisher's exact test

To evaluate the association between fertilization events and the occurrence of high N_2O fluxes, Fisher's Exact Test was employed. This test is particularly suitable for small sample sizes and provides exact p-values without relying on large-sample approximations (Connelly 2016; Fisher 1922). High N_2O flux events were defined as instances where flux measurements exceeded 0.005 μ mol m^{-2} s^{-1}. This threshold was established based on observed flux distributions and aligns with criteria used in similar studies (Ji et al. 2012). A 2×2 contingency table was constructed to categorize the data:

- **Rows**: Time periods relative to fertilization:
  - One month prior to fertilization
  - One month after fertilization
- **Columns**: Occurrence of high N_2O flux events:
  - Presence of high flux events
  - Absence of high flux events

The table was populated with the frequency of high flux events observed in each time period.

The hypotheses tested were:

- **Null Hypothesis (H_0)**: There is no association between fertilization events and the occurrence of high N_2O flux events.
- **Alternative Hypothesis (H_1)**: There is a significant association between fertilization events and the occurrence of high N_2O flux events.

Fisher's Exact Test was applied to determine the exact probability of observing the data under the null hypothesis.

The test was conducted using [statistical software], specifically the [function/package], with a significance level (α) set at 0.05. A two-tailed p-value was calculated to account for any direction of association.

The p-value obtained from Fisher's Exact Test was interpreted as follows:

- **$p \leq 0.05$**: Reject the null hypothesis, indicating a statistically significant association between fertilization events and high N_2O flux occurrences.
- **$p > 0.05$**: Fail to reject the null hypothesis, suggesting no significant association.

Fisher's Exact Test was chosen due to its appropriateness for small sample sizes and its ability to provide exact p-values, ensuring robust and reliable statistical inference.

2.4 Results

2.4.1 N_2O emission from beef cattle

Environmental factors

The cattle emission study was conducted at Kansas State University's beef cattle research unit near Manhattan, Kansas, from late November 2019 to early January 2020. This period allowed for the monitoring of gaseous emissions originating from both the cattle and area-distributed sources, primarily related to manure management. The temperature at the site fluctuated significantly, ranging from −10°C to 20°C, which introduced variability into emission processes. The research site was surrounded by open, ungrazed pasture, which provided a stable baseline for atmospheric background concentrations, consistent with typical ambient conditions. The dominant wind directions during the study were from the north and south.

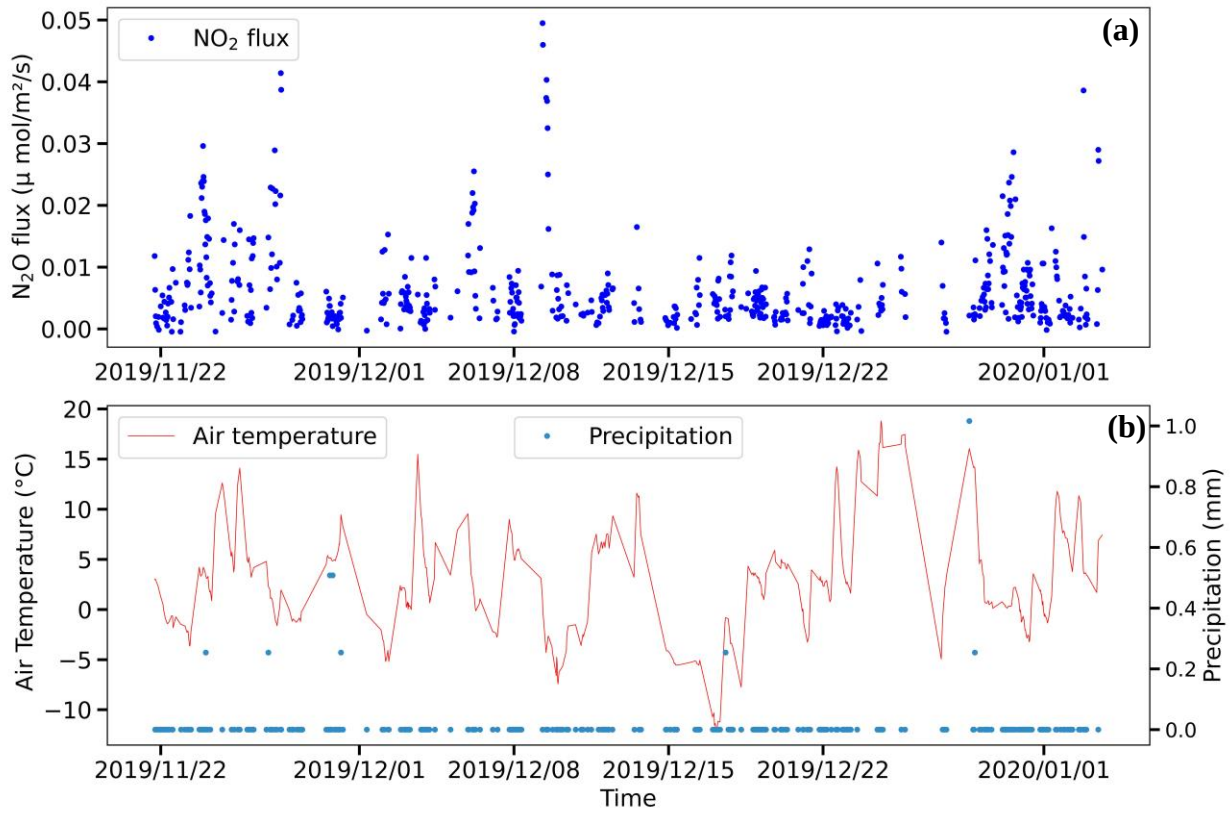

Figure 2-3: 30-min values of intervals (a) N_2O fluxes, and (b) air temperature and precipitation.

The 30-minute averaged flux measurements provided a detailed and high-resolution temporal record of N_2O emissions (Figure 2-3). The recorded N_2O flux values ranged from 0 to 0.05 μ mol m^{-2} s^{-1}, with an overall average flux of 0.0062 μ mol m^{-2} s^{-1}. This average aligns well with previous studies conducted during winter months, such as Aguilar et al., (2014), indicating that emissions during colder periods are typically low. Most of the time, flux values were near zero, reflecting minimal biological activity in the frozen soil. However, several notable N_2O emission events were recorded during the study period. These spikes in flux were not consistently correlated with temperature fluctuations or precipitation events, likely due to the frozen soil conditions, which suppressed typical emission responses that are usually observed in warmer seasons. Multiple snow precipitation events occurred during the study, but they did not lead to a discernible pattern of increased N_2O emissions, contrasting with patterns observed in warmer months when rainfall typically stimulates microbial activity and gas emissions. The lack of a temperature-driven emission pattern further underscores the impact of frozen soil, where biological activity is largely inhibited. This finding highlights the importance of seasonality in influencing emission dynamics and suggests that winter N_2O fluxes may be more influenced by sporadic factors rather than continuous environmental drivers.

Spatial variability of N_2O flux

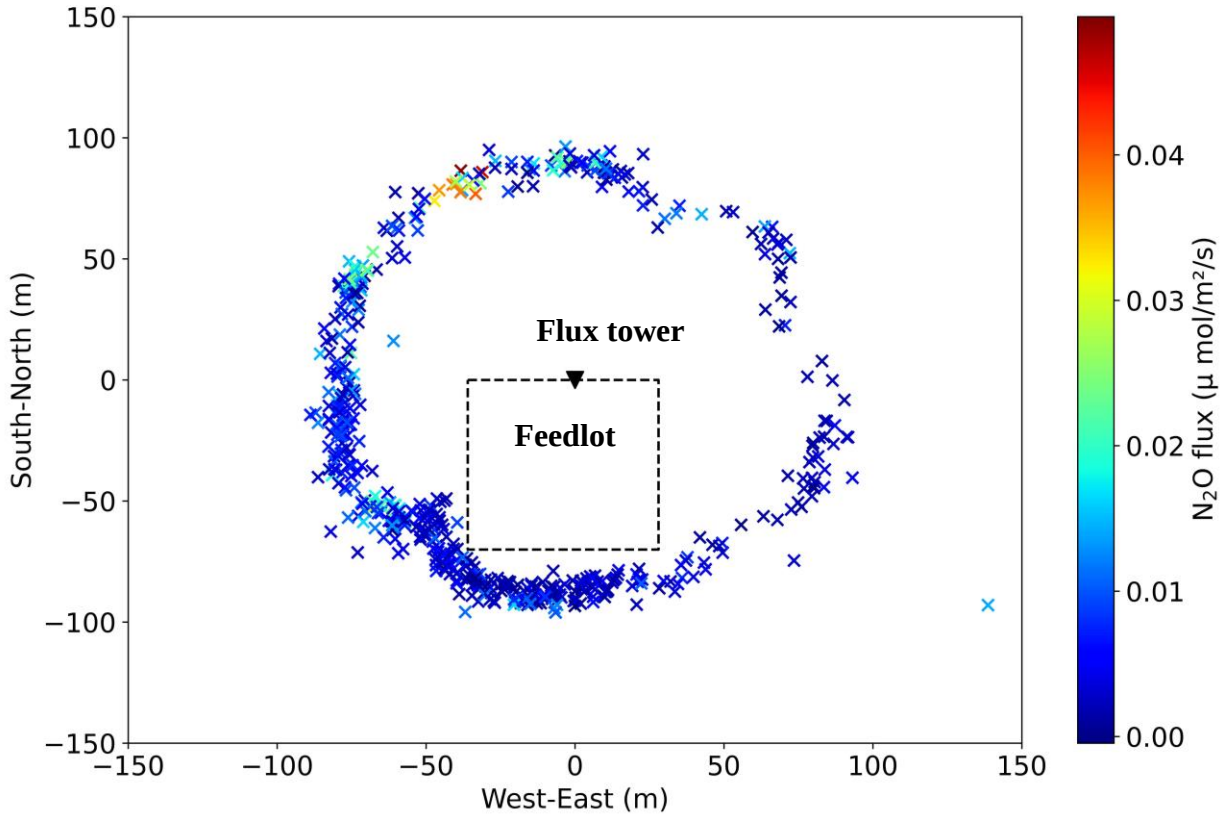

Figure 2-4: Distance from the flux tower to the 'x' mark representing the upwind distance from the tower contributing to 70% of the total flux for 30-minute intervals. Color of the 'x' represents the flux value.

Footprint analysis revealed that the flux tower's measurement area extended beyond the boundaries of the feedlot. As shown in Figure 2-4, the distance from the flux tower to the *'x'* mark represents the upwind distance contributing to 70% of the total flux for each 30-minute interval. A significant portion of this 70% contribution originated from areas outside the cattle feedlot, suggesting that emissions were primarily driven by manure runoff deposited beyond the cattle feedlot. These off-site emissions were particularly concentrated in the northwest and southwest directions, where runoff likely carried manure, creating localized hotspots for N_2O production.

The statistical analysis of N_2O fluxes grouped by wind direction further supports the evidence of spatial variability. The Kruskal-Wallis test revealed highly significant differences in flux distributions across wind directions (statistic = 94.04, p-value = 1.82×10^{-17}). Additionally,

Levene's test indicated substantial heterogeneity in variances (p-value = 9.07×10^{-29}), demonstrating that the variability in fluxes is influenced by wind direction. Normality tests confirmed that N_2O fluxes did not follow a normal distribution across the different wind direction groups, further highlighting the complexity of spatial patterns.

These results suggest that emissions are not uniformly distributed within the flux footprint and are instead strongly influenced by surface processes, particularly in areas downwind of manure deposition.

Temporal variability of N_2O flux

The analysis of N_2O flux data revealed statistically significant diurnal variability in emissions, as confirmed by the Kruskal-Wallis test (statistic = 38.09, p-value = 0.025). Median flux values remained low, generally ranging between 0.002 and 0.01 μ mol m^{-2} s^{-1} throughout the 24-hour period, but notable increases in variability were observed during midday hours (Figure 2-5). The largest spread in N_2O fluxes occurred between 10:00 and 13:00, with both the interquartile range and the occurrence of outliers peaking around 11:00. This heightened variability during midday may be attributed to increased microbial activity driven by elevated soil temperatures and moisture evaporation. In contrast, early morning and late evening hours exhibited more stable and lower emissions, likely due to cooler soil temperatures and reduced biological activity.

The results of Levene's test (p-value = 0.018) indicated significant differences in variance across time groups, further supporting the variability in flux patterns. Additionally, the presence of numerous outliers during midday suggests that certain environmental or management-related events may sporadically trigger spikes in N_2O emissions. These findings highlight the complex interactions between environmental factors, such as temperature and moisture, and N_2O flux dynamics over the course of the day, emphasizing the importance of temporal monitoring to capture the full range of flux variability.

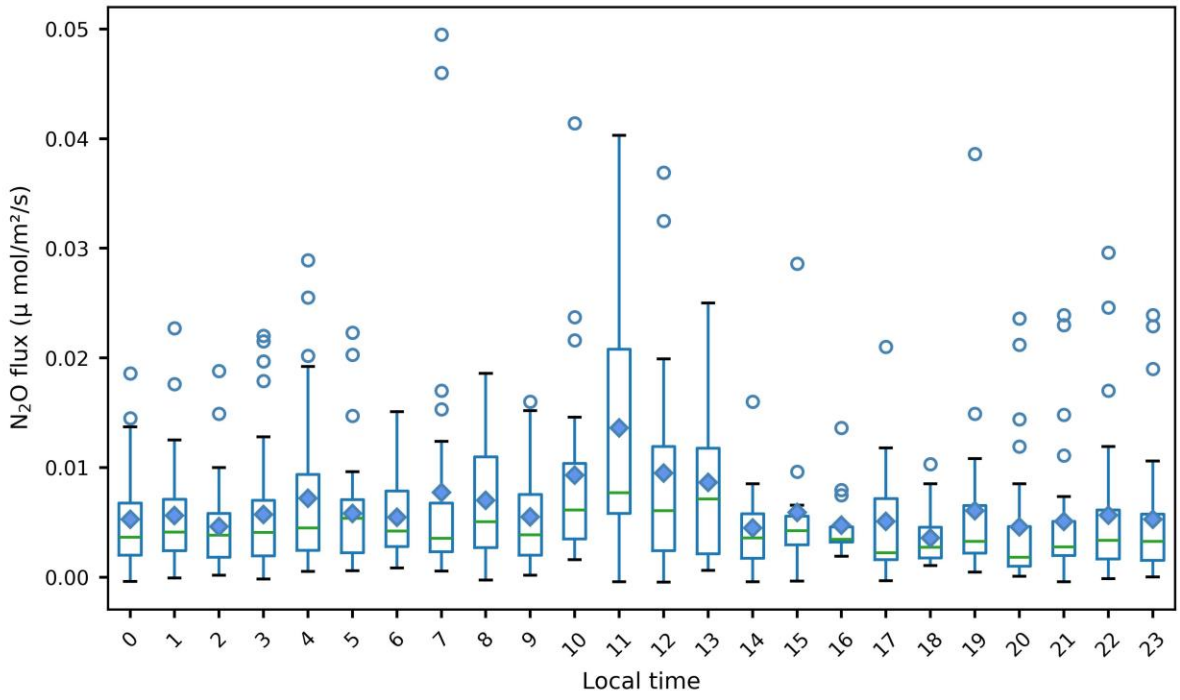

Figure 2-5: Hourly average of N_2O fluxes in Beef stocker unit. The central blue line in each box indicates the median, central diamond indicates the mean, and the bottom and top edges of the box indicate the 25th and 75th percentiles, respectively. The whiskers are extended to the most extreme data point that is no more than 1.5 times the interquartile range (IQR) from the edge of the box. The black circle sign represents outliers that lie beyond the whiskers.

2.4.2 N_2O emission from cropland

Environmental factors

The research experiment was conducted at the NEON Kona experimental field located near Manhattan, Kansas, from November 2020 to May 2021. The study period experienced notable variability in weather conditions. In December 2020 and January 2021, temperatures were relatively warm, but a significant cold spell occurred from early to mid-February, with the lowest recorded temperature plunging to -31°C. In contrast, the highest temperature during the experiment was 28°C, recorded in June 2021. Precipitation over the entire experiment totaled 100 mm, with the highest monthly rainfall of 30 mm occurring in March. March and April were particularly wet

months, with five days of rainfall exceeding 10 mm/day. In contrast, May and June were dry, marked by warm temperatures and minimal rainfall.

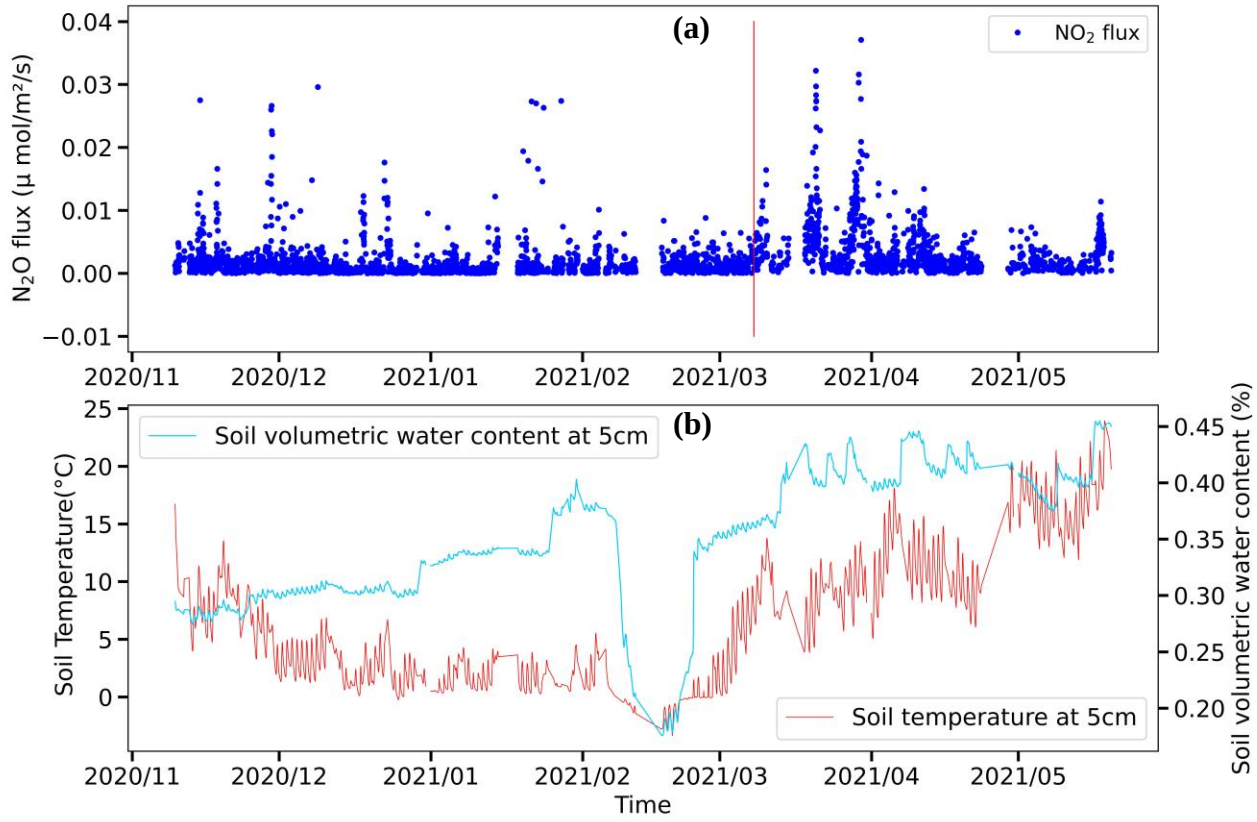

Figure 2-6: 30-min values of (a) N_2O fluxes with red vertical line indicating the fertilization event 07 March 2021 (47 kg N ha−1), (b) soil temperature and water content at 5cm depth.

The initial analysis of the 30-minute averaged N_2O flux data showed an average flux of 0.01 μ mol m^{-2} s^{-1}, with peak values reaching up to 0.039 μ mol m^{-2} s^{-1} (Figure 2-6). Although the majority of flux measurements were near zero, several significant emission spikes were observed throughout the study period.

To assess whether these high flux events were associated with fertilization, Fisher's Exact Test was employed. Table **2-1** presents the contingency table used in the analysis, with the odds ratio calculated at approximately 0.048. This indicates that the odds of a high flux event were about 20 times lower before fertilization compared to after fertilization. The p-value obtained was 2.08×10^{-44}, which is highly statistically significant, demonstrating a strong association between fertilization and the increase in high flux events. The extremely small p-value (<0.05) confirms

that fertilization significantly influences the occurrence of high flux events. Moreover, the odds ratio (<1) underscores that high flux events are far more likely to occur after fertilization than before. These findings strongly support the hypothesis that fertilization contributes to the occurrence of high flux events, likely due to increased nitrogen availability enhancing emissions.

These spikes in N_2O flux were closely associated with the fertilization event, showing significant increases that were strongly linked to changes in soil moisture and temperature. This relationship was particularly evident after rainfall events following fertilization, which appeared to trigger heightened emissions. Such observations highlight the combined effects of fertilization and environmental conditions in driving nitrous oxide emissions. The results suggest that soil temperature and moisture play crucial roles in regulating N_2O emissions, consistent with patterns reported in previous N_2O emission studies. The periods of higher flux occurred shortly after rain events, which likely enhanced microbial activity in the soil, leading to increased nitrification and denitrification processes. The combination of rainfall and fertilizer application further amplified this effect, causing sharp increases in N_2O emissions. This pattern is evident in the Figure 2-6 , where sharp spikes in N_2O flux align with increases in soil moisture content and temperature. The data illustrate that while overall fluxes were relatively low during the colder months of January and February, significant emissions were triggered by warm, wet conditions later in the study period.

	High flux events	No high flux events
Before fertilization	10	1430
After fertilization	182	1258

Table 2-1: Contingency table

Spatial variability of N_2O flux

Footprint analysis confirmed that the flux footprint remained entirely within the experimental field, ensuring that all measurements reflected on-site emissions. The accompanying wind rose diagram provides a detailed view of the directional distribution of N_2O flux values over time, categorized by flux intensity (Figure 2-7). The diagram shows that the dominant wind direction was from the south-southeast (SSE), with the majority of N_2O flux measurements influenced by winds from this

sector. Flux values between 0.000 and 0.010 μ mol m^{-2} s^{-1}, represented in green, were the most prevalent, particularly in the SSE and S directions, indicating that low N_2O emissions occurred most frequently under these conditions.

The statistical analysis further supports the significant spatial variability of N_2O fluxes based on wind direction. The Kruskal-Wallis test revealed a highly significant difference in N_2O fluxes across wind direction groups (statistic = 127.87, p-value = 1.75×10^{-24}). Additionally, Levene's test indicated substantial heterogeneity in variances among these groups (p-value = 3.85×10^{-10}). Normality tests confirmed that the N_2O flux distributions within each wind direction group deviated significantly from normality. These findings underscore the importance of wind direction in shaping the spatial patterns of N_2O emissions.

Interestingly, higher N_2O flux values, represented in orange, red, and brown, occurred more frequently when winds were coming from the south (S), southeast (SE), and SSE directions. These elevated fluxes, ranging from 0.010 to over 0.040 μ mol m^{-2} s^{-1}, were less common but suggest the presence of localized emission hotspots. These spikes in emissions are likely linked to specific environmental conditions, such as variations in soil moisture or agricultural activities like fertilization, which may have amplified N_2O production when winds came from these directions.

The results highlight the critical role of wind direction in shaping the spatial variability of N_2O fluxes within the study area. The association between elevated fluxes and specific wind directions suggests that emissions are not uniformly distributed but are instead strongly influenced by localized conditions and atmospheric dynamics.

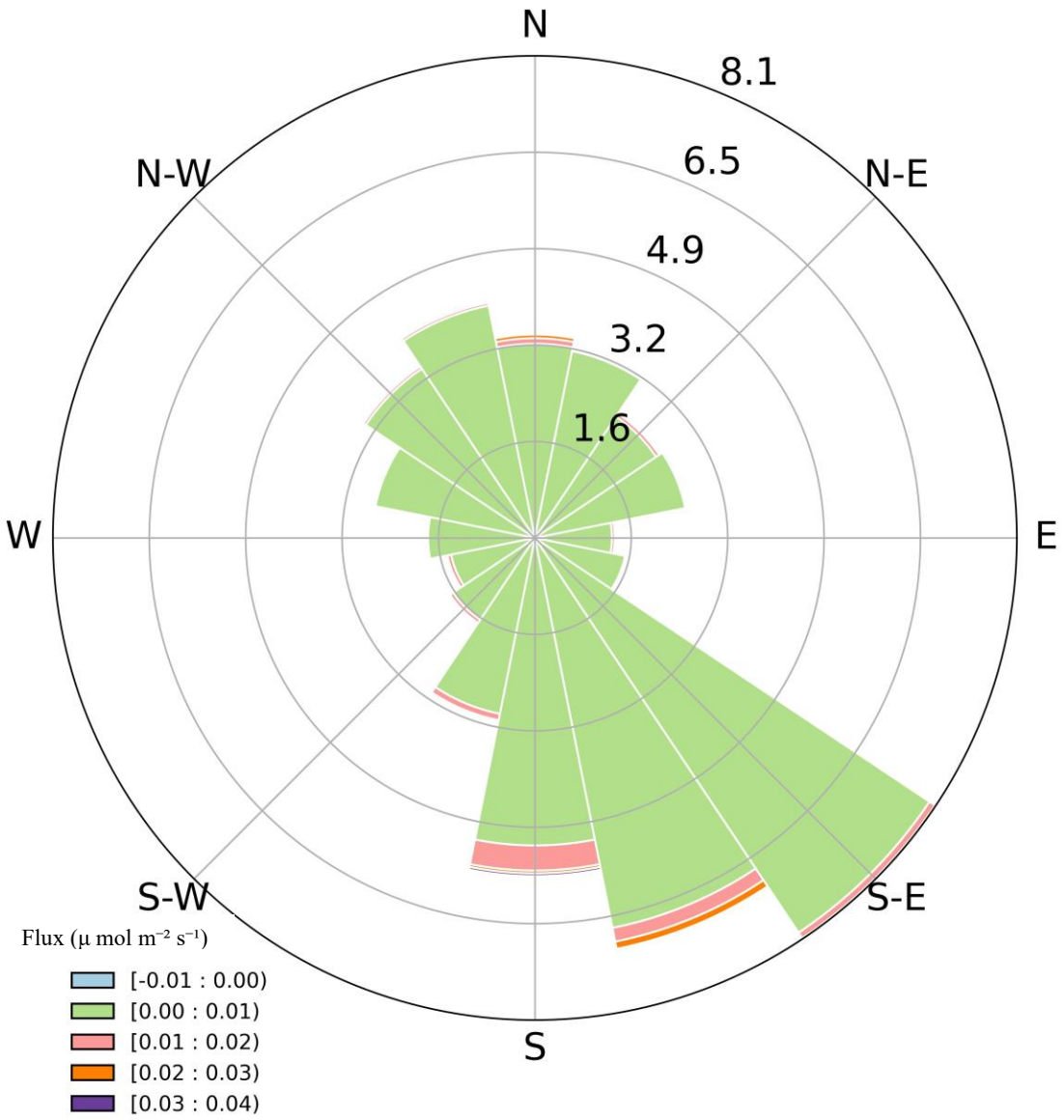

Figure 2-7:Wind rose and N_2O flux magnitudes during the experimental period. The N_2O flux was grouped based on the flux magnitude bins represented by the different colors in the graph.

Temporal variability of N_2O flux

The analysis of N_2O flux data revealed statistically significant diurnal variability in emissions, as confirmed by the Kruskal-Wallis test (statistic = 143.20, p-value = 2.36×10^{-19}). Median flux values were generally low, ranging between 0.000 and 0.005 μ mol m^{-2} s^{-1} throughout the 24-hour period (

Figure *2-8*). However, the variability across different times of the day was notable, with Levene's test (p-value = 0.048) indicating significant differences in variances. These results suggest that N_2O emissions are influenced by diurnal factors.

While the overall emissions exhibited low variability, several outliers were observed, indicating sporadic spikes in N_2O flux. These outliers were more frequent during the evening hours (16:00 to 21:00) and early morning hours (around 6:00), with fluxes occasionally exceeding 0.020 μ mol m^{-2} s^{-1}. These spikes in emissions may be driven by environmental factors such as changes in soil temperature, moisture content, or biological activity, which are influenced by diurnal cycles.

The presence of these spikes underscores the complexity of N_2O flux dynamics, highlighting the interplay of environmental and biological processes. While baseline flux levels remain relatively stable, specific conditions, potentially tied to diurnal variations in temperature and soil processes, can trigger bursts of emissions. This emphasizes the importance of continuous monitoring to capture the full temporal variability of N_2O emissions and identify key factors driving these fluctuations.

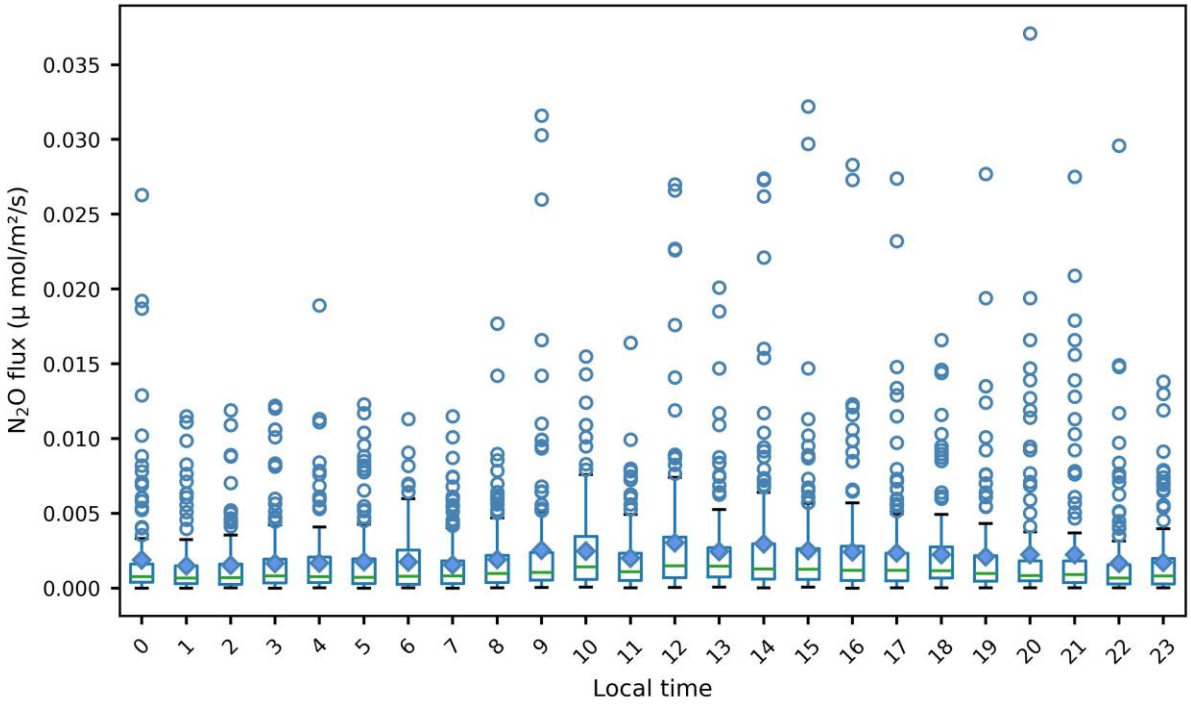

Figure 2-8: Hourly average of N_2O flux in winter wheat field. The central blue line in each box indicates the median, central diamond indicates the mean, and the bottom and top edges of the box indicate the 25th and 75th percentiles, respectively. The whiskers are extended to the most extreme data point that is no more than 1.5 times the interquartile range (IQR) from the edge of the box. The black circle sign represents outliers that lie beyond the whiskers.

2.5 Discussion

This study highlights the substantial temporal and spatial variability in N_2O fluxes, regardless of the type of agricultural field, beef cattle feedlot or cropland. N_2O emissions in both systems are influenced by a range of environmental factors, including soil temperature, moisture, and management practices such as fertilization. However, there are key differences in how these factors drive emissions, as well as significant challenges due to missing data caused by unfavorable weather conditions, equipment failures, or power outages.

2.5.1 Temporal and spatial variability

The beef cattle feedlot exhibited greater N_2O flux variability with multiple high-emission events. Median flux values were low, averaging 0.0062 μ mol m^{-2} s^{-1}, but several significant spikes were recorded. These spikes were likely driven by sporadic factors such as manure decomposition or thawing events, where microbial activity intensified during warmer midday hours due to increased soil temperature and manure moisture. Similar variability has been noted in studies such as that by Aguilar et al. (2014), who observed low emissions during colder months with spikes during warmer periods. Footprint analysis further revealed that much of the emissions were influenced by off-site sources, particularly runoff areas where manure deposited beyond the feedlot boundaries contributed to the variability in N_2O flux. This suggests that manure management practices and indirect emissions play a crucial role in determining the spatial distribution of emissions.

Conversely, cropland N_2O emissions were more stable, with an average flux of 0.01 μ mol m^{-2} s^{-1}, and peak values up to 0.039 μ mol m^{-2} s^{-1}. Emission spikes were closely tied to environmental events, particularly after rainfall and fertilization, as supported by studies like Flechard et al. (2007), which observed enhanced nitrification and denitrification processes in the soil driving increases in N_2O emissions. In contrast to the feedlot, the cropland exhibited more predictable patterns of N_2O flux, with significant spatial variability occurring within the field and influenced primarily by wind direction and localized environmental conditions.

2.5.2 Impact of missing data

The reliability of N_2O flux estimates is heavily compromised by significant data gaps, which are a persistent challenge in environmental research. These gaps are primarily due to unfavorable weather conditions, equipment malfunctions, and power outages, which disrupt continuous data collection. Such interruptions not only create incomplete records but can also lead to substantial underestimations of total N_2O emissions, skewing cumulative emission estimates and potentially leading to incorrect conclusions about the environmental impacts of these systems.

The intermittent nature of high-emission events exacerbates this issue. These events, critical for understanding the full impact of N_2O emissions, can often be missed entirely if they occur during periods of data loss. This problem is highlighted in research such as that by Rochette and Eriksen-Hamel (2008), which emphasizes the need for continuous monitoring to capture the episodic nature of N_2O emissions, particularly after specific events like rainfall or fertilization that significantly enhance microbial activity and gas flux.

To address these challenges, it is crucial to implement robust gap-filling techniques. One approach, as utilized in studies like Vickers and Mahrt (1997), involves statistical interpolation methods that estimate missing values based on the trends and patterns observed in the available data. This method can be particularly effective in cases where data gaps are short and environmental conditions are relatively stable.

However, when gaps are extended or occur during periods of significant environmental change, more sophisticated methods may be necessary. Machine learning models, which can predict missing N_2O flux values from related environmental variables, offer a promising solution. These models, as discussed by Nemitz et al. (2018), in the context of CH_4, demonstrate the potential to incorporate factors such as soil temperature, moisture levels, and historical emission data. While such approaches have not yet been extensively applied to N_2O, their successful use for CH_4 highlights the feasibility of adapting them for estimating missing N_2O fluxes.
In conclusion, both the beef cattle feedlot and cropland systems demonstrate significant temporal and spatial variability in N_2O emissions, driven by complex interactions between environmental factors and management practices. However, the variability is more pronounced in the feedlot due

to manure-related processes, whereas the cropland exhibits more predictable patterns linked to soil moisture and fertilization. Importantly, the presence of missing data due to equipment or environmental failures presents a major challenge in accurately quantifying total emissions. Therefore, reliable gap-filling methods must be employed to ensure that high-emission events are accounted for, allowing for more accurate cumulative emission calculations and a better understanding of the overall greenhouse gas footprint of these agricultural systems.

Chapter 3 - Evaluating the applicability of neural networks for gap filling N_2O flux data

3.1 Abstract

This study evaluates the applicability of artificial neural networks (ANN) for gap-filling in nitrous oxide (N_2O) flux datasets collected using the eddy covariance (EC) technique in agricultural fields. N_2O is a potent greenhouse gas, and its emissions from soils are highly variable, driven by processes like nitrification and denitrification. The EC technique provides high-frequency data, but gaps due to equipment failures, adverse weather, and low-turbulence periods can introduce significant uncertainties into emission estimates. Addressing these gaps accurately is crucial for improving greenhouse gas inventories.

The study was conducted in a winter wheat field in Kansas, USA, where N_2O and environmental variables were continuously monitored from November 2020 to May 2021. The data exhibited significant missing points 26.91% of the total observations which were classified into short-term, medium-term, and long-term gaps. Two gap-filling techniques were applied: linear interpolation and an ANN model. The performance of these methods was evaluated using root mean square error (RMSE), bias error (BE), and the coefficient of determination (R^2).

Results showed that ANN outperformed linear interpolation for medium- and long-term gaps, achieving better accuracy (R^2 = 0.60 for long-term gaps) and lower uncertainty. Linear interpolation performed better for short-term gaps, with lower RMSE values. Sensitivity analysis revealed that soil moisture and wind speed were the most influential predictors in the ANN model. Overall, combining both methods provided a robust approach to gap-filling, reducing uncertainty in daily N_2O emissions from agricultural systems.

This study demonstrates that ANN is an effective tool for gap-filling N_2O flux data, particularly for longer data gaps, and highlights the importance of accurate data reconstruction for improving GHG emission estimates from agriculture.

3.2 Introduction

Nitrous oxide (N_2O) is a potent greenhouse gas (GHG) with an estimated global warming potential approximately 300 times greater than that of carbon dioxide (CO_2) over a 100-year time frame (IPCC and others 2013). While its atmospheric concentration is relatively low, its impact on radiative forcing and climate change is substantial due to its long atmospheric residence time. Agricultural activities have been identified as a major source of anthropogenic N_2O emissions, primarily arising from the microbial processes of nitrification and denitrification within agricultural soils (Smith et al. 2014). N_2O emissions from agricultural systems have high temporal and spatial variability due to variations in environmental factors, such as soil water content, temperature, texture, pH, soil nitrogen and soil carbon content, and management (Freney 1997). Accurate measurement of N_2O emissions is essential for better understanding the dynamics of GHG emissions within agroecosystems, enabling the identification of hotspots and moments (Butterbach-Bahl et al. 2013), for determining national greenhouse gas inventories, and improving current biogeochemical models. In addition, these measurements are important in assessing the effectiveness of sustainable agricultural practices in reducing N_2O emissions. Several techniques can be used to quantify N_2O emissions from agricultural fields, ranging from gas chambers to micrometeorological methods (Del Grosso et al. 2008; Wang et al. 2020; Izaurralde et al. 2004).

The gas chamber technique has long been a popular method for quantifying the N_2O emissions, due to its precision and adaptability. The gas chamber method involves placing a chamber on the ground to trap gases emanating from the soil. The concentration changes of the trapped gases are monitored over time, providing a measure of the soil flux. In the context of N_2O, this method has seen various improvements over time to enhance its accuracy and versatility (Davidson, EA and Savage, KVLV and Verchot, LV and Navarro 2002). Chamber measurements have provided insights into the diurnal and seasonal patterns of N_2O emissions. Flessa et al. (2002) noted that chamber-based measurements helped identify peak emission times, often associated with specific environmental conditions or agronomic practices. The design and deployment strategy of chambers can influence the accuracy of flux measurements. Venterea et al. (2005) highlighted that chamber height, deployment frequency, and duration can impact the quantification of N_2O emissions. One concern with chamber techniques is the potential for creating microclimates inside the chamber that differ from ambient conditions. With advances in technology, automated chamber systems have been developed to allow for more frequent measurements and reduced labor needs.

Ambus & Robertson, (2006) explored the capabilities of these automated systems, concluding that they offer a higher temporal resolution of N_2O flux data, although they come with increased complexity and cost. Pihlatie et al. (2005) studied these microclimatic effects, noting that while they do exist, with careful calibration and methodology adjustments, the data can be corrected to minimize this bias. Wang et al. (2013) presented a side-by-side comparison of the chamber technique with the eddy covariance method. While both methods yielded comparable annual flux estimates, but differences in short-term fluxes.

The flux gradient method is another widely used technique in micrometeorology to quantify the exchange of trace gases between the Earth's surface and the atmosphere. The flux gradient method is built on the gradient-diffusion theory, which assumes that gas flux is proportional to the concentration gradient of the gas, multiplied by a transfer coefficient (typically turbulent diffusion) (Jayasundara et al. 2007). It offers an advantage in being stable compared to other methods and is often applied in environments where direct measurements are needed (Del Grosso et al. 2022). N_2O emissions can be sporadic and influenced by various environmental and management factors. (Wagner-Riddle et al. (1997) underscored the importance of year-round measurements, suggesting that capturing seasonal and sporadic fluxes is crucial for accurate annual emission estimates. The flux gradient method is well-suited for such continuous monitoring (Philippe and Eriksen-Hamel 2011). Variables like wind speed, atmospheric stability, and boundary layer depth can influence the accuracy of the flux gradient method (Wagner R et al. 2007). Some studies have addressed these intricacies, offering adjustments and corrections to improve measurement accuracy (Risk et al. 2013).

Compared to the chamber technique and the flux gradient method, Eddy covariance emerges as a robust and efficient method for the quantification of N_2O fluxes in agricultural fields. It is capable of providing continuous, high-frequency data, for long periods, making it invaluable in observing the diurnal, seasonal, and inter-annual variabilities of fluxes. Several studies have employed the eddy covariance technique to quantify N_2O emissions from agricultural soils. Abalos et al. (2016) utilized eddy covariance measurements to compare N_2O emissions from annual and perennial crops over a three-year period. Brown et al. (2018) evaluated the performance of a lower-powered analyzer and sampling system for eddy covariance measurements of N_2O fluxes. Jones et al.

(2011) compared eddy covariance and static chamber measurements of N_2O emissions from managed grasslands. Huang et al. (2014) measured N_2O emissions from a commercial cornfield using the eddy covariance technique. These studies collectively demonstrate the efficacy of the eddy covariance method in understanding and quantifying N_2O emissions from agricultural soils.

Low-turbulence conditions, equipment failures, power outages, field operations, and bad weather conditions (Papale et al. 2006; Nemitz et al. 2018) cause data gaps. Therefore, reliable gap-filling techniques are essential to ensure accurate N_2O emissions. Different gap-filling techniques have been used to fill data gaps in CO_2 and methane (CH_4) and measurements, such as linear interpolation, look-up tables, nonlinear regression, and artificial neural networks (ANN) (Wohlfahrt and Galvagno 2017; Bigaignon et al. 2020; Dorich et al. 2020; Goodrich et al. 2021; Ooba et al. 2006; Mishurov and Kiely 2011; Dengel et al. 2013; Taki et al. 2019). Unlike CH_4 and CO_2 emissions, N_2O emissions generally remain at baseline levels most of the time but experience episodic exponential increases periods (Congreves et al. 2018). This distinctive pattern adds complexity to gap-filling N_2O emission data, making it more challenging to effectively address data gaps. Therefore, most of the gap-filling methods mentioned above would not be statistically appropriate for addressing gaps in N_2O data set (Moffat et al., 2010). Currently, there is no widely accepted gap-filling technique for filling gaps in N_2O flux time series.

Several studies have explored the use of artificial neural networks (ANNs) to address data gaps in daily and monthly N_2O datasets. These studies have shown promising results, demonstrating the effectiveness of the ANN technique in filling gaps in daily and monthly N_2O flux data (Taki et al. 2019; Bigaignon et al. 2020). In this study, we extend this approach by applying the ANN method to fill gaps in high-frequency N_2O time series data, specifically focusing on 30-minute N_2O flux measurements. Additionally, we evaluate the performance of the ANN method in comparison to the linear interpolation method.

3.3 Material and methods

3.3.1 Site description

The research experiment was carried out at NEON Kona experimental field (N 39.110, W 96.612) located in Manhattan, Kansas, from November 2019 to May 2020. The field has a total area of 16.1 ha, with near-flat surface (slope < 5%). The field was tilled and planted with winter wheat on October 8th, 2020, at a seeding rate of 166.6 kg/ha.

The first nitrogen (N) fertilizer application was carried out on **September 16, 2020**, with a total application rate of **44.8 kg of nitrogen per hectare**. The fertilizer used was a combination of **UAN (28-0-0)** and **ATS (12-0-0-26)**, which were sprayed directly onto the soil surface.

The second application took place on **March 7, 2021**, at a rate of **47 kg of nitrogen per hectare**. This time, only **UAN (28-0-0)** was applied, and it was sprayed onto both the soil and the plant surfaces.

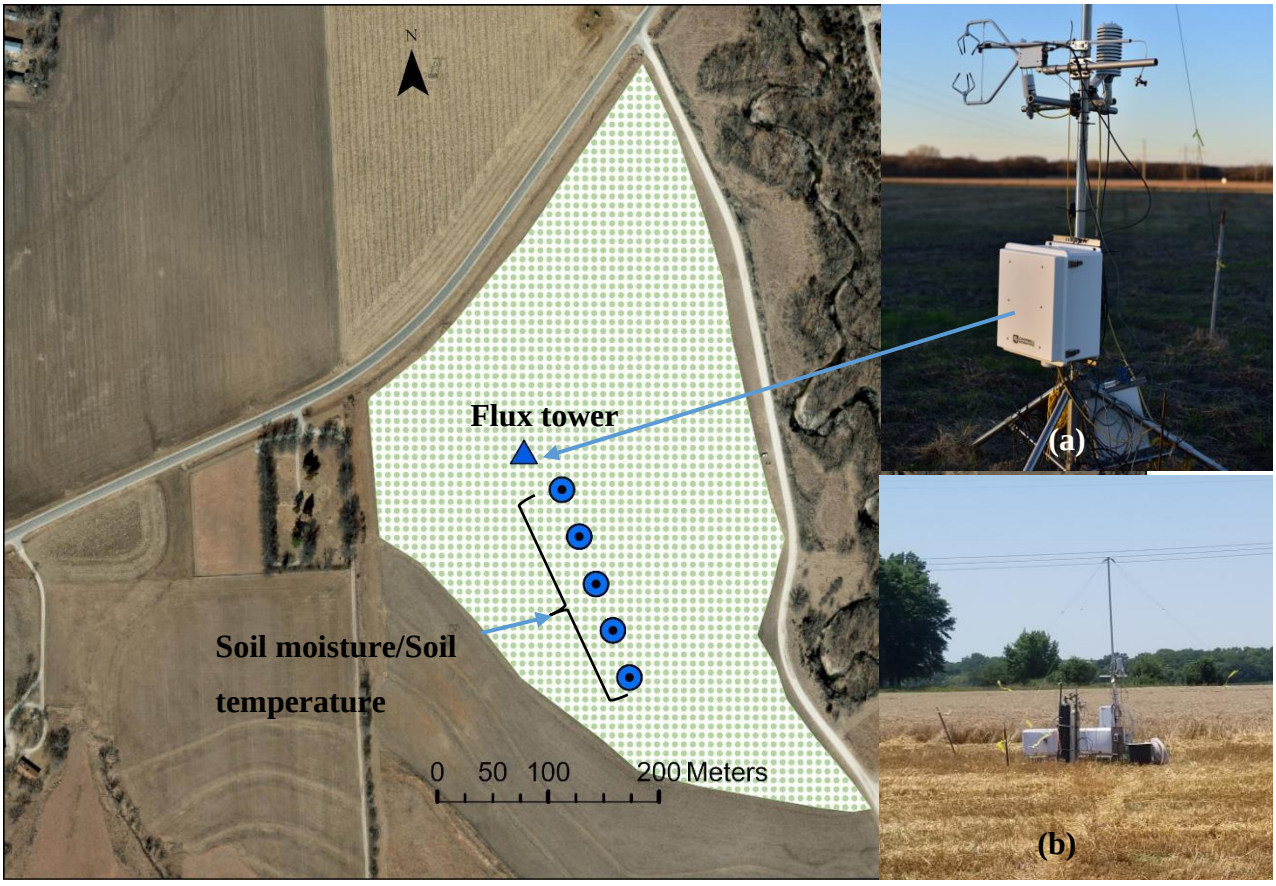

Figure 3-1: Layout of the NEON Kona experimental field. Blue circles show the location of the soil moisture and soil temperature sensors. Insets: (a) instrument setup, (b) Flux tower.

3.3.2 Flux measurements

Fluxes of N_2O and CO_2 fluxes were measured using the eddy covariance technique. Wind velocity three orthogonal components and temperature were measured using the sonic anemometer (CSAT3B, Campbell Sci., Logan, UT). Mixing ratios of CO_2 and N_2O were measured using a tunable-diode laser absorption spectroscopy (TDLAS) closed-path gas analyzer (TGA 200A, Campbell Sci., Logan, UT). Additionally, a well-established open-path gas analyzer (LI-7500, LI-COR, Lincoln, NE) was used to measure CO_2 and water vapor (H_2O) concentrations for comparison purposes. The closed-path analyzer's air intake, open path gas analyzer and the sonic anemometer were mounted onto the tower 2.25 m above the ground. The air samples were drawn to the gas analyzer through a 7.6 m long high-density polyurethane tube connected to the air intake. The air intake included vortex flow mechanism to filter out the air samples. In addition to that an insect screen, and a high-flow filter equipped with a 10 μm filter membrane to ensure particulates were removed. Air was drawn through the sampling tube by a vacuum pump (Edwards nXDS15i, Edwards Ltd, UK) at a rate of 5 liters/min. The signals from the sonic anemometer, the closed-path gas analyzer, and the open-path gas analyzer were recorded at 10 Hz using a datalogger (CR3000, Campbell Sci.).

The 30-minute average gas fluxes were calculated by the raw data being analyzed using the eddy covariance software package EddyPro (v. 7.6, Licor). The raw data eddy-covariance data processing steps followed the standard protocol described by Nemitz et al. (2018). Briefly, the data processing procedures included spike removal (Vickers and Mahrt 1997), double coordinate rotation, time lag compensation (Fan et al. 1990), and spectral corrections (Horst 1997) were mainly followed, and flux quality was controlled using flag values as suggested by Foken et al. (2004).

In addition to the filtering and processing methods described above, CO_2 flux values that were calculated using open-path gas analyzer data were utilized to validate the closed-path data. The frequency response and random error of the open-path gas analyzer have been extensively tested in several studies (Prajapati and Santos 2017), establishing it as one of the most accepted gas analyzers for eddy covariance systems. Therefore, we only accepted N_2O fluxes that corresponded to CO_2 fluxes where both analyzers exhibited congruence.

Air temperature and relative humidity were measured using a standard air temperature and moisture probe (HMP 50, Campbell Sci), with the data recorded via a data logger. Soil moisture and temperature data were retrieved from the NEON online data portal (KONA,NEON 2021). This data product includes soil temperature and moisture measurements for eight depth levels across five different locations within the field. Further details about the sensor locations can be found on the NEON data portal (NEON 2021).

The flux footprint represents the spatial area over which the sensors measure exchanges of gases and energy between the land surface and the atmosphere. The calculation of a flux footprint typically depends on various factors including measurement height, surface roughness, atmospheric stability conditions, wind direction, and the inherent characteristics of the turbulence itself. In this study the flux footprint was calculated using the parameterized approach proposed by Kljun et al. (2004). The calculated flux footprint length was then incorporated as an input variable into the artificial neural network (ANN) model.

3.3.3 Using cross-correlation to identify the lags between N_2O flux, soil temperature, and soil moisture content.

Cross-correlation is a powerful statistical tool that measures the similarity between two signals or datasets as a function of a time-lag applied to one of them (Bendat and Piersol 2000). It provides insights into how changes in one variable may be associated with shifts in another after a certain time lag. This method has found its application in various fields, and in recent years, has been used in understanding the key relationship between soil properties and gas emissions. By correlating the time series of specific soil properties (like soil moisture, temperature, or microbial activity) with gas emission rates, researchers have been able to identify driving factors behind emissions of greenhouse gases like CO_2, CH_4, and N_2O. For instance, a study by Kettunen et al. (1996) utilized cross-correlation to investigate the links between soil moisture, temperature, and CH_4 flux. Their findings indicated that soil temperature and soil moisture have a complex interaction with CH_4 emissions. Sexstone et al., (1985) , utilized cross-correlation to identify temporal lags between soil moisture variations and subsequent N_2O emission spikes and identified relationships between rainfall events and N_2O emissions. but the lag can vary based on soil type. Soil temperature has a

direct influence on microbial processes responsible for N_2O production and consumption. Cross-correlation has revealed that N_2O emissions often follow temperature changes and other meteorological variable changes (Kamata et al. 2002). Understanding these lags is crucial for modeling and predicting N_2O emissions. Here the “correlation_lags” function in the python scipy package (SciPy 2020) was used to identify the lags between N_2O flux and the soil moisture content and the soil temperature.

The analysis identified a 24-hour lag between N_2O flux and soil moisture content and a 9-hour lag between N_2O flux and soil temperature. These lag durations were observed to vary seasonally, reflecting the dynamic interactions between N_2O emissions and environmental conditions.

3.3.4 Gap filling approaches.

Linear interpolation

Linear interpolation is a fundamental technique used to estimate missing values within a dataset. It operates on the premise that changes between two known data points are uniform. By drawing a straight line between values adjacent to the missing data, it estimates the missing value based on its position on that line. However, this technique assumes a constant rate of change between points, which might not always accurately represent the true dynamics of a system. Linear interpolation has been employed for gap filling in meteorological time series data (Jones and others 2017 ;Six et al. 2007). When the rate of change is not uniform or when the gaps are extensive, linear interpolation can produce biased results (Smith and Richardson 2018). In this study, the 'interpolate' method from the Python pandas package (Pandas 2023) was used to estimate the missing data points.

Artificial neural network

Artificial Neural Networks (ANNs) are computational models that draw inspiration from the intricate neural structure of the human brain. These networks are designed to recognize patterns, identify relationships between variables, and make decisions. ANNs are capable of processing vast amounts of information. This is achieved by transmitting signals between neurons via weighted connections. During the training phase, the networks undergo iterative adjustments to these

weights based on the error of their predictions, typically using algorithms like back propagation (Rumelhart et al. 1986). ANNs are powerful tools for predicting complex relationships, making them particularly valuable in environmental studies where interactions are both intricate and dynamic. Artificial neural networks (ANNs) are powerful tools for predicting complex and non-linear relationships, making them especially valuable in environmental studies where interactions among variables are both intricate and dynamic. In the context of greenhouse gas emissions, ANNs have been utilized to integrate multiple variables, including soil characteristics, agricultural practices, and weather patterns, to predict emissions. For nitrous oxide (N_2O) specifically, studies such as those by Bigaignon et al. (2020), Taki et al. (2019), and Dorich et al. (2020) have demonstrated the ability of ANNs to predict N_2O fluxes with high accuracy across diverse soil types and climatic zones.

In addition, ANNs have shown promise in addressing data gaps in agricultural emission datasets. While studies like datasets Goodrich et al. (2021) and Mishurov and Kiely (2011) have focused on other greenhouse gases (e.g., CO_2 and CH_4), they provide a foundation for understanding how ANNs can be adapted to address gaps in N_2O datasets. However, most existing work has been limited to daily or monthly flux predictions, leaving a gap in high-frequency N_2O flux analysis. This study advances the field by applying ANNs to fill gaps in high-resolution (30-minute) N_2O flux measurements, a critical step in capturing the episodic and dynamic nature of N_2O emissions. By integrating additional variables, such as flux footprint length and environmental conditions, this research moves beyond previous approaches to improve the accuracy and applicability of gap-filling techniques in high-frequency GHG datasets.

Multi-layer perceptron (MLP) neural networks are well-suited for addressing classification and regression problems (Bishop 1995; Moffat et al. 2010; de Oliveira et al. 2013). In MLP configurations, data progresses linearly: starting at the input layer, moving through a series of hidden layers, and culminating at the output layer. In MLP, neural network, the number of hidden layers can vary depending on the complexity of the problem and the architecture of the network. For many problems, a single hidden layer is sufficient to capture the patterns in the data (Hornik et al. 1989). This simplifies the model and reduces the risk of overfitting. The optimal number of hidden layers and the number of neurons within each layer are often determined through

experimentation and cross-validation (Svozil et al. 1997; Saxén and Pettersson 2006; Stathakis 2009; Järvi et al. 2012). Adding too many hidden layers can make the network prone to overfitting (Goodfellow et al. 2016), where it performs very well on the training data but poorly on unseen or new data. On the other hand, too few layers can lead to underfitting, where the model can't adequately capture the patterns in the data.

Development and optimization of an artificial neural network

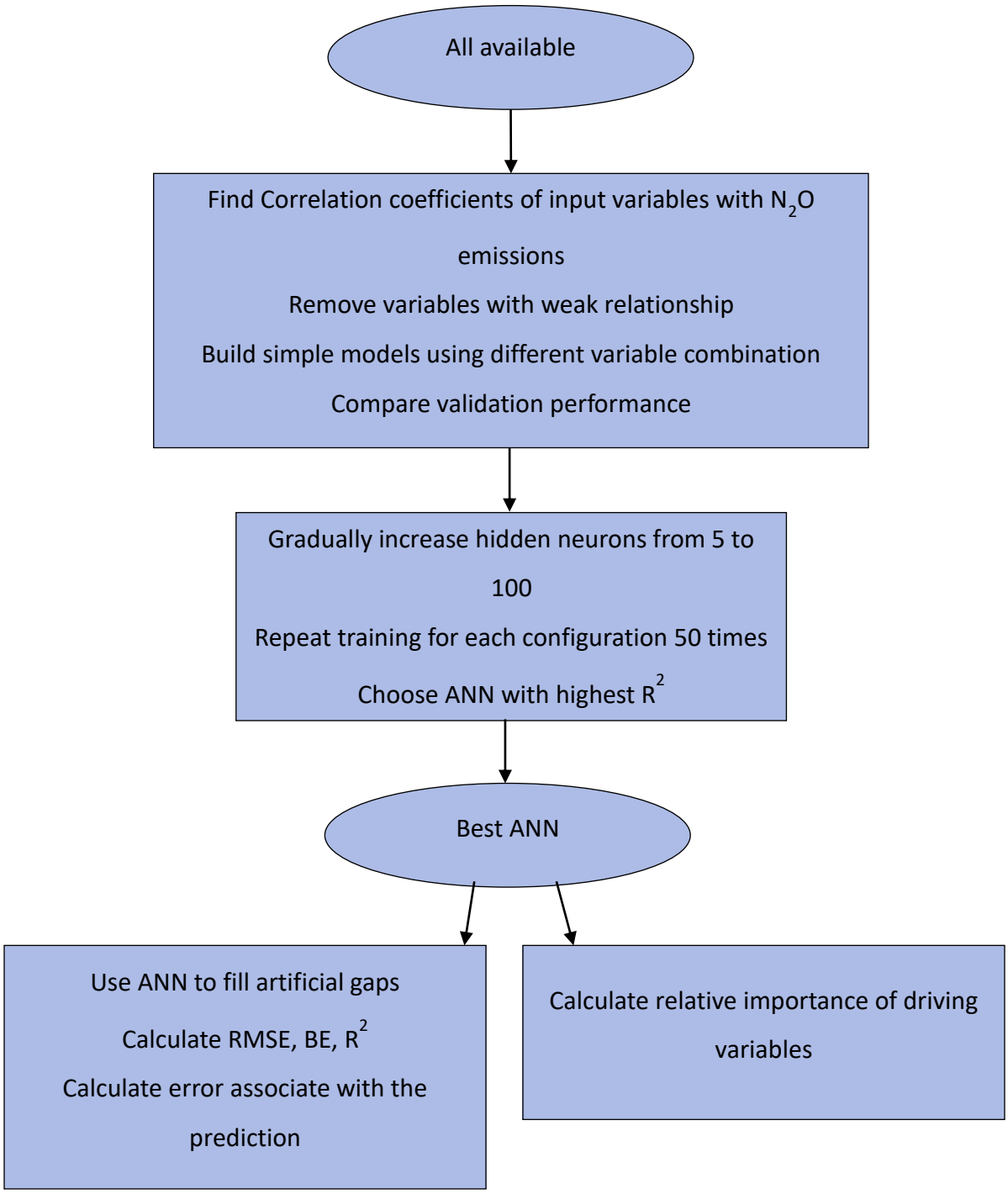

Figure 3-2: Workflow for developing and optimizing an artificial neural network (ANN) for filling gaps in N_2O flux data

To address gaps in the time series of N_2O fluxes, an ANN was developed using MATLAB™'s Deep Learning Toolbox. The ANN setup and training process involved several systematic steps, starting with the selection of input variables. Correlation coefficients between measured variables and N_2O fluxes were evaluated, and variables with no significant relationships to N_2O fluxes were excluded. Strong candidate variables were selected based on their relevance to N_2O emissions and previous studies. These variables included soil moisture content, soil temperature, wind speed, friction velocity, air temperature, relative humidity, and flux footprint length along the main wind direction. Among highly correlated variables, such as wind speed and friction velocity, wind speed was chosen to reduce model complexity and improve computational efficiency.

Simple ANN models were constructed using different combinations of these input variables, and their validation performance was evaluated. Each variable combination was tested through 50 runs, and the average R^2 value from these repetitions was used to identify the best-performing combination of input variables. Soil temperature (9 hours prior) and soil moisture (24 hours prior) were included to account for the observed time lags in N_2O flux responses to environmental changes. The optimal input variable set, selected based on its contribution to maximizing model performance, consisted of seven variables.

The next step involved determining the optimal number of hidden neurons. Using a trial-and-error approach, the number of neurons in the hidden layer was systematically increased from 5 to 100 in increments of 5. For each configuration, the training process was repeated 50 times, and the ANN configuration that achieved the highest average R^2 value was selected. The final ANN model consisted of one hidden layer with 15 neurons, a hyperbolic tangent activation function, and the Levenberg–Marquardt algorithm for training. Before training, the input data were normalized to the [-1, +1] range using MATLAB's 'mapminmax' function.

The dataset was divided into three subsets: 70% for training, 15% for validation, and 15% for testing. During training, the ANN minimized the mean square error (MSE) by adjusting the connection weights between neurons. The training process terminated either when the validation MSE reached a predefined cutoff or when no further improvement was observed after a specified

number of epochs. To ensure robustness, the training process was repeated 50 times with randomly assigned subsets, and the model with the highest R^2 value was selected as the best-trained network. The trained ANN was then employed to fill artificial data gaps in the 30-minute N_2O flux time series. Model performance was evaluated using the root mean square error (RMSE), bias error (BE), and R^2 values, which quantified the agreement between predicted and observed fluxes. Additionally, the relative importance of the driving variables was calculated to assess their contributions to N_2O emissions.

3.3.5 The relative importance of driving variables for the ANN model

In ANNs, understanding the relative importance of driving variables (often termed as features or inputs) is crucial for identifying the most influence variables to the network's predictions. Determining the significance of driving variables can lead to more efficient models. By identifying and subsequently removing less important inputs, one can often achieve similar predictive accuracy with a simpler model as achieved with more complex model, resulting in faster training and inference times. There are several methods to gauge the importance of features in ANNs. One popular approach is the sensitivity analysis, small changes in an input lead to significant changes in the output, that input is deemed important. Another method is using connection weights. In this approach, the magnitude of the weights connecting the input layer to the first hidden layer can provide insights into feature importance, especially when the network is relatively shallow. In this study a sensitivity analysis method proposed by Goh (1995) was used to identify the relative importance of each predictor variables and the relative importance of a predictor variable x_{ij} is defined by equation 8. x_{im} is the connection weight between the input neuron *i* and hidden neuron *m*; y_{mj} is the weight between hidden neuron m and output neuron j; *L* is the number of neurons in the input layer and L is the number of neurons in the hidden layer. $\sum_{r=1}^{L}|x_{rm}|$ corresponds to sum of the connection weights between *L*.

$$x_{ij} = \frac{\sum_{m=1}^{k}\left|x_{im}y_{mj}\right| / \sum_{r=1}^{L}|x_{rm}|}{\sum_{i=1}^{L}\sum_{m=1}^{k}\left|x_{im}y_{mj}\right| / \sum_{r=1}^{L}|x_{rm}|} \quad \textbf{8}$$

3.3.6 Evaluation of gap filling methods

Performance of Linear interpolation and the ANN method were assessed using three statistical metrics to ensure a comprehensive understanding of their efficacy. The root-mean-square error (RMSE) was utilized as an index of prediction accuracy, offering insights into the deviation of predicted values from observed ones (Smith et al. 2018). Furthermore, the coefficient of determination (R^2) was used to quantify the proportion of the variance in the dependent variable that is predictable from the independent variable(s); a higher R^2 indicates a better fit of the model to the observed data (Jones and Wilson 2019). Additionally, the bias error (BE) was examined to provide a measure of the systematic deviation of the predictions. This error metric is crucial as it identifies whether a model consistently overestimates or underestimates the values.

$$\boldsymbol{RMSE = \sqrt{\frac{1}{N}\sum\left(p_{i-o_i}\right)^2}} \quad \textbf{9}$$

$$\boldsymbol{R^2 = \frac{\left(\sum(p_i - \overline{p})\,(O_i - \overline{O})\right)^2}{\sum(p_i - \overline{p})^2 \sum(O_i - \overline{O})^2}} \quad \textbf{10}$$

$$\boldsymbol{BE = \frac{1}{N}\sum\left(p_{i-o_i}\right)} \quad \textbf{11}$$

3.3.7 Total flux uncertainty

Gap-filling methodologies inherently introduce uncertainties in the estimation of N_2O emission data, necessitating robust approaches to quantify these uncertainties. Several techniques have been employed to assess the uncertainty associated with gap-filled N_2O emissions. One widely used method is bootstrapping, which involves resampling the available data to generate multiple synthetic datasets. These datasets are then used for gap-filling, allowing researchers to evaluate the variability in outcomes (Hollinger and Richardson 2005). Another common approach involves applying bias error analysis to estimate the uncertainty in cumulative emissions over a specific period (Papale et al. 2006).

Since gap-filling techniques can introduce systematic biases in 30-minute flux estimations, they may result in either underestimation or overestimation of cumulative fluxes over time. The total offset introduced by gap-filling can be quantified by combining the average bias error with the total number of observed gaps (Moffat et al. 2007). In this study, bias error method was used to calculate the uncertainty associated with N_2O flux estimates resulting from gap-filling processes.

3.3.8 Data selection for training the ANN and the evaluation performance of the gap filling methods.

In the preliminary analysis, three distinct patterns of missing data were identified: short-term gaps (spanning 1 to 4 consecutive data points), medium-term gaps (ranging from 5 to 12 consecutive data points), and long-term gaps (extending beyond 12 consecutive data points). To assess the efficacy of two gap-filling methods across these varying data patterns, the primary dataset was divided into two distinct subsets. The first subset was used training the Artificial Neural Network (ANN), and the second was reserved for evaluating the performance of the gap-filling techniques. The eddy covariance time series consists of 30-minute average flux values, over a span of seven months. Initially, the most extended uninterrupted data sequences (those with a length exceeding 50 data points) were identified for each month. From the entirety of these identified sequences, seven were randomly chosen, ensuring that each month was represented by at least one such dataset. After separating out these seven data sets the rest of all the data was used to train, validate and test the ANN.

From the selected seven datasets, 420 synthetic missing data scenarios were created by randomly removing sequences of 1, 2, 4, 6, 12, and 24 consecutive data points. To ensure comprehensive representation, ten subsets were formulated for each monthly dataset to correspond to each type of data gap. Then, the artificially introduced gaps were filled using both gap-filling techniques. The predicted values were compared with the original data to evaluate the precision and effectiveness of each method.

3.4 Results

3.4.1 Environmental conditions

During the experimental period, there were significant fluctuations in the weather conditions. A notably warmer climate was observed in December 2020 and January 2021, while the subsequent period from early to mid-February experienced subzero temperatures, the recorded lowest temperature was -31°C. Conversely, the warmest temperature was 28°C in June (Figure 3-3). This extreme cold spell in February caused malfunctions in the soil moisture sensors, leading to significant gaps in soil moisture data for that month. Over the duration of the experiment, a total precipitation of 100 mm was recorded, with the maximum precipitation of 30 mm occurring in March. March and April alone had five days where the rainfall exceeded 10 mm per day. The month of May characterized by warm weather and sparse rainfall events.

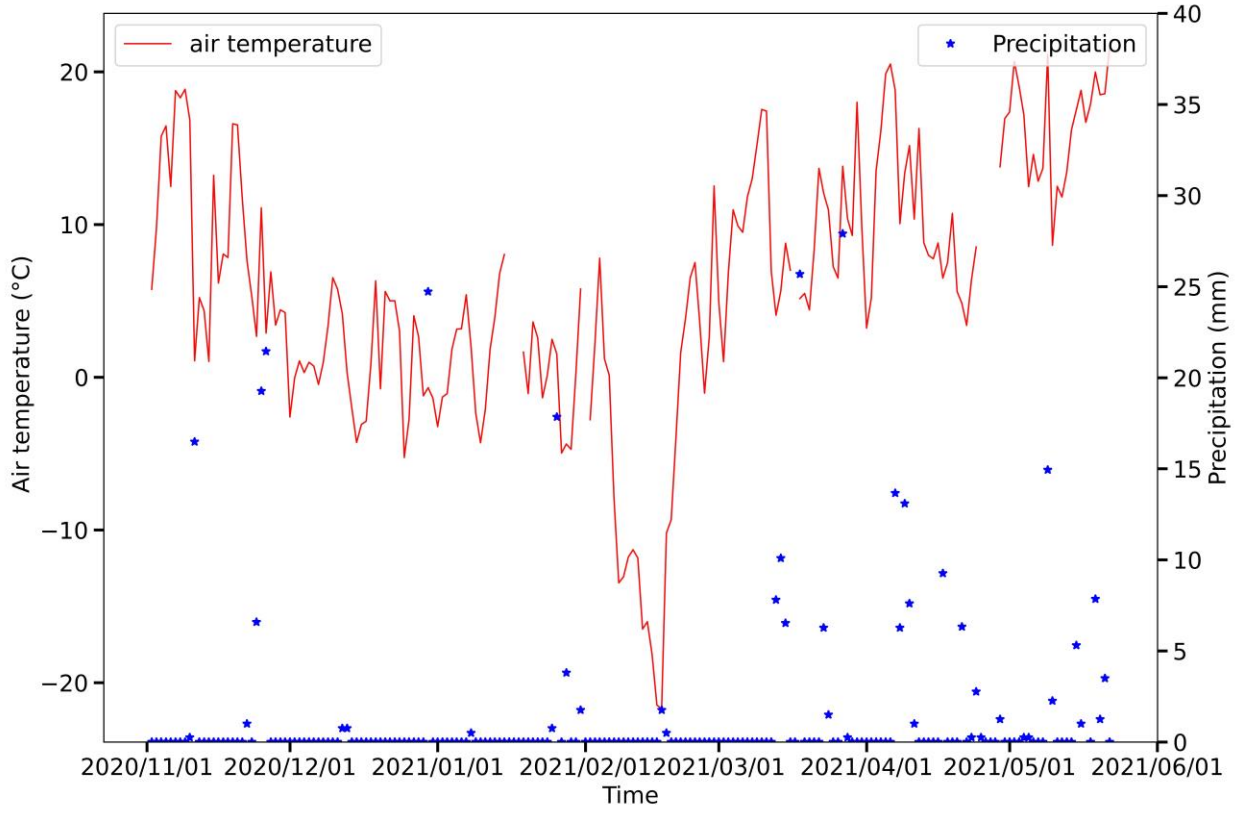

Figure 3-3: Daily values of air temperature and precipitation.

3.4.2 Data screening

In the preliminary analysis, 30-minute average flux data were examined to compare CO_2 flux measurements obtained from an open-path gas analyzer and a closed-path gas analyzer. The open-path gas analyzer, validated in multiple studies (Prajapati and Santos, 2017), is widely recognized for its reliability and frequency response in eddy covariance systems. Standard data screening procedures, such as filtering based on friction velocity and quality flags, were applied as part of the analysis. Subsequently, CO_2 fluxes from the open-path analyzer were used as a benchmark to assess and filter the closed-path data, ensuring that only high-quality measurements from the closed-path analyzer were retained for further analysis.

The scatterplot (Figure 3-4) illustrates the comparison between selected CO_2 flux values from the two analyzers, revealing a strong linear relationship between the datasets. The tight clustering of points around the 1:1 line (represented in red) demonstrates a high level of agreement between the two systems, with minimal deviation observed across a range of flux values. This consistency confirms that the closed-path system accurately captures CO_2 fluxes in a manner aligned with the well-established open-path system, with no obvious bias or systematic errors.

The agreement between the two analyzers justifies the use of CO_2 flux alignment as a filtering criterion for accepting N_2O flux data. By ensuring that N_2O fluxes are only included when the corresponding CO_2 fluxes show alignment between the two systems, the integrity of the dataset is enhanced. This filtering approach minimizes the risk of measurement errors, particularly those related to instrument limitations or environmental interferences, thereby improving the reliability of the N_2O flux data.

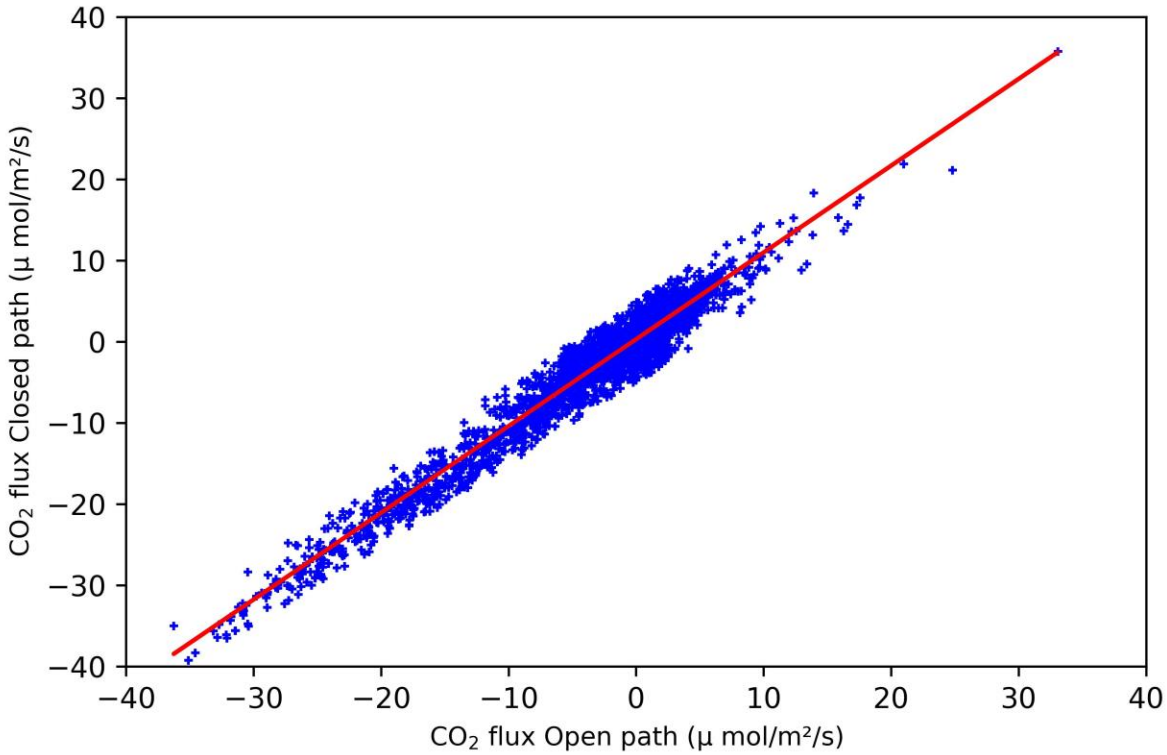

Figure 3-4: Comparisons between fluxes obtained using two different EC systems: closed-path and open-path systems. Data on the graphs are half-hourly fluxes. Redline is the 1:1 line.

After preliminary analysis and data filtering, it was found that 26.91% of data points were missing and three types of missing data types were identified. Short-term gaps: these comprise 1-4 consecutive missing 30-min data points and accounted for 37% of the total missing data. They mainly occurred due to unpredictable weather changes. Medium-term gaps: comprised of 5-12 consecutive missing data points, accounting for 40% of the missing data. Low turbulent conditions and inclement weather were the primary reasons for these gaps. Long-term gaps: considered to be gaps with twelve consecutive missing data points, making up the remaining 23% of the missing data. These gaps were largely attributed to equipment failures. The extreme cold in February pushed the closed path gas analyzer's temperature regulation system to its limits. This led to a shutdown from February 12 to February 17 to facilitate the replacement of the heating system. In addition, there were brief shutdowns in March and April due to maintenance and power failures, with each lasting less than three days.

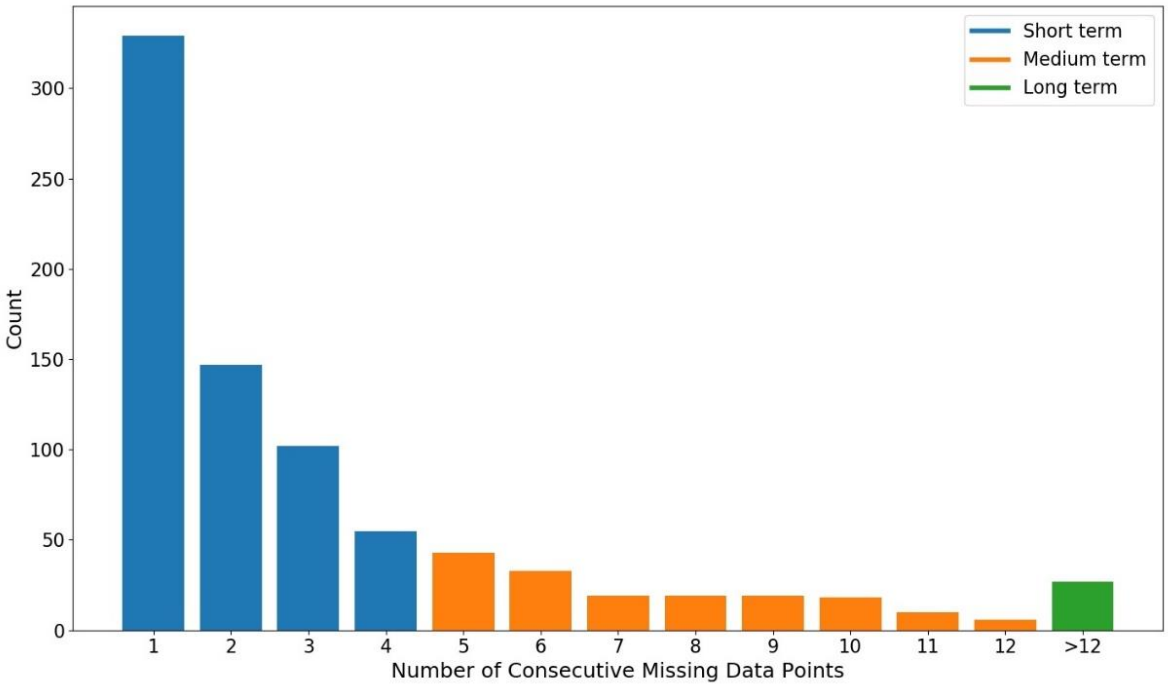

Figure 3-5: Frequency distribution of the consecutive missing data points.

3.4.3 Neural network training

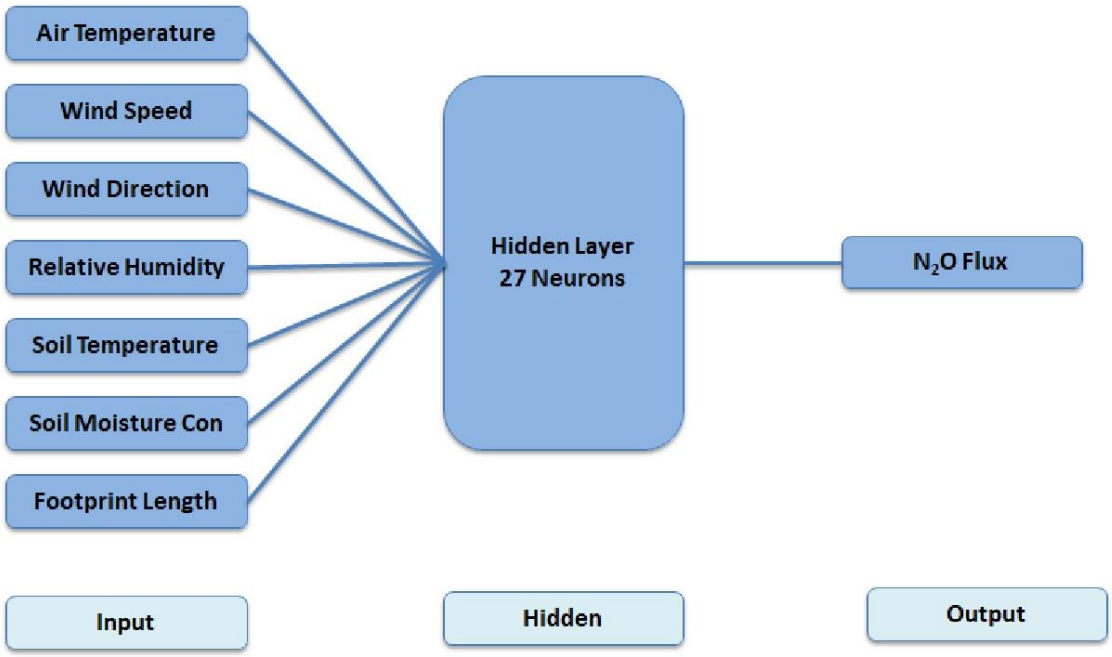

Figure 3-6: Architecture of the Artificial Neural Network (ANN) for N_2O Flux Prediction.

Based on the highest R^2 value of the test data from 50 runs, the optimum number of hidden neurons was determined to be 15, resulting in a final network configuration of 7-15-1 (seven input variables, 15 neurons in the hidden layer, and one output layer for N_2O flux). The network was trained using the training dataset, and the training process was repeated 100 times to ensure robustness. The best-performing network was selected based on the highest R^2 value for the testing data. The selected network achieved an R^2 of 0.64 for the testing dataset, with a correlation coefficient of 0.7994 (p=0.001) between the predicted and observed values(Figure 3-8), significant at the 1% confidence level.

The progression of mean square error (MSE) during the training process for the training, validation, and testing datasets is shown in Figure 3-7. The MSE for the validation dataset decreased until the 32nd epoch, after which it began to increase, indicating potential overfitting. Therefore, the ANN at the 32nd epoch was selected as the best-performing network. The predicted N_2O values generated by the trained network were subsequently used to evaluate the performance of the ANN relative to other gap-filling techniques.

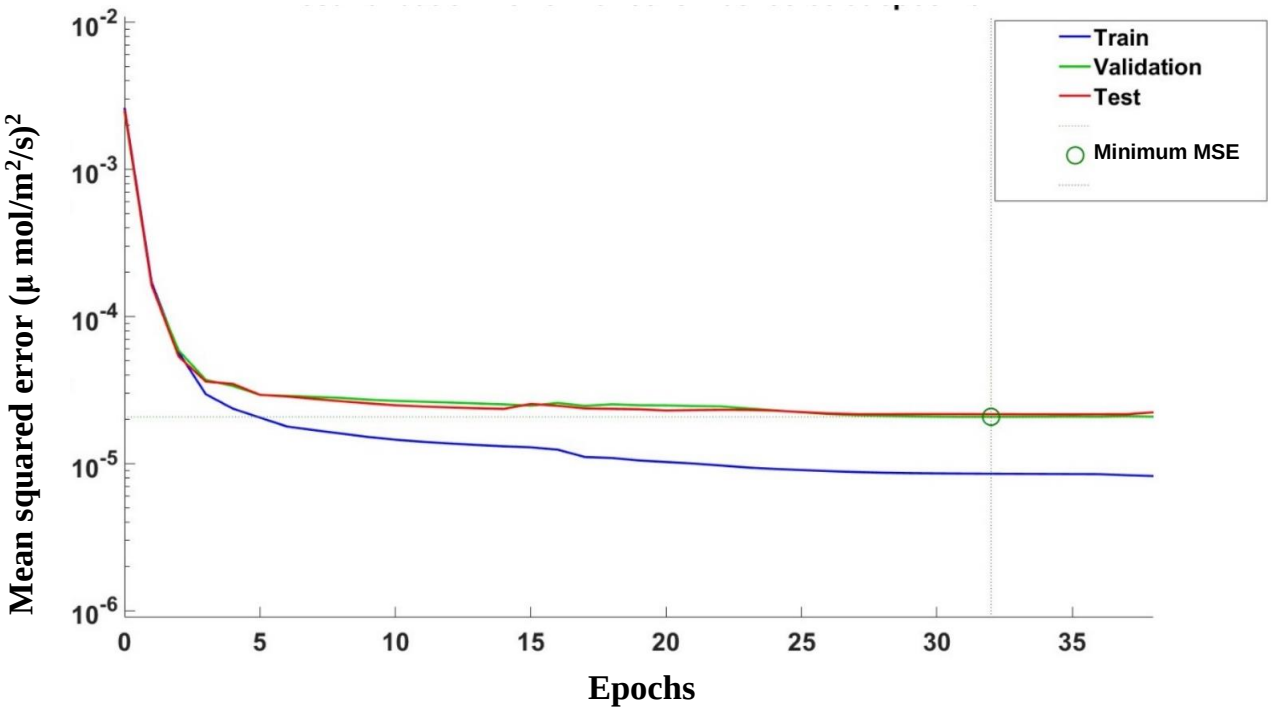

Figure 3-7: Training status of the artificial neural network (ANN) model using the MSE. MSE for the training data set shows in the blue line, green lines show the MSE for the validation data

set and the red shows the MSE for the test data set. The MSE for the validation data decreases from beginning up to 32nd epoch and minimum MSE achieved at the 32nd epoch.

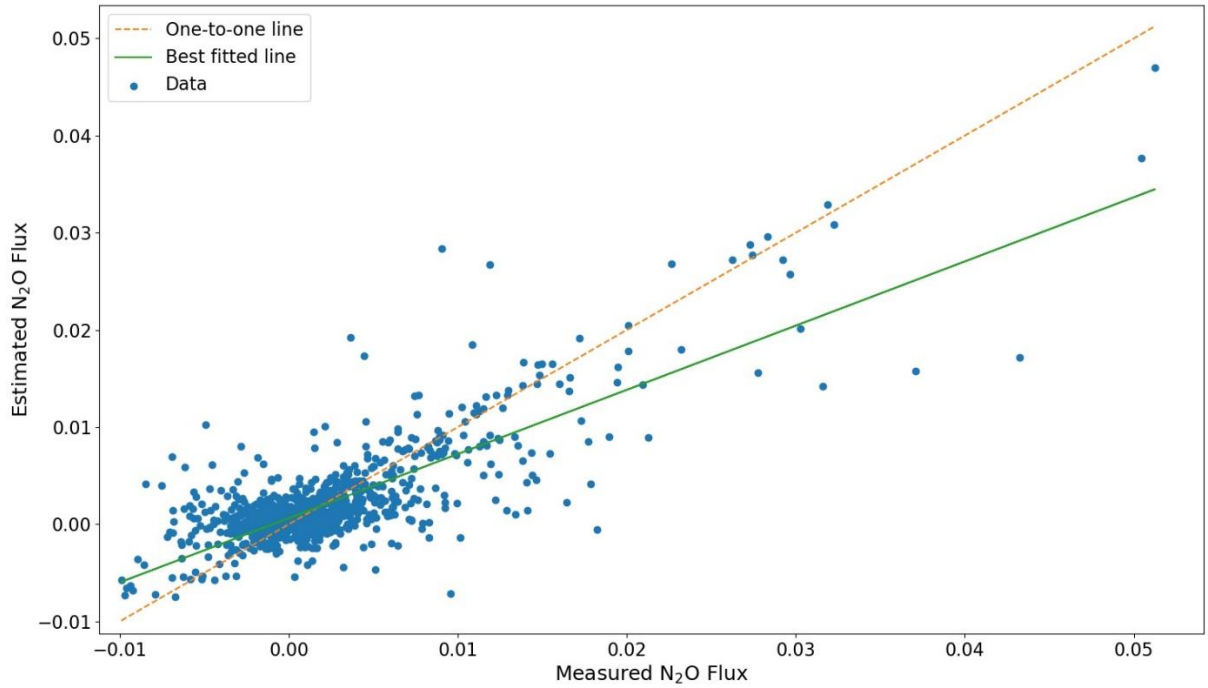

Figure 3-8: Correlation between the actual values and the ANN predicted values, orange line shows the hypothetical prefect correlation, and the green line shows the best fitted line to show the relationship between the actual values and the predicted values.

3.4.4 Performance of gap filling methods

The performance of the two gap-filling methods was evaluated for short term gaps, medium-term gaps and the long-term gaps using the MSE, BE, and the R^2. The performance of the methods to fill artificial gaps of different lengths in N_2O flux was initially assessed compared with the linear interpolation method.

The linear interpolation method had a noticeable increase in RMSE moving from short gap length towards very long gaps. For example, RMSE for single missing data was 0.0029 $\mu mols^{-1}m^{-2}$ and for the gaps that has more than 12 consecutive missing points was 0.00458 $\mu mols^{-1}m^{-2}$. Moreover, the R^2 values showed that the linear interpolation method does not explain the variability of the predictor values well when the data series has a large number of missing data points. The R^2 value dropped from 0.599 for a single missing point to 0.038 for gaps exceeding 12 missing data points. Similar behavior of the R^2 was observed by (Taki et al., 2019,Bigaignon et al., 2020a) who tested

the linear interpolation methods to fill the gaps in N_2O emission data. Furthermore, the Bias error for the short-term gaps predictors remains in the negative territory and for the long term gaps the linear interpolation predictor has large positive BE. For the ANN predictions RMSE increases with the number of consecutive gaps increases, The RMSE for the single missing data was 0.00306 and the more than 12 consecutive missing data points the RMSE was 0.00380. Compared to the linear interpolation methods the ANN predictions have low RMSE values when the data series has more than four consecutive missing data points. The BE moves from a large negative value to a small negative value when the number of missing data points increases. However, the BE remained in negative territory for all types of predictions. The R^2 of the ANN estimates slightly increase with the number of gaps increases. For the single missing point, the R^2 was 0.55 and for the very large gaps the R^2 was 0.60 (Figure 3-9).

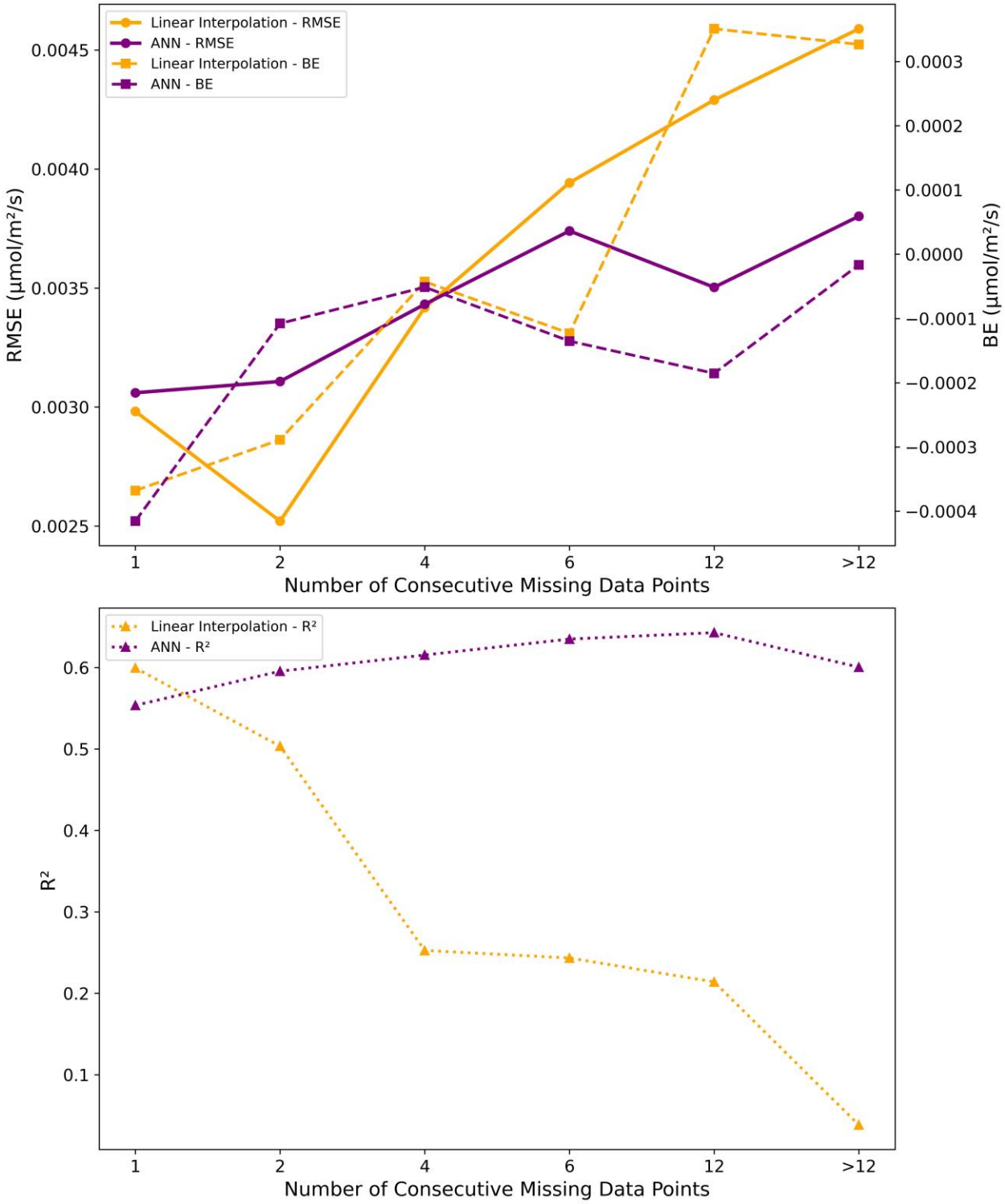

Figure 3-9: Relationship between missing data points and coefficient of determination (R^2), biased error (BE) and root mean square error (RMSE) for the relationship between measured N_2O fluxes and estimated fluxes using linear interpolation and artificial neural networks.

Based on the all the statistics described in the paragraph above, the linear interpolation method is more suitable to fill the gaps the length is less than or equal to four. For filling the large gaps, the ANN performs better compared to the linear interpolation method. The uncertainty associated with filling each type of gap using both methods evaluated, and the ANN consistently exhibited the least uncertainty had lowest uncertainty for all types of the gaps. Figure 3-10 shows the segment of original N_2O time series that filled using both gap filling methods along with the observation data. The error bars show the uncertainty of the correspondent estimation.

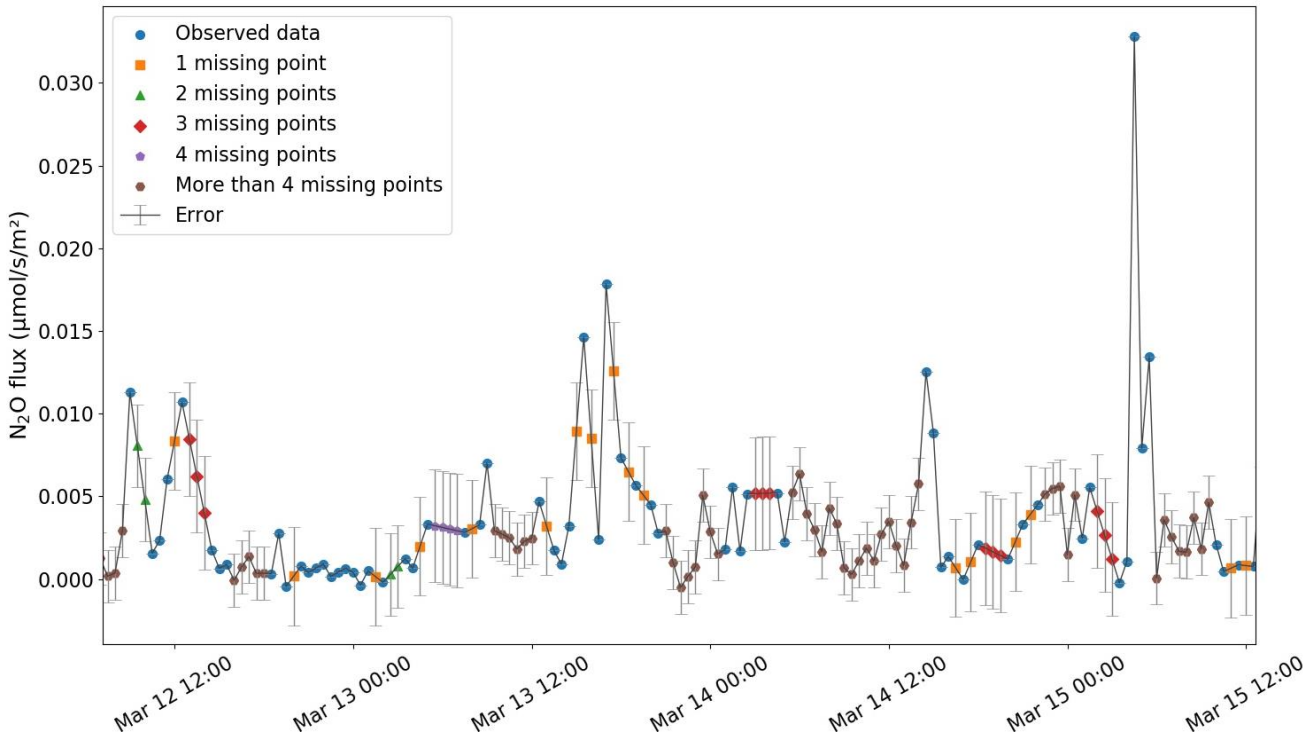

Figure 3-10: Segment of the gap filled N_2O time series that include original data and different data gap sizes. The error bar shows the standard error.

The measured N_2O time series was gap filled using both linear interpolation and the ANN in such a way that the small gaps (length<=4) using the linear interpolation and the medium-term to long-term(length>4) gaps using the ANN and daily average fluxes were calculated. From November 2020 the May 2021 the average N_2O emission was 21.08g N_2O-N ha^{-1} d^{-1} after filling the gaps. However, the emission value was 16.36 g N_2O-N ha^{-1} d^{-1} when without filling the gaps. The total BE associated with the estimated value was -1.16 N_2O-N ha^{-1} d^{-1}.

During the observation period, the highest N_2O emission occurred on March 2021 with the average emission of 21.84g N_2O-N ha^{-1} d^{-1} and the associated BE was 1.09 g N_2O-N ha^{-1} d^{-1}after filling the gaps. Data acquisition was conducted during both the dormant winter and fall and spring growing seasons. Emissions during the dormant season remained near zero, as this period is typically associated with minimal emission activity. However, relying solely on data from the growing season to estimate annual emissions may introduce a potential bias, as it fails to account for the reduced emission rates characteristic of the dormant season.

Garson's algorithm, as illustrated in equation (8) was used to calculate the relative importance of the variables used to in the ANN model. A comprehensive evaluation revealed that the individual contributions of these variables were relatively modest, with their significance spanning a range from 8.9% to 24.3%. Soil moisture content, which has relative importance 24%, was the most affecting variable among all the input variables. The soil temperature appeared to exert the least influence on the model, with its relative importance quantified at 8%. Other variables such as wind speed, air temperature, wind direction, flux footprint length along the prevailing wind trajectory, and relative humidity demonstrated relative importance of 16%, 15%, 14%, 11%, and 10%, respectively.

Here the flux footprint length and the wind direction both have notable relevance to the N_2O fluxes. This finding highlights a key point from our study: the pronounced spatial variability in N_2O fluxes, even within a homogenous agricultural landscape. Such variability suggests that local factors, possibly microclimatic or soil-related, can play a pivotal role in influencing N_2O emissions, underscoring the need for more granular data collection and analysis in future studies.

3.5 Discussion

In this study, the eddy covariance technique was used to measure N_2O fluxes within an agricultural setting, with flux averages computed at 30-minute intervals. The frequency of these measurements provided detailed insights into the duration of high flux events, their occurrence rates, the lags between these events, and the flux responses post-fertilization and rainfall. Notably, elevated emissions were typically observed between 2 days to 14 days following field fertilization. Recognizing these specific emission windows is crucial for research endeavors that lack the capability for continuous long-term monitoring, allowing for optimized resource allocation during these critical periods.

3.5.1 Challenges of data gaps in N_2O emission studies

Due to environmental and human factors, the N_2O fluxes time series had gaps ranging from short-term to long-term, with 26.91% of data points missing. This level of data loss aligns with findings from previous studies, such as those utilizing chamber and gradient techniques to estimate daily average fluxes, which reported approximately 30% missing data (Taki et al. 2019; Rochette and Eriksen-Hamel 2008). Given the high temporal variability of N_2O emissions, data gaps during high-emission events significantly impact overall N_2O emission estimates if not addressed properly.

3.5.2 Evaluation of gap-filling methods

This study evaluated two different gap-filling methods, linear interpolation and artificial neural networks (ANNs), to address short-term, medium-term, and long-term data gaps. The performance of these methods was assessed using RMSE, BE, and R^2 metrics. These findings demonstrated that ANNs were particularly effective for medium and long-term gap filling, outperforming linear interpolation, which only excelled for short-term gaps. This aligns with the study by Taki et al. (2019), which emphasized that ANNs could handle the non-linear, complex nature of N_2O emissions more effectively than simpler interpolation methods. Their comparison of gap-filling techniques showed that ANN's non-linear modeling capabilities allowed it to capture interactions between environmental variables and emissions, enhancing predictive accuracy during varied gap lengths.

Furthermore, Bigaignon et al. (2020) also validated the advantage of ANNs for N_2O data, demonstrating that combining ANNs with linear interpolation enhanced performance, especially for prolonged data gaps. This reinforces the conclusion from this study that hybrid approaches can optimize gap-filling strategies for better accuracy. Goodrich et al. (2021) expanded on this by highlighting the potential of advanced ANN algorithms to reduce uncertainties in N_2O flux estimates, which complements our findings where ANNs consistently exhibited lower uncertainty than linear interpolation.

Dengel et al. (2013) underscored the efficacy of ANNs for predicting CH_4 emissions, from high latitude wetlands; a gas that, like N_2O, has complex, episodic emission patterns influenced by environmental conditions. This study's use of cross-correlation methods alongside ANNs to identify the time lags between environmental variables and N_2O fluxes align with Dengel et al. approach to recognizing non-linear interactions and variability in GHG fluxes.

The analysis from this study also highlighted the significant role of soil moisture content as the most influential factor for N_2O flux prediction. This finding mirrors insights from Taki et al.(2019) and Ooba et al. (2006), who pointed out that ANN models, when trained with relevant environmental input variables, can prioritize factors based on their contribution to flux variability. The notable importance of wind direction in the ANN model, as shown in this research, points to spatial variability within fields, a point also suggested by Goodrich et al. (2021), where local microclimatic influences were found to affect N_2O emissions.

The comparative performance results of ANNs and linear interpolation reflect Taki et al. (2019) findings, where ANNs outperformed traditional methods in long-term data gaps, providing more reliable cumulative emission estimates. Bigaignon et al. (2020) and Goodrich et al. (2021) also corroborated the ability of ANNs to yield better RMSE and R^2 scores for larger gaps, emphasizing the robustness of neural network models in gap-filling applications.

Overall, the integration of ANNs for gap-filling demonstrated significant improvements in medium to long-term gaps, with ANN models showing resilience in capturing the variability and non-linearity of N_2O emissions. The proposed approach combining linear interpolation for short-

term gaps and ANNs for longer gaps proved to be effective, as evidenced by an estimated average N_2O emission of 21.08 g N_2O -N ha^{-1} d^{-1} for the study period. The difference of 4.72 g N_2O -N ha^{-1} d^{-1} between gap-filled and non-gap-filled time series underscores the importance of robust gap-filling techniques to avoid underestimation or overestimation of emissions.

3.5.3 Study limitations and future directions

This study, conducted from November 2019 to May 2020, did not include data from certain months, such as September, October, and early November, which could potentially exhibit comparable or even higher N_2O emissions than some of the monitored months due to harvest-related activities, soil preparation, and post-harvest nitrogen dynamics. While this temporal limitation could introduce bias in estimating annual emissions, the focus of this study was elucidating the controlling factors of N_2O emissions and evaluating gap-filling methodologies.
The selected study period provided critical insights into N_2O fluxes during specific management and environmental conditions, such as winter wheat growth phases and post-fertilization events. These conditions allowed us to capture key drivers of emissions, including soil moisture and temperature dynamics, and assess the performance of the artificial neural network (ANN) in addressing high-frequency data gaps. The study design was deliberately constrained to a shorter term to ensure detailed evaluation of these factors while maintaining manageable data complexity for modeling.

Future research should address the temporal limitations by incorporating year-round data collection to capture the full spectrum of seasonal variability in N_2O emissions. This aligns with recommendations by Taki et al. (2019) and Goodrich et al. (2021), advocating for comprehensive data collection to improve the accuracy of annual greenhouse gas inventories. However, the findings from this study, particularly the demonstrated ability of the ANN to fill high-frequency data gaps and identify driving variables, provide a robust foundation for expanding temporal coverage in future investigations.

.

Chapter 4 - Assessing the use of eddy covariance and flux scaling to estimate methane emissions from a simulated herd of cattle in a grazing system.

4.1 Abstract

This study evaluates the application of the eddy covariance (EC) technique combined with footprint analysis and flux scaling to estimate methane (CH_4) emissions from a simulated herd of cattle in a grazing system. Controlled CH_4 release experiments were conducted at Rannells' Ranch in Kansas to simulate emissions from cattle, with methane released at known rates multiple point sources. The EC system was used to measure the vertical CH_4 fluxes, allowing for the assessment of the technique's ability to accurately capture emissions in an extensive grazing environment. The results demonstrated significant underestimation of CH_4 emissions, with the estimated emission rates clustering around 30% of the actual release rate. Footprint analysis showed that the source area coverage increased when the fetch percentage was raised to 90%, improving the alignment with the intended source area. However, this improvement came at the cost of greater instability in the footprint model, introducing higher prediction errors in the flux estimates. Despite these adjustments, the calculated CH_4 fluxes were consistently lower than the known release rates.

The study further revealed that spatial variability within the footprint area and wind conditions had significant impacts on CH_4 emission measurements, emphasizing the challenges of applying the EC technique in complex grazing systems. The use of a homogeneous 20 m^2 source area in the release experiments highlighted the limitations of current footprint models in accurately representing real-world conditions, where cattle may spread over a much larger area. Overall, the findings suggest that while the EC technique holds potential for estimating CH_4 emissions in grazing systems, significant improvements are needed in footprint modeling to account for the spatial heterogeneity and dynamic nature of such environments. This research provides important insights into refining CH_4 measurement methodologies, contributing to more accurate greenhouse gas emission inventories for agriculture.

4.2 Introduction

Methane (CH_4), a potent greenhouse gas with a global warming potential 28 times that of carbon dioxide, significantly contributes to global radiative forcing (IPCC, 2014). In the United States, the agriculture sector is responsible for 9.3% of total greenhouse gas (GHG) emissions, with enteric fermentation and manure management being the primary sources (EPA, 2023). These processes are estimated to produce 9.31 Tg of CH_4 annually (EPA, 2023). Cattle, which spend 70% to 80% of their lives in grazing systems, significantly contribute to atmospheric CH_4 emissions from these often-overlooked grazing lands (Hristov et al. 2013). Current GHG inventories predominantly rely on measurements from individual animals or centralized hubs (Godde et al. 2020), rather than from grazing systems. This discrepancy highlights the inaccuracies in current estimations and underscores the necessity for accurate quantification of emissions in grazing systems to better understand and mitigate their impact and refine GHG inventories (Hristov et al. 2013). Various methodologies have been utilized to measure and estimate methane emissions from ruminants, each presenting distinct advantages and limitations (Hristov et al. 2013; Jungbluth et al. 2001; Kinsman et al. 1995).

Chamber techniques, including open-path and closed-path systems, are considered as the good standard for measuring CH_4 emissions from individual animals (Johnson et al. 1994). These techniques deliver highly accurate and direct measurements, enabling detailed analyses of individual animal variations and the impacts of different diets or ration additives (Troy et al. 2016). Despite their precision, chamber techniques have notable limitations. They are labor-intensive, restricting their use to a limited number of animals (Johnson et al. 1994). More critically, confining animals within chambers can alter their natural behavior and potentially affect CH_4 production, introducing uncertainties in the measurements (Harper et al. 2011). The artificial environment created by chambers raises concerns about the extrapolation of chamber-based data to larger, more representative scales, thereby putting into question the accuracy of current GHG emission estimates derived from these techniques (Johnson et al. 1994). Although chamber studies have contributed valuable insights, their inherent limitations underscore the need to explore alternative methods capable of providing more representative and scalable measurements of CH_4 emissions.

The SF_6 tracer technique has gained recognition as an effective method for measuring enteric CH_4 emissions from individual ruminants in grazing settings (Lassey et al. 2011; Johnson et al. 1994). This technique involves the administration of a small permeation tube containing sulfur hexafluoride (SF_6) into the rumen of the animal. The SF_6 gas is released at a known and consistent rate from the permeation tube, allowing it to act as a tracer for methane emissions. As the animal exhales, both SF_6 and CH_4 are emitted, and air samples from the exhaled breath are collected using a sampling apparatus placed near the animal's nostrils or mouth.

The air samples are later analyzed to determine the concentration ratio of CH_4 to SF_6. Since the release rate of SF_6 from the permeation tube is known, this ratio can be used to calculate the rate of methane emissions from the animal. This approach presents several benefits over conventional micrometeorological methods, particularly in its capacity to measure emissions under more natural grazing conditions, thereby reducing the impact of confinement on animal behavior (Harper 2005). By enabling animals to graze naturally, the SF_6 tracer technique offers a more accurate evaluation of methane emissions in their typical environment. This method improves the accuracy of CH_4 emission estimates by reflecting the animals' normal grazing activities and dietary habits (Johnson et al. 1994).

Despite its advantages, the SF_6 tracer technique also faces certain limitations. The labor-intensive nature of the method, which requires specialized equipment for gas analysis, poses challenges for widespread implementation (Johnson et al. 1994). The necessity for precise calibration and maintenance of the equipment adds to the complexity and cost of the technique (Lassey et al. 2011). Additionally, the SF_6 tracer technique is not well-suited for measuring emissions from large groups of animals, thereby limiting its practicality for large-scale assessments (Lassey et al. 2011). Furthermore, the handling and administration of SF_6 gas necessitate stringent safety and environmental precautions due to its potent greenhouse gas properties (Harper 2005).

Despite these limitations, the SF_6 tracer technique remains a valuable tool for measuring enteric CH_4 emissions from individual ruminants under grazing conditions. Its ability to capture emissions in a natural grazing environment provides a more accurate representation of methane production in real-world settings, which is crucial for developing effective mitigation strategies and refining

greenhouse gas inventories (Johnson et al., 1994; Harper 2005; Lassey et al., 2011). The technique's contribution to the field underscores the importance of continuous innovation in measurement methodologies to enhance the reliability and applicability of emission data.

Inverse dispersion modeling (IDM) presents a compelling alternative for estimating CH_4 emissions from agricultural fields (Flesch et al. 1995). IDM works by using measurements of CH_4 concentrations and wind statistics at a single location within the emission plume to deduce the emission rate from the source. This method offers numerous advantages over traditional approaches, such as reduced setup time, lower costs, and the capability to assess emissions from extensive areas (Wilson et al. 2013; FLESCH et al. 2005; Flesch et al. 2014) . The accuracy of IDM hinges on the model's ability to accurately represent atmospheric dispersion. A variety of dispersion models have been utilized in IDM research, ranging from straightforward Gaussian plume models to more sophisticated models that incorporate atmospheric turbulence and local advection (Gimson and Uliasz 2003). Several studies have validated the efficacy of IDM in estimating CH_4 emissions from agricultural sources. For example, Flesch et al. (1995) successfully applied IDM to measure CH_4 emissions from cattle feedlots, demonstrating the method's practical applicability. Similarly, Bühler et al. (2022) employed IDM to estimate CH_4 emissions from bio gas and water treatment plants, further showcasing the technique's versatility. Despite its promise, IDM remains a relatively novel method for quantifying CH_4 emissions from agricultural fields. Continued research is essential to refine dispersion models, enhance measurement techniques, and validate IDM findings against traditional methods. Ongoing advancements in these areas will be crucial for increasing the reliability and acceptance of IDM. Nonetheless, IDM holds significant potential as a cost-effective and efficient tool for estimating CH_4 emissions from agricultural sources, offering a viable alternative to more established methodologies (Gao et al. 2009; Ro et al. 2013; FLESCH et al. 2005; Wilson et al. 2013).The development and application of IDM are vital for improving our understanding of CH_4 emissions in agricultural contexts. By providing accurate and scalable emission estimates, IDM can contribute to better greenhouse gas inventories and more effective mitigation strategies, ultimately helping to address the environmental impacts of agricultural practices.

The backward Lagrangian stochastic (bLS) model, developed by Flesch et al. (1995, 2004), has become an essential tool for estimating greenhouse gas emissions, particularly methane (CH_4), from agricultural sources. Its non-intrusive methodology allows for emission measurements on a landscape scale without interfering with livestock or farming activities (FLESCH et al. 2005; Laubach 2010). This micrometeorological technique utilizes gas concentration measurements, wind data, and turbulence statistics to calculate gas advection by predicting particle trajectories from the source to the sensor (Flesch et al. 1995, 2004, 2005; FLESCH et al. 2005; Wilson et al. 2013). The model operates under the assumption of horizontally homogeneous flow, as described by Monin-Obukhov similarity theory. Theoretically, it can estimate GHG emissions over an ideal surface layer from any source, regardless of size or shape. However, the model's applicability is limited to non-uniform, complex wind environments. To address this limitation, one approach involves incorporating predicted turbulent wind data into the inverse dispersion model, as suggested by Wilson and Yee (2003). Alternatively, an idealized dispersion model can be used, which simplifies the complexities of wind patterns (Wilson et al. 2001). Modeling disturbed wind patterns remains challenging, and the accuracy of the results is highly dependent on the model's ability to replicate atmospheric conditions accurately (Wilson and Yee, 2003). Using standard wind data in a Monin-Obukhov similarity theory-based bLS model, while acknowledging its limitations, could be a straightforward approach. Understanding the model's accuracy in turbulent wind situations is crucial for its effective application.

Several studies have validated the effectiveness of the bLS model in estimating emissions from agricultural plots. Feitz et al. (2018) conducted a controlled release experiment of CH_4 and CO_2, comparing various emission quantification techniques, including the bLS model. Their findings indicated that most CH_4 estimates using the bLS model were within 20% of the actual release rate, underscoring its efficacy when parameters are optimized. Prajapati and Santos (2018) specifically evaluated the bLS model's performance in estimating CH_4 emissions from beef cattle feedlots. Additionally, the bLS model's adaptability has been demonstrated through modifications such as incorporating terrain models to enhance accuracy in regions with varied topography (Gao et al. 2009). A notable limitation of the bLS model is its reliance on precise background and downwind concentration data, necessitating the complex process of cross-calibrating multiple gas analyzers (Laubach et al. 2013; McGinn 2013). The model's accuracy is significantly influenced by specific

atmospheric conditions; low wind speeds and highly stable or unstable atmospheric stratifications can adversely affect the reliability of bLS estimates (McGinn 2013). Despite these challenges, the bLS model remains a promising tool for estimating greenhouse gas emissions from agricultural sources. Continued research is necessary to refine its application and improve its accuracy across diverse environmental settings.

The eddy covariance (EC) technique has emerged as a widely used method for directly quantifying gas exchanges, including carbon dioxide (CO_2), methane (CH_4), and water vapor, between ecosystems and the atmosphere (Baldocchi 2003). Its direct and non-intrusive approach, coupled with its ability to deliver continuous, long-term measurements, has established its importance in micrometeorological studies. The EC technique operates on the principle of turbulent transport, where eddies mix gases within the atmospheric boundary layer (Aubinet et al. 2012). By capturing high-frequency fluctuations in gas concentrations and vertical wind speeds, the EC method quantifies the net gas exchange between the surface and the atmosphere. This is achieved by calculating the covariance between the vertical wind speed and the gas concentration, which reflects the gas flux (Baldocchi 2003).

The EC technique has been extensively used to measure CO_2 fluxes in various ecosystems, including forests, grasslands, and agricultural fields (Baldocchi 2008). These measurements have significantly advanced our understanding of the carbon cycle and the role of different ecosystems in carbon sequestration. For instance, EC measurements have demonstrated that forests are significant carbon sinks, absorbing more CO_2 from the atmosphere than they emit (Curtis Hanson et al. 2002).

Recent advancements in fast-response optical sensors have expanded the application of the EC technique to other trace gases, such as CH_4, nitrous oxide (N_2O), and ammonia (NH_3) (Xu et al. 2014; Sun et al. 2015; Peltola et al. 2013; Detto et al. 2011; Curtis Hanson et al. 2002). The EC technique has proven particularly valuable in quantifying CH_4 emissions from livestock, a significant source of anthropogenic greenhouse gases (Nalon et al. 2013). Numerous studies have utilized EC to measure CH_4 fluxes from feedlots, providing crucial data for improving emission inventories and developing mitigation strategies (Prajapati and Santos 2017).

The eddy covariance (EC) technique measures the vertical flux of gases between the land surface and the atmosphere at a single point, providing a continuous and high-frequency assessment of gas exchanges. However, the measured flux is not solely a localized value but represents a spatially weighted average of emissions from the upwind area contributing to the flux. This contributing area is known as the flux footprint, which is influenced by factors such as sensor height, surface roughness, wind direction, and atmospheric stability (Schuepp et al. 1990).

The emission footprint is critical in interpreting EC data, particularly in non-homogeneous landscapes like grazing systems. It delineates the spatial area from which emissions are measured, allowing researchers to attribute fluxes to specific sources, such as cattle or microbial soil activity. Accurate footprint analysis is essential for several reasons:

1. **Source Attribution:** By identifying the specific areas contributing to the flux, footprint analysis ensures that emissions are attributed to the correct sources, minimizing errors caused by extraneous contributions.
2. **Measurement Accuracy:** Footprint modeling accounts for spatial variability, ensuring that flux measurements reflect the actual emission patterns in heterogeneous environments.
3. **Scaling Emission Estimates:** In complex systems, such as grazing environments, footprint analysis enables the scaling of localized measurements to larger areas, improving the accuracy of regional or national greenhouse gas inventories.
4. **Experimental Design:** Understanding the footprint helps optimize the placement of EC towers and other sensors to maximize data representativeness and reduce uncertainties.

While footprint analysis is often less critical in homogeneous systems, such as large feedlots where cattle are evenly distributed (Gao et al. 2011), it becomes indispensable in grazing systems. Here, cattle movement, uneven emission distribution, and dynamic environmental conditions can significantly influence the flux footprint. Accurate interpretation of EC data in these settings requires advanced footprint models that account for the spatial and temporal variability of emissions. Without such analysis, flux measurements may underestimate or misrepresent the true emission dynamics, as they fail to account for contributions from sources outside the assumed area.

To improve the accuracy of CH_4 emission estimates, several studies have combined the EC technique with other methods. Neftel et al. (2008) developed a footprint weighting tool based on a 2-dimensional analytical footprint model by Kormann and Meixner (2001), which allowed them to account for the spatial variability of N_2O sources within the measurement area. Their results demonstrated that the EC technique, when combined with footprint analysis, provided reliable estimates of N_2O emissions, capturing the spatial heterogeneity of the fluxes. Dengel et al. (2011) utilized the EC technique to measure CH_4 emissions from grazing sheep and found close agreement with IPCC estimates. They emphasized the importance of considering the spatial distribution of sheep within the measurement footprint. Felber et al. (2015) advanced this approach by integrating GPS tracking of dairy cows to interpret CH_4 emissions from a grazing system. They combined EC flux measurements, an analytical footprint model, and GPS data to estimate CH_4 emissions, reporting consistency with other studies. However, Felber et al. (2015) observed a systematic underestimation of CH_4 emissions from animals far from the flux tower, attributing this to uncertainties in the analytical footprint model and suggesting that more sophisticated Lagrangian footprint model could improve predictability.

Coates et al. (2017) enhanced the accuracy of CH_4 emission estimates by combining the EC technique with a Lagrangian stochastic model. In a controlled CH_4 release study, they demonstrated that this combined approach provided accuracy comparable to other micrometeorological techniques. Their study confirmed that the estimated CH_4 emissions per animal were consistent with reported values, reinforcing the reliability of the EC technique for estimating livestock CH_4 emissions.

Overall, while the EC technique holds great promise for accurately measuring greenhouse gas emissions from agricultural sources, ongoing research is needed to refine its application and enhance its accuracy in diverse environmental settings. For instance, Prajapati and Santos (2017) emphasized the importance of footprint analysis in EC studies by comparing two footprint models (Kljun et al. 2015; Kormann and Meixner 2001) to estimate CH_4 emissions from beef cattle in a feedlot, revealing significant differences in source area estimates.

The objective of the current study is to evaluate the efficacy of the eddy covariance method with footprint parameterization to estimate CH_4 flux in grazing systems using a synthetic source.

4.3 Material and methods

4.3.1 Site description and instrument setup

The field experiment was conducted at Rannells' Ranch, a Flint Hills Prairie Preserve manage by Kansas State University near Manhattan, Kansas, USA (39° 08' 28"N, 96° 31' 31"W, 324 m asl), from November 2022 to April 2024. The selected grazing unit spans 31 hectares and is burned annually in late April. This unit was chosen due to its topography, which is ideal for micrometeorological measurements.

A custom-built gas manifold was used to control the release of CH_4 at a rate of 600 to 9000 g CH_4 day^{-1}, through 10-point sources spread across 12 m^2 area on the southwest side of the experimental area. CH_4 gas of 99.97% purity was delivered from a compressed tank to a proportional solenoid valve (PVQ13, SMC, Noblesville, IN) via high-density polyethylene tubing (I.D. 5.3 mm). The gas pressure was initially controlled by a two-stage pressure regulator. The proportional valve was connected to an aluminum manifold with the same type of tubing. A pressure transducer (PX119-030GI, Omega, Norwalk, CT) monitored the manifold pressure. CH_4 flowed from the manifold through ten 0.253-mm precision orifice assemblies (K2-10-SS, O'Keefe Controls Co., Monroe, CT) connected to 8m high-density polyethylene tubing. These tubes were mounted on metal rods at a height of 0.7 m above the ground. During CH_4 release campaigns, the manifold pressure was maintained at a constant value to achieve the desired flow rate, by adjusting the voltage applied to the proportional valve using a datalogger (CR1000, Campbell Scientific). The CH_4 tank was weighed at the beginning and end of the release campaigns to determine the mass of gas released using a scale (D125WQL, Ohaus, Parsippany, NJ).

Wind velocity, including three orthogonal components and temperature, was measured using a sonic anemometer (CSAT3, Campbell Scientific, Logan, UT). A closed-path gas analyzer (G2311-f, Picarro Inc., Santa Clara, CA) was used to measure concentrations of CH_4, CO_2, and H_2O. The air intake of the analyzer featured a rain diverter connected to an inline filter (10 µm membrane, Pall Corporation, Ann Arbor, MI) positioned 15 cm from the sonic anemometer. Air was drawn through 5.8 m high-density polyethylene tube with an inner diameter of 5.3 mm into the analyzer. A vacuum pump (MD 4 NT, Vacuubrand GmbH, Wertheim, Germany) and the analyzer's internal

mass flow controller maintained a flow rate of 5 L min^{-1}. The sonic anemometer and the closed-path analyzer air inlet were mounted on a tower approximately 5.3 m above the ground. Given that the prevailing wind direction in this area is southwest, the flux tower was strategically positioned 60 m northeast of the gas release points. This placement ensured that the sonic anemometer and the gas analyzer air intake were oriented towards the southwest to maximize airflow over the source area.

Data from the sonic anemometer was recorded using a datalogger (CR3000, Campbell Scientific), while the gas analyzer data was recorded internally and later synchronized using timestamps. The Python Pandas package was employed for data synchronization. To minimize synchronization errors, the datalogger clock and the gas analyzer clock were synchronized daily using the clock from another datalogger (CR1000x, Campbell Scientific).

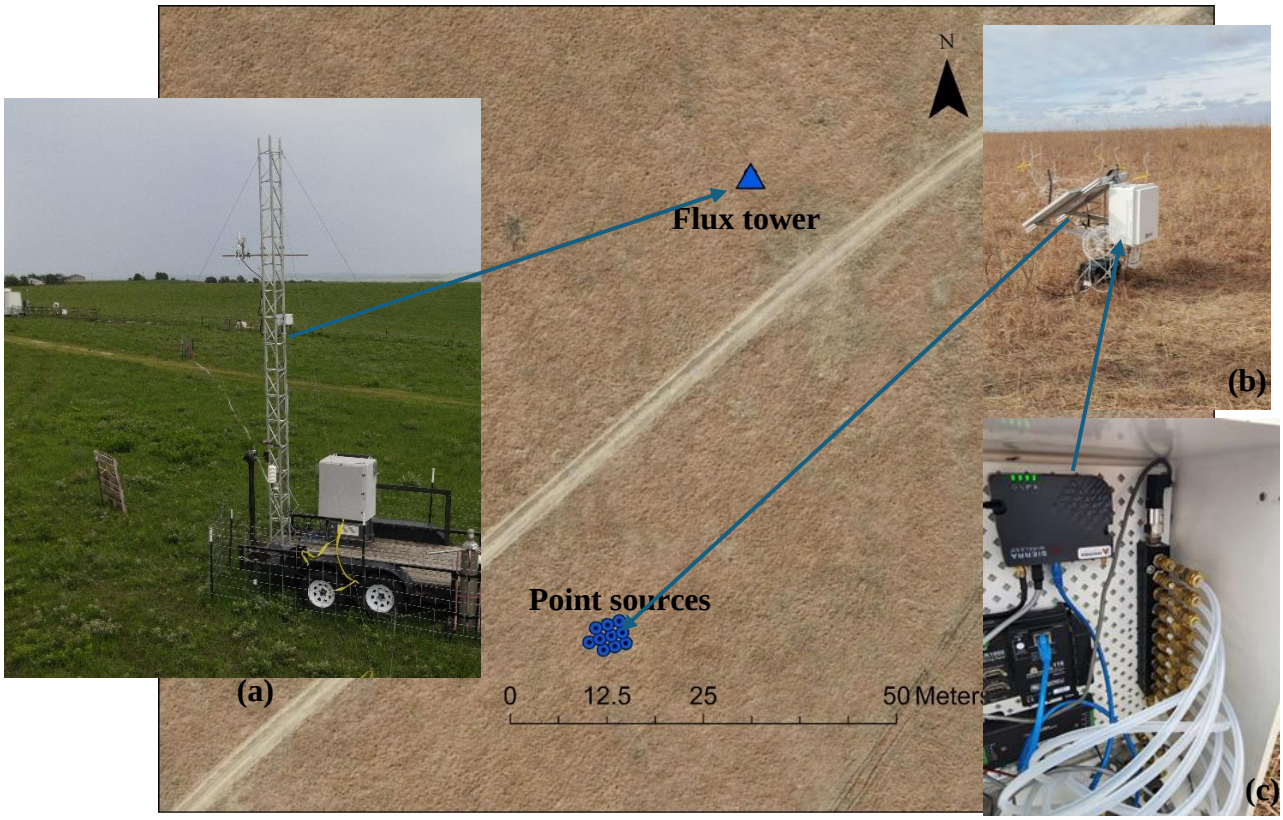

Figure 4-1: Layout of the experimental site the Rannells' Flint Hills Prairie Preserve. Insets: (a) flux tower, (b) gas manifold enclosure and point sources used to release CH_4 at a known rate, and (c) gas manifold and manifold control system.

4.3.2 Flux calculation

The half-hour high-frequency data were processed and analyzed using the EddyPro software (v. 7.0.9, LI-COR). Fluxes of CH_4, CO_2, and H_2O were estimated through this analysis. Turbulent fluctuations were calculated using the block averaging method, while the double rotation method was employed to eliminate the average cross-stream and vertical components of the wind velocity (Wilczak et al. 2001).

Time lags between the sonic anemometer and gas analyzer signals are caused by several factors, including spatial separation of the instruments and differences in signal processing (Aubinet et al. 2012). In closed-path systems, the air travel time through the sampling tube and interactions with the tube walls further delay gas concentration measurements relative to wind velocity readings

(Moravek et al. 2013). To ensure accurate flux calculations and prevent underestimation, it is essential to accurately determine these time lags.

In this study, time lag issues were addressed by using the covariance maximization method (Fan et al. 1990). For the closed-path EC system, time lags were identified within a predefined plausible search window. This process is particularly important in low flux conditions, where noise can produce unrealistic time lag values (Detto et al. 2011). The EddyPro software was used in a preprocessing step to statistically determine the time lags and their variability range.

The closed-path analyzer calculates CO_2 and CH_4 mixing ratios using high-frequency measurements of H_2O in the air. An internal algorithm (Chen et al. 2010) handles this process. This method eliminates the need for density corrections.

Frequency losses in EC systems arise from various factors such as insufficient sensor sampling frequency, separation between sensors, and limited sampling duration. In closed-path systems, additional factors like sampling tubes, filters, and the residence time in the sampling cell contribute to spectral attenuation and flux underestimation (Aubinet et al. 2012). To address these issues, the method proposed by Moncrieff et al. (2006) was applied to correct low frequency losses. For spectral correction, the procedure outlined by Horst (1997) was utilized.

4.3.3 Flux footprint calculation

In this study, footprint calculations were performed using the model proposed by Kljun et al. (2015). This two-dimensional flux footprint parameterization (FFP) is based on the Lagrangian stochastic particle dispersion model LPDM-B (Kljun et al. 2002). The parameterization provides a source weight footprint function ($\emptyset_k$) for various boundary layer conditions and measurement heights.

$$\emptyset_k = \tilde{f}^y(x)\frac{1}{\sigma_{y\sqrt{2\pi}}} exp\left(\frac{-y^2}{2\sigma_y^2}\right) \quad \textbf{(12)}$$

where y represents the crosswind distance from the x-axis, and σ_y is the standard deviation of the crosswind distance, and $\tilde{f}^y(x)$ is the crosswind dispersion function.

The function the crosswind-integrated footprint given by

$$\tilde{f}^{y} = F^{y*}(x^{*})\left(1 - \frac{z_m}{h}\right)\frac{u^{*}}{\widetilde{U}(Z_m)kZ_m} \quad \textbf{(13)}$$

where: $\tilde{f}^{y}$ is the crosswind-integrated footprint function, representing the influence of source areas on the measured flux at a given point, $F^{y*}(x^{*})$ is the scaled crosswind-integrated footprint function, which depends on the non-dimensional distance from the source area to the measurement point x^{*}. This term incorporates the effect of horizontal distance from the source area to the measurement point. $\left(1 - \frac{z_m}{h}\right)$ is a factor accounting for the relative height of the measurement above ground, normalized by the boundary layer height *h*. This term adjusts the footprint for the vertical position of the measurement within the boundary layer. u^{*} is the friction velocity, representing the shear stress exerted by the wind on the surface. It is a measure of turbulence and plays a crucial role in determining the footprint. $\widetilde{U}$ is the mean horizontal wind speed at the measurement height Z_m . This term accounts for the transport of gases by the mean wind flow. *k* is the von Kármán constant, approximately equal to 0.4. It is a dimensionless constant used in boundary layer meteorology.

Here, F^{y*} is the scaled crosswind-integrated footprint, x^{*} is the scaled non-dimensional distance, h is the boundary layer height (*h*), (u*) is the friction velocity, Z_m is the measurement height above, Monin–Obukhov length (*L*), standard deviation of the cross wind component, wind direction, and mean horizontal wind speed (*u*).

The boundary layer height was calculated using the methodology suggested by Kljun et al. (2015), following Batchvarova and Gryning (1991). This calculation required several input parameters, including friction velocity (u*), Monin–Obukhov length (*L*), the Coriolis parameter, sensible heat flux, measurement height above the displacement height (Z_m), standard deviation of the crosswind component, wind direction, and mean horizontal wind speed (u).

4.3.4 Flux scaling

The CH_4 flux per unit surface area was estimated by scaling EC flux measurements using the relative contributions of artificial CH_4 point sources. This approach follows the methodologies proposed by Baum et al. (2008) and Neftel et al. (2008). During time intervals where the majority of the measured flux contributions originate within the grazing system, the observed EC CH_4 flux (F_{obs}) can be attributed to the cumulative effects of artificial CH_4 sources and the sinks from microbial activities in the surrounding area.

The equation used for this estimation is:

$$\boldsymbol{F_{obs} = P_t F_{Release} + (1 - P_t) F_{other}} \quad \textbf{(14)}$$

where P_t represents the normalized footprint contribution from the artificial sources, ranging from 0 to 1, $F_{Release}$ is the CH_4 flux from the artificial sources, and F_{other} is the CH_4 flux from the surrounding area. Assuming F_{other} remains constant over the short period of gas release, CH_4 background concentration was determined using a conditional sampling procedure based on wind direction (Wilson et al. 2013), the equation can be rearranged to estimate $F_{Release}$

$$\boldsymbol{F_{Release} = \frac{F_{obs} - (1 - P_t) F_{other}}{P_t}} \quad \textbf{(15)}$$

This adjusted equation was employed to scale F_{obs} from the landscape scale to the source area scale. Half-hourly values of P_t were estimated by superimposing arrays of $\emptyset_k$ onto a digital map of the grazing area, with polygon representing the artificial source areas. For illustration, Figure 4-1 shows the grazing system map and the calculated source weight function for a selected half-hour period. The digital map was created using high-resolution satellite imagery from ESRI (Esri, California, U.S), with an accuracy of less than 1 meter, and GPS coordinates of the artificial source area points collected using a survey-grade RTK GPS (EMLID Reach RS2, Emlid Tech, Budapest, Hungary).

Arrays of $\emptyset_k$ were computed using Equation (1) for grid cells in the x-y plane. The coordinates of the grid cells and the feedlot digital map were specified such that the flux tower was located at the origin (x = 0, y = 0). Half-hourly values of $\emptyset_k$ and contributions of different surfaces to the measured flux were calculated using MATLAB (MathWorks, Inc.) functions provided by Felber et al. (2015), based on the original footprint tool developed by Neftel et al. (2008). The MATLAB function computed $\emptyset_k$using a grid size of 0.2 × 0.2 m².

The values of $\emptyset_k$ for all grid cells within the artificial source area (i) were summed to calculate the integral footprint contribution $\emptyset_{\Omega_i}$ from a given grazing area surface:

$$\boldsymbol{\phi_{\Omega_i}} = \sum_{j=1}^{M} \boldsymbol{\phi_j A_{cell}} \quad \textbf{(16)}$$

where ϕ_j is the footprint weighting function calculated using Equations (1), M is the number of cells within a given polygon, and A_{cell} is the area of a grid cell. The normalized integral footprint contribution (P_i) given by:

$$\mathbf{P_i} = \frac{\boldsymbol{\phi_{\Omega_i}}}{\boldsymbol{\phi_{\Omega_P}}} \quad \textbf{(17)}$$

Half-hourly P_t values were estimated by summing all P_i values corresponding to the artificial source areas.

4.4 Results

4.4.1 Eddy covariance fluxes

The dates and times for gas releases were determined using weather forecasts from the National Weather Service (https://www.weather.gov/). When the wind blew from the south - southwest, it effectively carried the released gas from source to the flux tower. For these wind conditions, flux footprint got good coverage of the artificial source area. Therefore, gas releases were always planned during favorable wind conditions. In this study, a total of 145 successful half-hour intervals of gas release were achieved. Eddy covariance (EC) fluxes were successfully computed for 95% of these intervals.

4.4.2 Footprint analysis

Footprint analysis revealed that with an 80% footprint fetch, 76% of the flux measurements did not include the intended artificial source area. Extending the footprint fetch to 90% reduced this discrepancy, leaving 60% of the flux measurements outside the coverage of the artificial source area. While the 90% footprint fetch improved the detection rate of flux originating from the artificial source, it also introduced greater instability in the footprint calculation model and increased the prediction error, highlighting a trade-off between coverage and model reliability. However, under certain conditions, the artificial source area was covered by 90% of the footprint fetch, even though it was not included within the 80% footprint fetch. This allowed for flux estimates to be made. Figure 4-2 illustrates a similar scenario on December 1, 2022, at 9:00 PM, where the 80% flux footprint did not cover the artificial source area, while the 90% footprint fetch barely covered it. Consequently, this resulted in no flux estimate for the 80% footprint fetch, whereas a flux estimate of 2000 g/day was obtained for the 90% footprint fetch. However, when the artificial source area was completely covered by both the 90% and 80% footprint fetch, the estimated flux values were nearly equal.

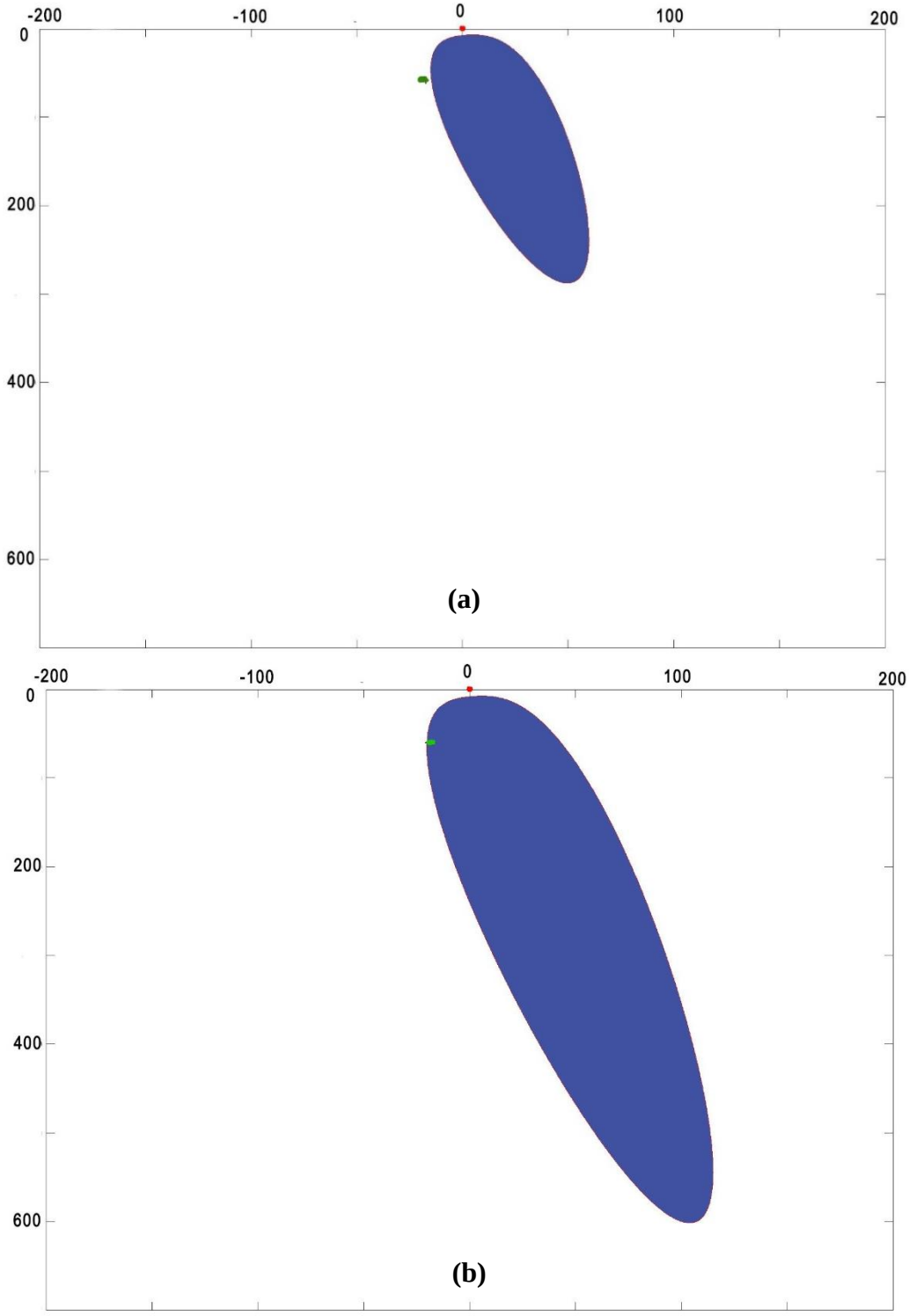

Figure 4-2: Coverage of the source area by (a) 80% footprint fetch and (b) 90% footprint fetch at 9.00 p.m. December 01st 2022. Red point represents the position of the flux tower and green box represents the artificial source area.

4.4.3 Fluxes from the surrounding area

This study area is surrounded by other grazing lands. For the gas released period, the fluxes from the surrounding area (F_{other}) were calculated using conditional sampling, and these values were either negative or close to zero. These values were used to correct the background fluxes.

4.4.4 Emissions from the artificial source

The emissions from the artificial source area were calculated according to equation 15. The estimated flux values for the selected two days are shown in Figure 4-3(c) and Figure 4-4 (c).

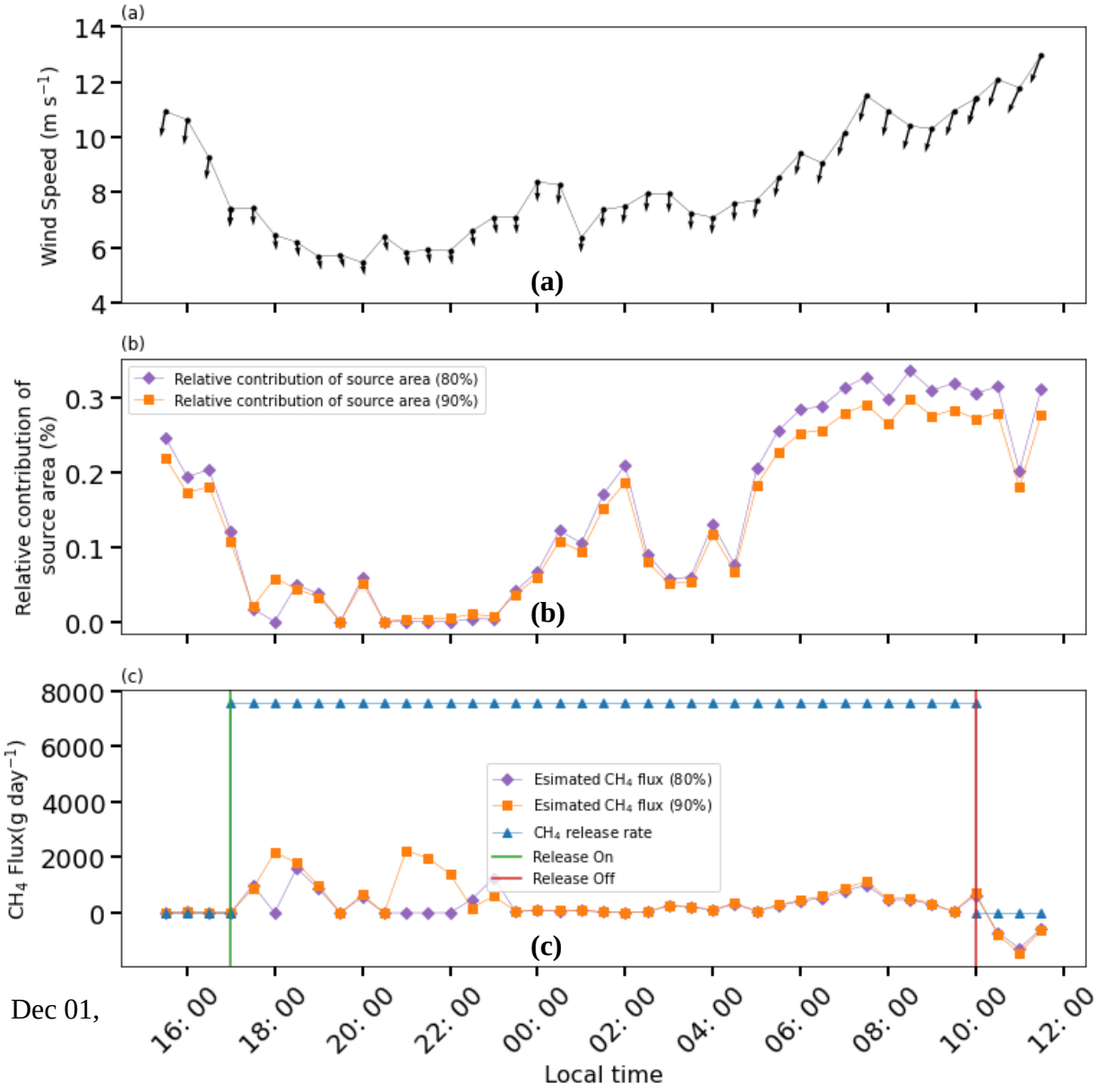

Figure 4-3: Time series of 30-min values of (a) wind speed and direction, (b) relative contribution of the source area provided by the footprint model, and (c) estimated CH_4 flux during controlled CH_4 release event on December 01 2022.

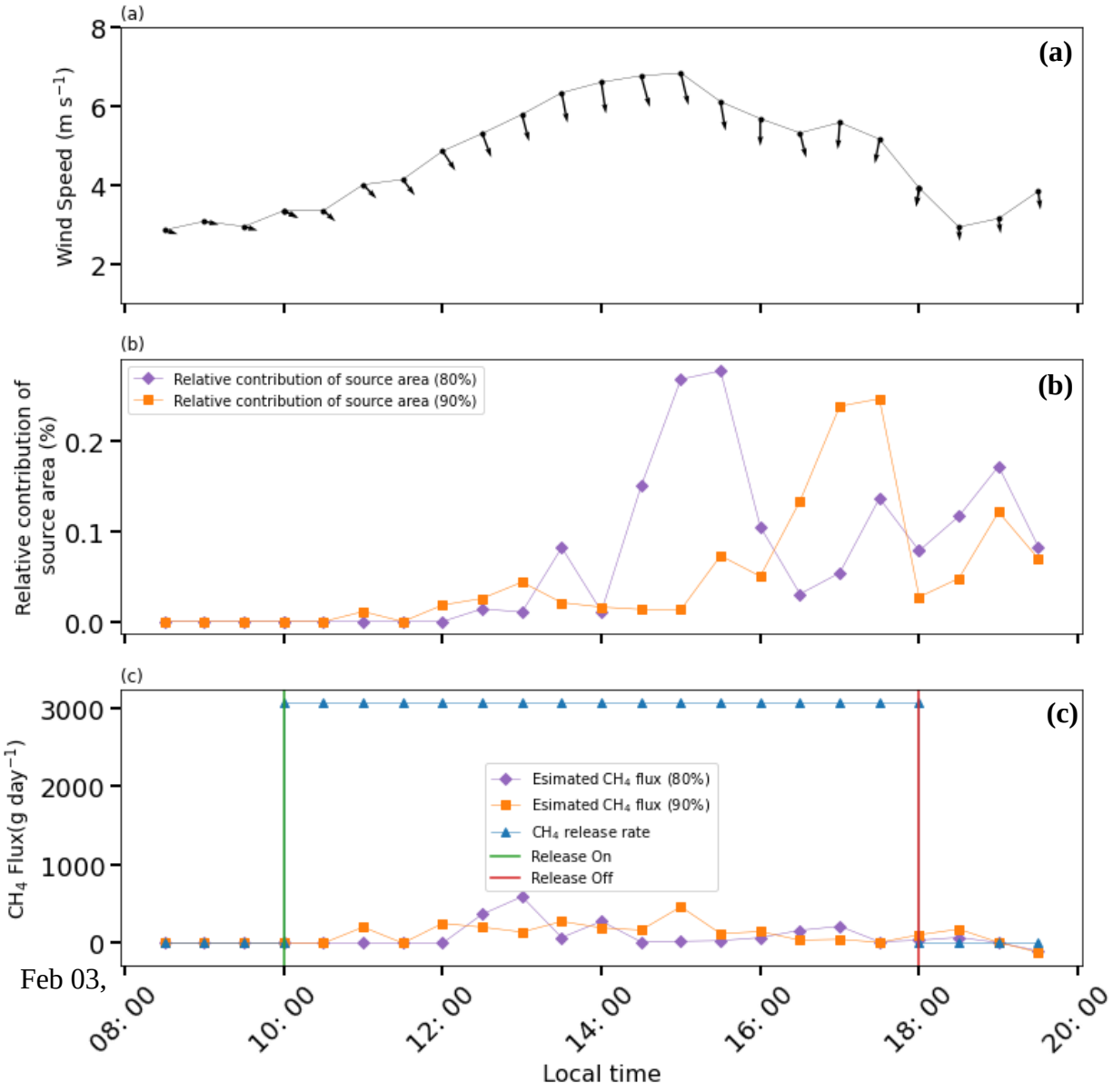

Figure 4-4:Time series of 30 min of (a) wind speed and direction, (b) relative contribution of the source area, and (c) estimated CH_4 flux during controlled CH_4 release event on February 03, 2023.

The analysis incorporates three interconnected aspects: wind speed, the relative contribution of the source area, and CH_4 flux. In Figure 4-4(a), the wind speed shows significant fluctuations over the observed period, with notable peaks and troughs, and the arrows represent variations in both the magnitude and direction of the wind. These fluctuations are crucial as they affect gas dispersion patterns and influence the footprint area from which the measured fluxes originate. Figure 4-4 (b) examines the relative contribution of the source area to the measured fluxes using two different

footprint fetches: 80% and 90%. Generally, the 80% footprint fetch captures a larger contribution to the measured fluxes compared to the 90% fetch. However, the artificial source area falls outside the boundary of the 80% fetch more frequently, leading to its exclusion in the flux measurements. In contrast, the 90% fetch extends to include the artificial source area, thus reflecting its contribution, which the 80% fetch does not capture. Figure 4-4(c) presents the estimated CH_4 flux alongside the CH_4 release rate and the moments when CH_4 release is turned on and off. The estimated flux at both 80% and 90% fetches is consistently lower than the actual release rate but demonstrates similar temporal patterns, increasing when the CH_4 release is activated and decreasing when it is deactivated. This alignment, despite the lower flux estimates, suggests that the eddy covariance analysis effectively captures the release trends. However, the differences between the 80% and 90% fetches highlight that while a larger fetch might initially capture a wider area, it introduces greater instability and error in prediction. This observation underscores the importance of selecting an appropriate fetch percentage to balance between capturing the source area contribution and maintaining model stability and accuracy.

Accurate emission rate estimates can only be achieved if the artificial source area is within the tower footprint. We used the ratio of the calculated emission rate to the true emission rate (QLS/Q) as our metric for evaluating the accuracy of our calculations. An ideal emission calculation would result in QLS/Q = 1. However, our data shows significant clustering around QLS/Q < 0.3, with 89% of the data having QLS/Q < 0.3.

4.5 Discussion

In this study, we explored the use of the eddy covariance (EC) technique combined with footprint analysis to estimate methane (CH_4) emissions from artificial point sources simulating beef cattle. The results demonstrated both the potential and limitations of this approach, with key factors influencing the accuracy of CH_4 flux estimations, such as temporal resolution, footprint coverage, and scaling methodologies. These findings are consistent with various studies that have highlighted similar challenges and proposed enhancements to improve EC-based flux measurements.

4.5.1 Impact of temporal resolution on flux estimates

One of the primary factors affecting flux estimation is the temporal resolution of data collection. While 30-minute intervals were used for calculating fluxes in this study, many inverse dispersion model (IDM) applications for agricultural sources recommend shorter intervals, such as 15-minute averaging periods, to better constrain animal locations and capture high-resolution data in dynamic grazing scenarios (Harper et al. 2011). However, shorter intervals risk missing low-frequency flux contributions, which are important in accurately capturing the full range of CH_4 emissions.

4.5.2 Footprint analysis and source area coverage

The footprint analysis in this study revealed consistent underestimation of CH_4 emissions, particularly at lower fetch percentages. This underestimation can be attributed to the footprint model's limitations in capturing the full contributions of the artificial source area, an issue also identified by Felber et al. (2015). Their work demonstrated that footprint analysis is essential for understanding spatial variability and that underestimations often occur when emissions from animals positioned far from the measurement point are not fully captured.

Increasing the fetch percentage to 90% improved source area coverage but introduced instability and increased prediction errors. This reflects findings by Coates et al. (2017), who found that larger fetch areas enhance source area representation but comes with the trade-off of model instability. These observations emphasize the importance of developing more dynamic footprint models that can adapt to changes in wind conditions and source distribution, as recommended by Neftel et al. (2008), who used footprint weighting tools to better capture the spatial variability of emissions.

4.5.3 Challenges in scaling methodologies

The scaling approach used in this study, relying on footprint-derived estimates of CH_4 contributions, highlighted the inherent difficulties of assuming a homogeneous source area, particularly in real-world grazing systems. Grazing environments are inherently heterogeneous, with animals dispersed unevenly across large areas, resulting in varied emission intensities that are influenced by factors such as animal activity, grazing patterns, and manure deposition. This spatial variability presents a significant challenge for accurately estimating emissions within the footprint. Felber et al. (2015) and Dengel et al. (2011) emphasized the critical role of tracking animal movement and distribution within the flux footprint to improve the accuracy of emission estimates. By considering dynamic animal locations and activity patterns, these studies demonstrated the importance of integrating spatial data to refine CH_4 flux calculations. In our study, the assumption of a uniform 20 m^2 source area oversimplified these complex dynamics, potentially leading to discrepancies in the representation of actual CH_4 emissions within the footprint.

This limitation aligns with observations by Prajapati and Santos (2017), who found significant variations in source area estimates when comparing different footprint models. These discrepancies underscore the sensitivity of footprint analyses to input assumptions and the need for models to account for heterogeneous source distributions. In particular, static assumptions about source area size and uniformity may fail to capture the spatial variability associated with grazing systems, leading to under- or overestimation of emissions.

Moreover, the footprint models applied here were originally derived for smooth surface conditions, which may not accurately capture the effects of surface roughness and topographical variation. This can result in further underestimations, as Neftel et al. (2008) suggested when demonstrating the necessity of parameterizing models for complex terrains to improve emission accuracy.

Several studies have proposed potential improvements to EC-based flux measurements. Laubach et al. (2013) pointed out that increasing the horizontal distance between the EC tower and the source area could enhance accuracy by capturing more representative data. However, as noted by Coates et al. (2017), increasing the sensor height can extend the coverage of the source area but may decrease data retention due to larger fetch requirements. This highlights the need for balancing data quality and sensor capabilities to optimize flux measurement.

Ground-level CH_4 emissions, which were assumed to be negligible in this study, could significantly impact the observed EC fluxes. Felber et al. (2015) highlighted that soil microbial activity can result in CH_4 uptake, a factor that should be considered to more accurately estimate background levels and account for variability.

4.5.4 Future directions and methodological advancements

Our approach, while demonstrating potential in estimating CH_4 emissions from a controlled artificial source, did not perform well when applied to real-world grazing systems characterized by low-concentration and highly variable sources. The traditional flux scaling method used in this study has inherent limitations, particularly in capturing the complexities of spatial heterogeneity and dynamic source distributions in such environments. More refined methods, such as those proposed by Weerasekara et al. (2024), provide improved strategies for quantifying trace gas emissions by incorporating these critical factors.

Addressing these challenges will require the development of more sophisticated approaches. Future studies should integrate real-time tracking of animal movement and spatially explicit data on emission hot spots within the flux footprint. Techniques like GPS tracking and sensor networks can enhance the spatial resolution of CH_4 flux estimates, allowing for a more accurate representation of emissions. Additionally, incorporating variability in environmental conditions, such as wind direction and speed, could improve the robustness of footprint models, enabling them to allocate emissions more precisely to their sources.

Furthermore, adaptive footprint models and scaling techniques need to be refined to better represent the complexities of agricultural emissions. Such advancements should focus on capturing the dynamic interactions between emission sources and environmental conditions, providing a more comprehensive assessment of CH_4 sources.

In summary, while footprint-based scaling approaches offer a valuable framework for estimating CH_4 emissions in grazing systems, their effectiveness depends on the ability to account for spatial heterogeneity and animal behavior. Continued research should prioritize refining footprint models and integrating dynamic data, ultimately improving the accuracy and reliability of emission

estimates in complex grazing environments. These efforts are crucial for advancing our understanding and mitigation of agricultural greenhouse gas emissions.

Chapter 5 - Overall discussion and conclusion

This dissertation addresses the challenge of accurately measuring and estimating greenhouse gas (GHG) emissions from agricultural systems, with a focus on nitrous oxide (N_2O) and methane (CH_4) emissions. The studies presented span across different systems, employing advanced methodologies such as the eddy covariance (EC) technique, artificial neural networks (ANN) for gap-filling, and footprint analysis to estimate and model emissions in both crop and livestock systems. Each study highlights the complexity of measuring GHG emissions, the limitations of existing techniques, and opportunities for refining these methods to improve emission estimates. The collective findings from these three studies provide important insights into the measurement and modeling of N_2O and CH_4 emissions from agricultural systems, offering a critical evaluation of the eddy covariance technique, the use of artificial neural networks, and footprint models. The research highlights the strengths and limitations of current methodologies, while also providing potential pathways for improving GHG emission estimates in agriculture.

5.1 Summary and conclusions

Study 1: N_2O emissions from agricultural fields using the eddy covariance technique

The first study focused on quantifying N_2O emissions from a cattle feedlot and a winter wheat field, highlighting the significant variability of N_2O emissions in response to environmental and management factors. In both systems, N_2O emissions were low on average but punctuated by large emission events, which were likely triggered by soil moisture changes, nitrogen application, and temperature variations. For instance, in the winter wheat field, the study found strong emissions spikes following rainfall and fertilization, indicating increased microbial activity in response to favorable conditions for nitrification and denitrification processes.

Footprint analysis in the cattle feedlot revealed that a substantial portion of N_2O emissions originated from areas outside the feedlot, suggesting that indirect emissions due to manure runoff were significant contributors to the overall flux. This finding underscores the complexity of

capturing total N_2O emissions in open agricultural environments where emissions may not originate directly from the expected source. These results emphasize the need for continuous, high-frequency measurements to fully capture the episodic nature of N_2O emissions, particularly given the disproportionate contribution of these high-emission events to the total GHG budget.

The study also highlighted the importance of soil drivers to N_2O emissions. Frozen soils during the winter period suppressed emission patterns, illustrating that environmental conditions significantly alter microbial activity and thus influence emission levels. This variability stresses the need for long-term monitoring to understand and accurately model GHG emissions from agricultural systems.

The eddy covariance technique is shown to be effective for capturing high-frequency emissions data, particularly in dynamic environments where episodic fluxes are important. However, the technique's limitations in accurately capturing emissions from heterogeneous landscapes, such as grazing systems, underscore the need for further improvements in footprint modeling and sensor placement.

Study 2: Gap-filling of N_2O flux data using artificial neural networks

The second study evaluated the use of artificial neural networks (ANNs) to address gaps in 30-minute N_2O flux data caused by equipment malfunctions, adverse weather conditions, and periods of low turbulence. Unlike previous studies, which predominantly focused on filling gaps in daily or monthly flux data, this study represents a novel application of ANN to high-frequency (30-minute) flux measurements. High-frequency data is crucial for capturing the episodic and dynamic nature of N_2O emissions in agricultural systems, where emissions are influenced by complex interactions between environmental and management factors.

Missing data poses a significant challenge to long-term greenhouse gas (GHG) estimates, particularly in dynamic systems like agricultural fields. Traditional gap-filling methods, such as linear interpolation, often fail to account for the non-linear relationships that govern emissions, making them insufficient for reconstructing accurate datasets. In this study, ANN models were trained using a comprehensive set of environmental variables, including soil moisture, temperature, and wind speed, to predict missing N_2O fluxes. By capturing these intricate

relationships, the ANN approach significantly outperformed traditional gap-filling methods, particularly for medium- and long-term gaps.

The results of this study revealed that ANN models not only reduced bias but also improved the accuracy of cumulative N_2O emission estimates by accounting for underlying environmental patterns influencing flux variability. For short-term gaps, linear interpolation performed adequately; however, for longer gaps where the complexity of environmental drivers became more prominent, ANNs provided a more robust and reliable solution.

A key innovation in this study was the detailed sensitivity analysis, which identified soil moisture and wind speed as the most influential predictors in the ANN model. This finding adds new insights into the environmental drivers of high-frequency N_2O flux variability and underscores the importance of integrating these variables into predictive models. Additionally, by addressing high-frequency data gaps, this study highlights the potential of ANNs to enhance the resolution and reliability of GHG datasets, moving beyond the limitations of coarser temporal scales used in previous research.

In summary, this study not only demonstrated the effectiveness of ANNs for gap-filling in high-frequency N_2O flux data but also advanced the field by addressing a critical gap in the literature. The results showcase the ability of ANNs to reconstruct complex, non-linear datasets, offering a robust tool for reducing uncertainties in cumulative GHG flux estimates and improving the accuracy of emission inventories in agricultural systems.

.

Study 3: CH_4 emissions from grazing systems using eddy covariance and footprint analysis

The third study investigated CH_4 emissions from grazing systems using the eddy covariance technique combined with footprint analysis. The study involved controlled CH_4 release experiments designed to simulate cattle emissions, allowing for an assessment of the EC system's ability to capture CH_4 fluxes in a complex, heterogeneous grazing environment.

The results showed that CH_4 fluxes were consistently underestimated, with estimated emission rates clustering around 30% of the actual release rate. This underestimation was linked to the difficulty in accurately capturing the entire source area using simple footprint models, particularly when wind conditions and terrain introduced spatial variability. Increasing the footprint fetch improved source coverage but introduced greater instability in the model, leading to higher prediction errors. This pattern illustrates the challenges of applying EC in dynamic, open systems like grazing environments, where the movement of animals, variable wind conditions, and uneven terrain can all affect emission estimates.

Additionally, the use of a homogeneous 20 m^2 source area in the controlled release experiments highlighted the limitations of current footprint models in real-world grazing scenarios, cattle are typically dispersed over much larger areas, leading to lower CH_4 concentration enhancements that can challenge detection capabilities. This limitation emphasizes the need for EC and footprint models to accommodate the dispersed and variable nature of emissions in grazing systems.

The use of footprint analysis in the CH_4 emission study highlighted the importance of accurately representing the spatial distribution of emissions in open agricultural systems. The consistent underestimation of CH_4 emissions points to the need for more sophisticated footprint models that can better account for the dynamic nature of grazing systems.

The consistent underestimation of CH_4 fluxes highlights the critical need for refinement in footprint models. Accurate representation of spatial variability in open agricultural systems is essential for improving the reliability of CH_4 emission estimates. Developing more sophisticated footprint models that account for the dynamic and uneven nature of grazing systems will be crucial for advancing livestock emissions research.

5.2 Implications for agriculture in the United States

This dissertation presents a comprehensive framework for improving the accuracy of greenhouse gas (GHG) emission measurements and modeling in agricultural systems, with a focus on nitrous oxide (N_2O) and methane (CH_4). The findings have significant implications for enhancing sustainable agricultural practices, informing policy, and supporting the development of market-based solutions across the United States.

5.2.1 Advancing sustainable practices in U.S. agriculture

The methodologies developed and applied in this research such as the use of eddy covariance (EC) techniques, footprint analysis, and artificial neural networks (ANNs) address critical gaps in understanding and managing GHG emissions. These tools enable a more precise quantification of emissions, which is vital for designing targeted mitigation strategies. For instance:

- **N_2O Emission Management:** Insights into the episodic and spatially variable nature of N_2O emissions provide a foundation for precision nitrogen management practices. By optimizing fertilizer application based on the timing and environmental conditions identified in this research, U.S. farmers can minimize emissions while maintaining productivity. This aligns with efforts to reduce nitrogen losses to the atmosphere and waterways, improving environmental sustainability.
- **CH_4 Mitigation in Livestock Systems:** The improved understanding of CH_4 emission dynamics in grazing systems highlights opportunities to adopt practices such as rotational grazing, feed additives, and manure management strategies. These practices not only reduce CH_4 emissions but also improve overall livestock efficiency, offering economic and environmental benefits.

5.2.2 Enhancing national GHG inventories

Accurate GHG inventories are essential for the United States to meet its international climate commitments under agreements like the Paris Accord. The advanced methodologies in this dissertation contribute to reducing uncertainties in emission estimates by addressing key challenges in agricultural systems:

- The use of high-frequency measurements captures short-term emission events that are often missed in traditional inventory methods, leading to more accurate long-term estimates.
- ANN-based gap-filling techniques provide reliable tools for reconstructing missing data, ensuring that emission inventories reflect the full variability of agricultural emissions.

These improvements position the U.S. agricultural sector to lead in developing transparent, science-based emission reporting systems that can serve as a model for other countries.

5.2.3 Supporting policy and incentive programs

This work provides a scientific basis for developing federal and state-level policies that incentivize sustainable agricultural practices. For example:

- **Carbon Credits and Market-Based Solutions:** By improving the accuracy of emission measurements, this research supports the inclusion of agriculture in carbon markets. Programs that reward emission reductions or carbon sequestration could provide financial incentives for farmers to adopt sustainable practices.
- **Climate-Smart Agriculture Initiatives:** The findings align with national efforts to promote climate-smart agriculture, providing actionable data and methodologies to enhance the resilience and sustainability of U.S. farming systems.

5.3 Positioning U.S. agriculture as a global leader

Finally, the research contributes to positioning U.S. agriculture as a leader in sustainable practices and climate mitigation. By addressing the complexities of measuring and modeling GHG emissions, this work enhances the sector's ability to adopt evidence-based practices, meet sustainability goals, and contribute to global climate solutions. The integration of advanced tools like ANNs and footprint models into GHG inventories and mitigation strategies offers a pathway for the U.S. to lead in developing innovative solutions to one of agriculture's most pressing challenges.

This dissertation not only advances the scientific understanding of GHG emissions in agriculture but also provides practical tools and insights for transforming the sector. The implications for sustainable practices, policy development, and global leadership make this work a critical contribution to addressing the dual challenges of food security and climate change in the United States.

References

Abalos, D., S. E. Brown, A. C. Vanderzaag, R. J. Gordon, K. E. Dunfield, and C. Wagner-Riddle, 2016: Micrometeorological measurements over 3 years reveal differences in N2O emissions between annual and perennial crops. *Glob. Chang. Biol.*, **22**, 1244–1255, https://doi.org/10.1111/GCB.13137.

Aguilar, O. A., R. Maghirang, C. W. Rice, S. L. Trabue, and L. E. Erickson, 2014: Nitrous oxide fluxes from a commercial beef cattle feedlot in Kansas. *Air, Soil Water Res.*, **7**, 35–45, https://doi.org/10.4137/ASWR.S12841.

Ambus, P., and G. P. Robertson, 2006: Automated soil and chamber CO2 flux systems: State of the art, problems and future perspectives. *Eur. J. Soil Sci.*, **57**, 541–554.

Aubinet, M., A. Grelle, A. Ibrom, and others, 2000: Estimates of the annual net carbon and water exchange of European forests: the EUROFLUX methodology. *Adv. Ecol. Res.*, **30**, 113–175.

Aubinet, M., T. Vesala, and D. Papale, 2012: *Eddy covariance: a practical guide to measurement and data analysis*. Springer Science \& Business Media,.

Baldocchi, Dennis and Falge, Eva and Gu, Lianhong and Olson, Richard and Hollinger, David and Running, Steve and Anthoni, Peter and Bernhofer, Ch and Davis, Kenneth and Evans, R. and others, 2001: FLUXNET: A New Tool to Study the Temporal and Spatial Variability of Ecosystem-Scale Carbon Dioxide, Water Vapor, and Energy Flux Densities. *Bull. Am. Meteorol. Soc.*, **82**, 2415–2434, https://doi.org/10.1175/1520-0477(2001)082<2415:FANTTS>2.3.CO;2.

Baldocchi, D., 2008: “Breathing” of the terrestrial biosphere: lessons learned from a global network of carbon dioxide flux measurement systems. *Aust. J. Bot.*, **56**, 1,

https://doi.org/10.1071/BT07151.

Baldocchi, D. D., 2003: Assessing the eddy covariance technique for evaluating carbon dioxide exchange rates of ecosystems: past, present and future. *Glob. Chang. Biol.*, **9**, 479–492, https://doi.org/10.1046/j.1365-2486.2003.00629.x.

Bartlett, 1937: Properties of sufficiency and statistical tests. *Proc. R. Soc. London. Ser. A - Math. Phys. Sci.*, **160**, 268–282, https://doi.org/10.1098/rspa.1937.0109.

Batchvarova, E., and S.-E. Gryning, 1991: Applied model for the growth of the daytime mixed layer. *Boundary-Layer Meteorol.*, **56**, 261–274.

Baum, K. A., J. M. Ham, N. A. Brunsell, and P. I. Coyne, 2008: Surface boundary layer of cattle feedlots: implications for air emissions measurement. *Agric. For. Meteorol.*, **148**, 1882–1893.

Bendat, J. S., and A. G. Piersol, 2000: Random data analysis and measurement procedures. *Meas. Sci. Technol.*, **11**, 1825–1826.

Bigaignon, L., R. Fieuzal, C. Delon, and T. Tallec, 2020: Combination of two methodologies, artificial neural network and linear interpolation, to gap-fill daily nitrous oxide flux measurements. *Agric. For. Meteorol.*, **291**, https://doi.org/10.1016/j.agrformet.2020.108037.

Bishop, C. M., 1995: *Neural networks for pattern recognition*. Oxford University Press,.

Brown, M. B., and A. B. Forsythe, 1974: Robust tests for the equality of variances. *J. Am. Stat. Assoc.*, **69**, 364–367, https://doi.org/10.1080/01621459.1974.10482955.

Brown, S. E., S. Sargent, and C. Wagner-Riddle, 2018: Evaluation of a lower-powered analyzer and sampling system for eddy-covariance measurements of nitrous oxide fluxes. *Atmos. Meas. Tech.*, **11**, 1583–1597, https://doi.org/10.5194/amt-11-1583-2018.

Bühler, M., C. Häni, C. Ammann, S. Brönnimann, and T. Kupper, 2022: Using the inverse dispersion method to determine methane emissions from biogas plants and wastewater treatment plants with complex source configurations. *Atmos. Environ. X*, **13**, 100161.

Butterbach-Bahl, K., E. M. Baggs, M. Dannenmann, R. Kiese, and S. Zechmeister-Boltenstern, 2013: Nitrous oxide emissions from soils: How well do we understand the processes and their controls? *Philos. Trans. R. Soc. B Biol. Sci.*, **368**, https://doi.org/10.1098/rstb.2013.0122.

Campbellsci, *INSTRUCTION MANUAL TGA Series Trace Gas Analyzers*.

Chadwick, D., S. Sommer, R. Thorman, D. Fangueiro, L. Cardenas, B. Amon, and T. Misselbrook, 2011: Manure management: Implications for greenhouse gas emissions. *Anim. Feed Sci. Technol.*, **166**, 514–531.

Chen, H., and Coauthors, 2010: High-accuracy continuous airborne measurements of greenhouse gases (CO₂ and CH₄) using the cavity ring-down spectroscopy (CRDS) technique. *Atmos. Meas. Tech.*, **3**, 375–386, https://doi.org/10.5194/amt-3-375-2010.

Ciais, P., C. Sabine, G. Bala, L. Bopp, V. Brovkin, and E. House, 2013: *Carbon and other biogeochemical cycles. In Climate Change 2013: The Physical Science Basis. Contribution of Working Group I to the Fifth Assessment Report of the Intergovernmental Panel on Climate Change*. 465–570 pp. https://www.ipcc.ch/report/ar5/wg1/.

Coates, T. W., T. K. Flesch, S. M. McGinn, E. Charmley, and D. Chen, 2017: Evaluating an eddy covariance technique to estimate point-source emissions and its potential application to grazing cattle. *Agric. For. Meteorol.*, **234**–**235**, 164–171,

https://doi.org/10.1016/J.AGRFORMET.2016.12.026.

Congreves, K. A., C. Wagner-Riddle, B. C. Si, and T. J. Clough, 2018: Nitrous oxide emissions and biogeochemical responses to soil freezing-thawing and drying-wetting. *Soil Biol. Biochem.*, **117**, 5–15, https://doi.org/10.1016/j.soilbio.2017.10.040.

Connelly, L. M., 2016: Fisher's exact test. *MEDSURG Nurs.*, **25**, https://doi.org/10.2307/2982890.

Cowan, N. J. and Famulari, D. and Levy, P. E. and Anderson, M. and Reay, D. S. and Skiba, U. M., 2014: Investigating uptake of N2O in agricultural soils using a high-precision dynamic chamber method. *Atmos. Meas. Tech.*, **7**, 4455–4462, https://doi.org/10.5194/amt-7-4455-2014.

Cowan, N. J. and Norman, P. and Famulari, D. and Levy, P. E. and Reay, D. S. and Skiba, U. M., 2015: Spatial variability and hotspots of soil N2O fluxes from intensively grazed grassland. *Biogeosciences*, **12**, 1585–1596, https://doi.org/10.5194/bg-12-1585-2015.

Cowan, N. J., D. Famulari, P. E. Levy, M. Anderson, M. J. Bell, R. M. Rees, D. S. Reay, and U. M. Skiba, 2014: An improved method for measuring soil N2O fluxes using a quantum cascade laser with a dynamic chamber. *Eur. J. Soil Sci.*, **65**, 643–652, https://doi.org/10.1111/EJSS.12168.

Curtis Hanson, P. J., P. Bolstad, C. Barford, J. C. Randolph, H. P. Schmidt, and D. Wilson, K.B., 2002: Biometric and eddy covariance based estimates of annual carbon storage in five eastern North American deciduous forests. *Agric. For. Meteorol.*, **113**, 3–19.

Davidson, EA and Savage, KVLV and Verchot, LV and Navarro, R., 2002: Minimizing artifacts and biases in chamber-based measurements of soil respiration. *Agric. For. Meteorol.*, **113**, 21–37.

Davidson, Eric A. Verchot, L. V., 2000: Testing the hole-in-the-pipe model of nitric and nitrous oxide emissions from soils using the TRAGNET database. *Global Biogeochem. Cycles*, **14**, 1035–1043, https://doi.org/10.1029/1999GB001223.

Davidson, E. A., 2009: The contribution of manure and fertilizer nitrogen to atmospheric nitrous oxide since 1860. *Nat. Geosci.*, **2**, 659–662, https://doi.org/10.1038/ngeo608.

Davidson, E. A., M. Keller, H. E. Erickson, L. V Verchot, and E. Veldkamp, 2000: Testing a conceptual model of soil emissions of nitrous and nitric oxides: using two functions based on soil nitrogen availability and soil water content, the hole-in-the-pipe model characterizes a large fraction of the observed variation of nitric oxide . *Bioscience*, **50**, 667–680.

Dengel, S., P. E. Levy, J. Grace, S. K. Jones, and U. M. Skiba, 2011: Methane emissions from sheep pasture, measured with an open-path eddy covariance system. *Glob. Chang. Biol.*, **17**, 3524–3533, https://doi.org/10.1111/j.1365-2486.2011.02466.x.

Dengel, S., D. Zona, T. Sachs, M. Aurela, M. Jammet, F. J. W. Parmentier, W. Oechel, and T. Vesala, 2013: Testing the applicability of neural networks as a gap-filling method using CH4 flux data from high latitude wetlands. *Biogeosciences*, **10**, 8185–8200, https://doi.org/10.5194/bg-10-8185-2013.

Desjardins, R. L., E. Pattey, W. N. Smith, D. Worth, B. Grant, R. Srinivasan, J. I. MacPherson, and M. Mauder, 2010: Multiscale estimates of N2O emissions from agricultural lands. *Agric. For. Meteorol.*, **150**, 817–824, https://doi.org/10.1016/j.agrformet.2009.09.001.

Detto, M., J. Verfaillie, F. Anderson, L. Xu, and D. Baldocchi, 2011: Comparing laser-based open- and closed-path gas analyzers to measure methane fluxes using the eddy covariance method. *Agric. For. Meteorol.*, **151**, 1312–1324, https://doi.org/10.1016/j.agrformet.2011.05.014.

Dorich, C. D., and Coauthors, 2020: Improving N 2 O emission estimates with the global N 2 O database $. https://doi.org/10.1016/j.cosust.2020.04.006.

Dunn, O. J., 1964: Multiple Comparisons Using Rank Sums. *Technometrics*, **6**, 241–252, https://doi.org/10.1080/00401706.1964.10490181.

Edwards, A. W. F., 2005: R.A. Fischer, statistical methods for research workers, first edition (1925). *Landmark Writings in Western Mathematics 1640-1940*, Elsevier Science, 856–870.

EPA, 2023: *EPA (2023). Inventory of U.S. Greenhouse Gas Emissions and Sinks: 1990-2021. U.S. Environmental Protection Agency, EPA 430-R-23-002. https://www.epa.gov/ghgemissions/inventory-us-greenhouse-gas-emissions-andsinks-1990-2021*. 205 pp.

Fan, S. M., S. C. Wofsy, P. S. Bakwin, D. J. Jacob, and D. R. Fitzjarrald, 1990: Atmosphere-biosphere exchange of CO2 and O3 in the central Amazon forest. *J. Geophys. Res. Atmos.*, **95**, 16851–16864.

Feitz, A., and Coauthors, 2018: The Ginninderra CH4 and CO2 release experiment: An evaluation of gas detection and quantification techniques. *Int. J. Greenh. Gas Control*, **70**, 202–224, https://doi.org/10.1016/j.ijggc.2017.11.018.

Felber, R., A. Münger, A. Neftel, and C. Ammann, 2015: Eddy covariance methane flux measurements over a grazed pasture: effect of cows as moving point sources. *Biogeosciences*, **12**, 3925–3940, https://doi.org/10.5194/bg-12-3925-2015.

Firestone, M. K., and E. A. Davidson, 1989: Micorbiological basis of NO and N2O production and consumption in soil. *Exch. trace gases between Terr. Ecosyst. Atmos.*, 7–21.

Fisher, R. A., 1922: On the Interpretation of χ 2 from Contingency Tables, and the Calculation of P. *J. R. Stat. Soc.*, **85**, 87, https://doi.org/10.2307/2340521.

Flechard, C. R., and Coauthors, 2007: Effects of climate and management intensity on nitrous oxide emissions in grassland systems across Europe. *Agric. Ecosyst. Environ.*, **121**, 135–152, https://doi.org/10.1016/j.agee.2006.12.024.

FLESCH, T., J. WILSON, L. HARPER, and B. CRENNA, 2005: Estimating gas emissions from a farm with an inverse-dispersion technique. *Atmos. Environ.*, **39**, 4863–4874, https://doi.org/10.1016/j.atmosenv.2005.04.032.

Flesch, T. K., J. D. Wilson, and E. Yee, 1995: Backward-time Lagrangian stochastic dispersion models and their application to estimate gaseous emissions. *J. Appl. Meteorol.*, **34**, 1320–1332, https://doi.org/https://www.jstor.org/stable/26186846.

Flesch, T. K., J. D. Wilson, L. A. Harper, B. P. Crenna, and R. R. Sharpe, 2004: Deducing ground-to-air emissions from observed trace gas concentrations: a field trial. *J. Appl. Meteorol.*, **43**, 487–502, https://doi.org/10.1175/1520-0450(2004)043<0487:DGEFOT>2.0.CO;2.

Flesch, T. K., J. D. Wilson, and L. A. Harper, 2005: Deducing ground-to-air emissions from observed trace gas concentrations: a field trial with wind disturbance. *J. Appl. Meteorol.*, **44**, 475–484, https://doi.org/10.1175/JAM2214.1.

Flesch, T. K., S. M. McGinn, D. Chen, J. D. Wilson, and R. L. Desjardins, 2014: Data filtering for inverse dispersion emission calculations. *Agric. For. Meteorol.*, **198**, 1–6, https://doi.org/10.1016/j.agrformet.2014.07.010.

Flessa, H., P. D"orsch, F. Beese, and J. Prenzel, 2002: Seasonal variation of N2O and CH4 fluxes in differently managed arable soils in southern Germany. *J. Geophys. Res. Atmos.*, **107**, ACL 4-1--ACL 4-12.

Foken, T., M. Göockede, M. Mauder, L. Mahrt, B. Amiro, and W. Munger, 2004: Post-field data

quality control. *Handbook of micrometeorology: a guide for surface flux measurement and analysis*, Springer, 181–208.

Fowler, D., and Coauthors, 2013: The global nitrogen cycle in the twenty-first century. *Philos. Trans. R. Soc. B Biol. Sci.*, **368**, 20130164.

Freney, J. R., 1997: Emission of nitrous oxide from soils used for agriculture. *Nutr. Cycl. Agroecosystems*, **49**, 1–6.

Galloway, J. N., and Coauthors, 2008: Transformation of the nitrogen cycle: Recent trends, questions, and potential solutions. *Science (80-.).*, **320**, 889–892, https://doi.org/10.1126/science.1136674.

Gao, Z., M. Mauder, R. L. Desjardins, T. K. Flesch, and R. P. van Haarlem, 2009: Assessment of the backward Lagrangian Stochastic dispersion technique for continuous measurements of CH4 emissions. *Agric. For. Meteorol.*, **149**, 1516–1523, https://doi.org/10.1016/j.agrformet.2009.04.004.

Gao, Z., H. Yuan, W. Ma, X. Liu, and R. Desjardins, 2011: Methane emissions from a dairy feedlot during the fall and winter seasons in Northern China. *Environ. Pollut.*, **159**, 1183–1189.

Gimson, N. R., and M. Uliasz, 2003: The determination of agricultural methane emissions in New Zealand using inverse modelling techniques. *Atmos. Environ.*, **37**, 3903–3912, https://doi.org/10.1016/S1352-2310(03)00504-1.

Godde, C. M., I. J. M. De Boer, and E. Ermgassen, 2020: Soil carbon sequestration in grazing systems : managing expectations. 385–391.

Goh, A.-C., 1995: *Back-propagation neural networks for modeling and control*. Imperial College Press,.

Goodfellow, I., Y. Bengio, and A. Courville, 2016: *Deep learning*. MIT Press,.

Goodrich, J. P., A. M. Wall, D. I. Campbell, D. Fletcher, A. R. Wecking, and L. A. Schipper, 2021: Improved gap filling approach and uncertainty estimation for eddy covariance N2O fluxes. *Agric. For. Meteorol.*, **297**, 108280, https://doi.org/10.1016/j.agrformet.2020.108280.

Groffman, P. M., and Coauthors, 2009: Challenges to incorporating spatially and temporally explicit phenomena (hotspots and hot moments) in denitrification models. *Biogeochemistry*, **93**, 49–77, https://doi.org/10.1007/s10533-008-9277-5.

Del Grosso, S. J., T. Wirth, S. M. Ogle, and W. J. Parton, 2008: Estimating agricultural nitrous oxide emissions. *Eos (Washington. DC).*, **89**, 529, https://doi.org/10.1029/2008EO510001.

Del Grosso, S. J., and Coauthors, 2022: An agricultural systems approach for nitrous oxide mitigation in the United States. *Glob. Chang. Biol.*, **28**, 85–104.

Harper, L. A., 2005: Ammonia: measurement issues. *Micrometeorology in agricultural systems*, Vol. 47 of, Wiley Online Library, 345–379.

Harper, L. A. A., O. T. T. Denmead, and T. K. K. Flesch, 2011: Micrometeorological techniques for measurement of enteric greenhouse gas emissions. *Anim. Feed Sci. Technol.*, **166**, 227–239.

Hollinger, D. Y., and A. D. Richardson, 2005: Uncertainty in eddy covariance measurements and its application to physiological models. *Tree Physiology*, Vol. 25 of, Oxford Academic, 873–885.

Hornik, K., M. Stinchcombe, and H. White, 1989: Multilayer feedforward networks are universal approximators. *Neural Networks*, **2**, 359–366.

Horst, T. W., 1997: A simple formula for attenuation of eddy fluxes measured with first-order-

response scalar sensors. *Boundary-Layer Meteorol.*, **82**, 219–233, https://doi.org/10.1023/A:1000229130034.

Hristov, A. N., J. Oh, J. L. Firkins, J. Dijkstra, E. Kebreab, G. Waghorn, and H. P. S. Makkar, 2013: SPECIAL TOPICS — Mitigation of methane and nitrous oxide emissions from animal operations : I . A review of enteric methane mitigation options 1. https://doi.org/10.2527/jas2013-6583.

Huang, H., and Coauthors, 2014: Nitrous oxide emissions from a commercial cornfield (Zea mays) measured using the eddy covariance technique. *Atmos. Chem. Phys.*, **14**, 12839–12854, https://doi.org/10.5194/acp-14-12839-2014.

IPCC, 2014: *Climate change 2014: synthesis report*. R.K. Pachauri and L.A. Meyer, Eds. IPCC,.

IPCC, A., and others, 2013: Climate change 2013: the physical science basis. *Contrib. Work. Gr. I to fifth Assess. Rep. Intergov. panel Clim. Chang.*, **1535**.

Izaurralde, R. C., R. L. Lemke, T. W. Goddard, B. McConkey, and Z. Zhang, 2004: Nitrous Oxide Emissions from Agricultural Toposequences in Alberta and Saskatchewan. *Soil Sci. Soc. Am. J.*, **68**, 1285–1294, https://doi.org/10.2136/sssaj2004.1285.

Järvi, T., J. Lampinen, and E. Talvitie, 2012: *Bayesian optimization for neural networks*. Springer Science & Business Media,.

Jayasundara, S., C. Wagner-Riddle, G. Parkin, and P. Voroney, 2007: Flux-gradient relationships for methane and nitrous oxide emissions from a boreal forest soil. *J. Geophys. Res. Atmos.*, **112**.

Ji, Y., G. Liu, J. Ma, H. Xu, and K. Yagi, 2012: Effect of controlled-release fertilizer on nitrous oxide emission from a winter wheat field. *Nutr. Cycl. Agroecosystems*, **94**, 111–122, https://doi.org/10.1007/s10705-012-9532-y.

Johnson, K., M. Huyler, H. Westberg, B. Lamb, and P. Zimmerman, 1994: Measurement of methane emissions from ruminant livestock using a sulfur hexafluoride tracer technique. *Environ. Sci. Technol.*, **28**, 359–362.

Jones, D., and L. Wilson, 2019: An in-depth guide to understanding and interpreting R^2 in predictive modeling. *Stat. Sci. Rev.*, **23**, 475–487.

Jones, P. D., and others, 2017: Gap filling techniques in climate datasets: Applications and implications. *Clim. Res.*, **24**, 151–166.

Jones, S. K., D. Famulari, C. F. Di Marco, E. Nemitz, U. M. Skiba, R. M. Rees, and M. A. Sutton, 2011: Nitrous oxide emissions from managed grassland: A comparison of eddy covariance and static chamber measurements. *Atmos. Meas. Tech.*, **4**, 2179–2194, https://doi.org/10.5194/amt-4-2179-2011.

Jungbluth, T., E. Hartung, and G. Brose, 2001: Greenhouse gas emissions from animal houses and manure stores. *Nutr. Cycl. Agroecosystems*, **60**, 133–145.

Kamata, Y., A. Matsunami, K. Kitagawa, and N. Arai, 2002: FFT analysis of atmospheric trace concentration of N2O continuously monitored by gas chromatography and cross-correlation to climate parameters. *Microchem. J.*, **71**, 83–93.

Kettunen, A., V. Kaitala, J. Alm, J. Silvola, H. Nykänen, and P. J. Martikainen, 1996: Cross-correlation analysis of the dynamics of methane emissions from a boreal peatland. *Global Biogeochem. Cycles*, **10**, 457–471.

Kinsman, R., F. D. Sauer, H. A. Jackson, and M. S. Wolynetz, 1995: Methane and Carbon Dioxide Emissions from Dairy Cows in Full Lactation Monitored over a Six-Month Period. *J. Dairy Sci.*, **78**, 2760–2766, https://doi.org/10.3168/jds.S0022-0302(95)76907-7.

De Klein, C. A. M., and M. Harvey, 2012: Nitrous oxide chamber methodology guidelines.

Minist. Prim. Ind. Wellington, New Zeal.,.

De Klein, C., and M. Harvey, 2013: Nitrous Oxide Chamber Methodology Guidelines, Global Research Alliance on Agricultural Greenhouse Gases. *Publ. Minist. Prim. Ind. Wellington, New Zeal.*,.

Kljun, N., M. Rotach, and H. Schmid, 2002: A three-dimensional backward Lagrangian footprint model for a wide range of boundary-layer stratifications. *Boundary-Layer Meteorol.*, **103**, 205–226.

Kljun, N., P. Calanca, M. W. Rotach, and H. P. Schmid, 2004: A simple parameterisation for flux footprint predictions. *Boundary-Layer Meteorol.*, **112**, 503–523, https://doi.org/10.1023/B:BOUN.0000030653.71031.96.

Kljun, N., P. Calanca, M. W. Rotach, and H. P. Schmid, 2015: A simple two-dimensional parameterisation for Flux Footprint Prediction (FFP). *Geosci. Model Dev.*, **8**, 3695–3713, https://doi.org/10.5194/gmd-8-3695-2015.

Kormann, R., and F. X. Meixner, 2001: An analytical footprint model for non-neutral stratification. *Boundary-Layer Meteorol.*, **99**, 207–224, https://doi.org/10.1023/A:1018991015119.

Kroon, P. S., A. Hensen, H. J. J. Jonker, M. S. Zahniser, W. H. Van't Veen, and A. T. Vermeiden, 2007: Suitability of quantum cascade laser spectroscopy for CH4 and N2O eddy covariance flux measurements. *Biogeosciences*, **4**, 715–728, https://doi.org/10.5194/bg-4-715-2007.

Kruskal, W. H., and W. A. Wallis, 1952: Use of Ranks in One-Criterion Variance Analysis. *J. Am. Stat. Assoc.*, **47**, 583–621, https://doi.org/10.1080/01621459.1952.10483441.

Lassey, K. R., C. S. Pinares-Patiño, R. J. Martin, G. Molano, and A. M. S. McMillan, 2011:

Enteric methane emission rates determined by the SF6 tracer technique: Temporal patterns and averaging periods. *Anim. Feed Sci. Technol.*, **166**, 183–191.

Laubach, J., 2010: Testing of a Lagrangian model of dispersion in the surface layer with cattle methane emissions. *Agric. For. Meteorol.*, **150**, 1428–1442, https://doi.org/10.1016/j.agrformet.2010.07.006.

Laubach, J., M. Bai, C. S. Pinares-Patio, F. A. Phillips, T. A. Naylor, G. Molano, E. A. C. Rocha, and D. W. Griffith, 2013: Accuracy of micrometeorological techniques for detecting a change in methane emissions from a herd of cattle. *Agric. For. Meteorol.*, **176**, 50–63, https://doi.org/10.1016/j.agrformet.2013.03.006.

McGinn, S. M., 2013: Developments in micrometeorological methods for methane measurements. *Animal*, **7 Suppl 2**, 386–393, https://doi.org/10.1017/S1751731113000657.

Merbold, L., W. Eugster, J. Stieger, M. Zahniser, D. Nelson, and N. Buchmann, 2014: Greenhouse gas budget (CO2, CH4 and N2O) of intensively managed grassland following restoration. *Glob. Chang. Biol.*, **20**, 1913–1928, https://doi.org/10.1111/GCB.12518.

Mishurov, M., and G. Kiely, 2011: Gap-filling techniques for the annual sums of nitrous oxide fluxes. *Agric. For. Meteorol.*, **151**, 1763–1767, https://doi.org/10.1016/J.AGRFORMET.2011.07.014.

Moffat, A. M., and Coauthors, 2007: Comprehensive comparison of gap-filling techniques for eddy covariance net carbon fluxes. *Agric. For. Meteorol.*, **147**, 209–232, https://doi.org/10.1016/j.agrformet.2007.08.011.

MOFFAT, A. M., C. BECKSTEIN, G. CHURKINA, M. MUND, and M. HEIMANN, 2010: Characterization of ecosystem responses to climatic controls using artificial neural networks. *Glob. Chang. Biol.*, **16**, 2737–2749, https://doi.org/10.1111/j.1365-

2486.2010.02171.x.

Moncrieff, J., R. Clement, J. Finnigan, and T. Meyers, 2006: Averaging, Detrending, and Filtering of Eddy Covariance Time Series. *Handbook of Micrometeorology*, Kluwer Academic Publishers, 7–31.

Moncrieff, J. B., and Coauthors, 1997: A system to measure surface fluxes of momentum, sensible heat, water vapour and carbon dioxide. *J. Hydrol.*, **188**–**189**, 589–611, https://doi.org/10.1016/S0022-1694(96)03194-0.

Moravek, A., I. Trebs, and T. Foken, 2013: Effect of imprecise lag time and high-frequency attenuation on surface-atmosphere exchange fluxes determined with the relaxed eddy accumulation method. *J. Geophys. Res. Atmos.*, **118**, 10,210-10,224, https://doi.org/10.1002/jgrd.50763.

Nalon, E., S. Conte, D. Maes, F. A. M. Tuyttens, and N. Devillers, 2013: Assessment of lameness and claw lesions in sows. *Livest. Sci.*, **156**, 10–23, https://doi.org/10.1016/j.livsci.2013.06.003.

Neftel, A., C. Spirig, and C. Ammann, 2008: Application and test of a simple tool for operational footprint evaluations. *Environ. Pollut.*, **152**, 644–652.

Nemitz, E., and Coauthors, 2018: Standardisation of eddy-covariance flux measurements of methane and nitrous oxide. *Int. Agrophysics*, **32**, 517–549, https://doi.org/10.1515/intag-2017-0042.

NEON, 2021: NEON | Site management and event reporting. https://data.neonscience.org/data-products/DP1.10111.001 (Accessed September 14, 2023).

de Oliveira, A. L., L. N. de Castro, and L. dos Santos Coelho, 2013: Convolutional neural networks for text recognition: A survey. *arXiv Prepr. arXiv1312.4236*,.

Ooba, M., T. Hirano, J. I. Mogami, R. Hirata, and Y. Fujinuma, 2006: Comparisons of gap-filling methods for carbon flux dataset: A combination of a genetic algorithm and an artificial neural network. *Ecol. Modell.*, **198**, 473–486, https://doi.org/10.1016/j.ecolmodel.2006.06.006.

Pandas, 2023: Pandas Documentation 2.0.3. *Pandas.org*,. https://pandas.pydata.org/docs/index.html (Accessed December 1, 2024).

Papale, D., and Coauthors, 2006: Towards a standardized processing of Net Ecosystem Exchange measured with eddy covariance technique: Algorithms and uncertainty estimation. *Biogeosciences*, **3**, 571–583, https://doi.org/10.5194/bg-3-571-2006.

Peltola, O., I. Mammarella, S. Haapanala, G. Burba, and T. Vesala, 2013: Field intercomparison of four methane gas analyzers suitable for eddy covariance flux measurements. *Biogeosciences*, **10**, 3749–3765, https://doi.org/10.5194/bg-10-3749-2013.

Philippe and Eriksen-Hamel, N. S. R., 2011: Towards a standard non-steady-state chamber methodology for measuring soil N2O emissions. *Anim. Feed Sci. Technol.*, **166**–**167**, 141–146, https://doi.org/10.1016/j.anifeedsci.2011.04.063.

Pihlatie, M., and Coauthors, 2005: Nitrous oxide emissions from a beech forest floor measured by eddy covariance and soil enclosure techniques. *Biogeosciences*, **2**, 377–387, https://doi.org/10.5194/bg-2-377-2005.

Prajapati, P., and E. A. Santos, 2017a: Estimating methane emissions from beef cattle in a feedlot using the eddy covariance technique and footprint analysis. *Agric. For. Meteorol.*, https://doi.org/10.1016/j.agrformet.2017.08.004.

Prajapati, P., and E. A. Santos, 2017b: Measurements of methane emissions from a beef cattle feedlot using the eddy covariance technique. *Agric. For. Meteorol.*, **232**, 349–358,

https://doi.org/10.1016/j.agrformet.2016.09.001.

Prajapati, P., and E. A. Santos, 2018: Comparing methane emissions estimated using a backward-Lagrangian stochastic model and the eddy covariance technique in a beef cattle feedlot. *Agric. For. Meteorol.*, **256**–**257**, 482–491, https://doi.org/10.1016/j.agrformet.2018.04.003.

Ravishankara, A. R., J. S. Daniel, and R. W. Portmann, 2009: Nitrous oxide (N2O): The dominant ozone-depleting substance emitted in the 21st century. *Science (80-.).*, **326**, 123–125, https://doi.org/10.1126/science.1176985.

Risk, D., C. Ammann, M. Leuenberger, C. Spirig, A. Neftel, C. R"odenbeck, L. Sch"utz, and G. Wohlfahrt, 2013: Correction of flux-gradient relationships measured with relaxed eddy accumulation using a Lagrangian model. *Agric. For. Meteorol.*, **171**, 245–258.

Ro, K. S., M. H. Johnson, K. C. Stone, P. G. Hunt, T. Flesch, and R. W. Todd, 2013: Measuring gas emissions from animal waste lagoons with an inverse-dispersion technique. *Atmos. Environ.*, **66**, 101–106, https://doi.org/10.1016/J.ATMOSENV.2012.02.059.

Rochette, P., and N. S. Eriksen-Hamel, 2008: Chamber Measurements of Soil Nitrous Oxide Flux: Are Absolute Values Reliable? *Soil Sci. Soc. Am. J.*, **72**, 331–342, https://doi.org/10.2136/sssaj2007.0215.

Rumelhart, D. E., G. E. Hinton, and R. J. Williams, 1986: Learning representations by back-propagating errors. *Nature*, **323**, 533–536.

Saxén, H., and J. Pettersson, 2006: *Introduction to artificial neural networks*. CreateSpace Independent Publishing Platform,.

Schuepp, P. H., M. Y. Leclerc, J. I. MacPherson, and R. L. Desjardins, 1990: Footprint prediction of scalar fluxes from analytical solutions of the diffusion equation. *Boundary-*

Layer Meteorol., **50**, 355–373.

SciPy, 2020: Numpy and Scipy Documentation — Numpy and Scipy documentation. https://docs.scipy.org/doc/ (Accessed December 3, 2024).

Sexstone, A. J., T. B. Parkin, and J. M. Tiedje, 1985: Temporal response of soil denitrification rates to rainfall and irrigation. *Soil Sci. Soc. Am. J.*, **49**, 99–103.

SHAPIRO, S. S., and M. B. WILK, 1965: An analysis of variance test for normality (complete samples). *Biometrika*, **52**, 591–611, https://doi.org/10.1093/biomet/52.3-4.591.

Shen, F., D. Chen, G. Wang, J. Lu, X. Hu, X. Gao, E. Fertein, and W. Chen, 2024: Real-time monitoring of CH4 and N2O emissions from livestock using mid-infrared external cavity quantum cascade laser absorption spectroscopy. *J. Quant. Spectrosc. Radiat. Transf.*, **327**, 109131.

Six, J., J. W. van Groenigen, and K. Denef, 2007: Nitrous oxide emissions from agricultural soils: A gap-filling approach using linear regression. *Soil Biol. Biochem.*, **39**, 2787–2795, https://doi.org/10.1016/j.soilbio.2007.06.003.

Smith, J. Q., B. L. Jones, and B. J. Wilson, 2018: A neural network approach to predicting the performance of manufacturing systems. *Int. J. Prod. Res.*, **56**, 6942–6957.

Smith, K., and L. Richardson, 2018: Pitfalls in linear interpolation of missing data: A case study in hydrology. *J. Hydrol. Process.*, **32**, 558–565.

Smith, P., and Coauthors, 2014: Agriculture, forestry and other land use (AFOLU). *Climate change 2014: mitigation of climate change. Contribution of Working Group III to the Fifth Assessment Report of the Intergovernmental Panel on Climate Change*, Cambridge University Press, 811–922.

Stathakis, D., 2009: *Artificial neural networks*. Springer Science & Business Media,.

Stull, R., 1988: *Boundary conditions and surface forcing*. 251–289 pp.

Sun, K., L. Tao, D. J. Miller, M. A. Zondlo, K. B. Shonkwiler, C. Nash, and J. M. Ham, 2015: Open-path eddy covariance measurements of ammonia fluxes from a beef cattle feedlot. *Agric. For. Meteorol.*, **213**, 193–202, https://doi.org/10.1016/j.agrformet.2015.06.007.

Svozil, D., V. Kvasnicka, and J. Pospichal, 1997: Introduction to multi-layer neural networks. *Phys. D Nonlinear Phenom.*, **109**, 239–268.

Taki, R., C. Wagner-Riddle, G. Parkin, R. Gordon, and A. VanderZaag, 2019: Comparison of two gap-filling techniques for nitrous oxide fluxes from agricultural soil. *Can. J. Soil Sci.*, **99**, 12–24, https://doi.org/10.1139/cjss-2018-0041.

Thomson, A. J., G. Giannopoulos, J. Pretty, E. M. Baggs, and D. J. Richardson, 2012: Biological sources and sinks of nitrous oxide and strategies to mitigate emissions. *Philos. Trans. R. Soc. B Biol. Sci.*, **367**, 1157–1168, https://doi.org/10.1098/rstb.2011.0415.

Troy, S. M., C. A. Duthie, D. W. Ross, J. J. Hyslop, R. Roehe, A. Waterhouse, and J. A. Rooke, 2016: A comparison of methane emissions from beef cattle measured using methane hoods with those measured using respiration chambers. *Anim. Feed Sci. Technol.*, **211**, 227–240, https://doi.org/10.1016/j.anifeedsci.2015.12.005.

Tukey, J. W., 1949: Comparing Individual Means in the Analysis of Variance. *Biometrics*, **5**, 99, https://doi.org/10.2307/3001913.

Venterea, R. T., M. Burger, and K. A. Spokas, 2005: Chamber-based trace gas flux measurements: A review of methods, applications, and sources of error. *Methods for measuring greenhouse gas balances and evaluating mitigation options in agricultural production,* Springer Netherlands, 145–185.

Vickers, D., and L. Mahrt, 1997: Quality control and flux sampling problems for tower and

aircraft data. *J. Atmos. Ocean. Technol.*, **14**, 512–526, https://doi.org/10.1175/1520-0426(1997)014<0512:QCAFSP>2.0.CO;2.

Vitousek, P. M., J. D. Aber, R. W. Howarth, G. E. Likens, P. A. Matson, D. W. Schindler, W. H. Schlesinger, and D. G. Tilman, 1997: Human alteration of the global nitrogen cycle: sources and consequences. *Ecol. Appl.*, **7**, 737–750.

Wagner-Riddle, C., G. W. Thurtell, G. E. Kidd, E. G. Beauchamp, and R. Sweetman, 1997: Annual emissions of nitrous oxide and carbon dioxide from agricultural soils in eastern Canada. *Can. J. Soil Sci.*, **77**, 673–685.

Wagner R, C., T. B. Parkin, and R. T. Venterea, 2007: N2O emissions from agricultural soils: implications for N2O emissions inventories and mitigation strategies. *Can. J. Soil Sci.*, **87**, 359–369.

Wang, K., and Coauthors, 2013: Comparison between static chamber and tunable diode laser-based eddy covariance techniques for measuring nitrous oxide fluxes from a cotton field. *Agric. For. Meteorol.*, **171**–**172**, 9–19, https://doi.org/10.1016/j.agrformet.2012.11.009.

Wang, R., and Coauthors, 2020: Using field-measured soil N2O fluxes and laboratory scale parameterization of N2O/(N2O+N2) ratios to quantify field-scale soil N2 emissions. *Soil Biol. Biochem.*, **148**, 107904, https://doi.org/10.1016/j.soilbio.2020.107904.

Webb, E. K., G. I. Pearman, and R. Leuning, 1980: Correction of flux measurements for density effects due to heat and water vapour transfer. *Q. J. R. Meteorol. Soc.*, **106**, 85–100, https://doi.org/10.1002/qj.49710644707.

Weerasekara, C., and Coauthors, 2024: Using Open-Path Dual-Comb Spectroscopy to Monitor Methane Emissions from Simulated Grazing Cattle. *EGUsphere*, **2024**, 1–19.

Wilczak, J. M., S. P. Oncley, and S. A. Stage, 2001: Sonic anemometer tilt correction algorithms.

Boundary-Layer Meteorol., **99**, 127–150, https://doi.org/10.1023/A:1018966204465.

Wilk, M. B., and R. Gnanadesikan, 1968: Probability plotting methods for the analysis for the analysis of data. *Biometrika*, **55**, 1–17, https://doi.org/10.1093/BIOMET/55.1.1.

Wilson, J. D., and E. Yee, 2003: Calculation of winds disturbed by an array of fences. *Agric. For. Meteorol.*, **115**, 31–50, https://doi.org/10.1016/S0168-1923(02)00169-7.

Wilson, J. D., T. K. Flesch, and L. A. Harper, 2001: Micro-meteorological methods for estimating surface exchange with a disturbed windflow. *Agric. For. Meteorol.*, **107**, 207–225, https://doi.org/10.1016/S0168-1923(00)00238-0.

Wilson, J. D., T. K. Flesch, and B. P. Crenna, 2013: Estimating Surface-Air Gas Fluxes by Inverse Dispersion Using a Backward Lagrangian Stochastic Trajectory Model. *Geophysical Monograph Series, edited by: Lin, J., Brunner, D., Gerbig, C., Stohl, A., Luhar, A., and Webley, P*, Vol. 200 of, American Geophysical Union, 149–162.

Wohlfahrt, G., and M. Galvagno, 2017: Revisiting the choice of the driving temperature for eddy covariance CO 2 flux partitioning. *Agric. For. Meteorol.*, 135–142, https://doi.org/10.1016/j.agrformet.2017.02.012.

Woodward, A., and Coauthors, 2014: Climate change and health: on the latest IPCC report. *Lancet*, **383**, 1185–1189.

Xu, L., X. Lin, J. Amen, K. Welding, and D. McDermitt, 2014: Impact of changes in barometric pressure on landfill methane emission. *Global Biogeochem. Cycles*, **28**, 679–695, https://doi.org/10.1002/2013GB004571.